PAVOL JOZEF ŠAFÁRIK UNIVERSITY IN KOŠICE
Faculty of Medicine
Department of Forensic Medicine

ATLAS OF FORENSIC MEDICINE

Autopsy findings in violent and non-violent deaths

Dorota Sopková

Košice 2025

Publication is an output of the project KEGA No. 009UPJŠ-4/2023: Innovation of teaching forensic medicine with an electronic atlas of autopsy findings.

ATLAS OF FORENSIC MEDICINE: Autopsy findings in violent and non-violent deaths

University Textbook

Author:

Dorota Sopková, MD, PhD., MBA

Department of Forensic Medicine, Faculty of Medicine, Pavol Jozef Šafárik University in Košice

Reviewers:

prof. Jozef Šidlo, MD, CSc. MPH, FIALM
Department of Forensic Medicine, Faculty of Medicine, Comenius University in Bratislava

assoc. prof. Martin Janík, MD, PhD.
Department of Forensic Medicine and Medical Expertises, Jessenius Faculty of Medicine in Martin, Comenius University in Bratislava

Available at: www.unibook.upjs.sk
Publication date: 30.09.2025

DOI: https://doi.org/10.33542/AFM-0442-2
ISBN 978-80-574-0442-2 (e-publication)

CONTENTS

Preface

The Atlas of Forensic Medicine: Autopsy Findings in Violent and Non-violent Deaths is a full-color atlas including a series of more than 266 images of autopsy pathology recorded by the Department of Forensic Medicine of Pavol Jozef Šafárik University in Košice, Faculty of Medicine. Depicted are external and internal autopsy findings and histopathological findings, representing three major components to morphological autopsy diagnosis.

The Atlas aims to serve as a visual aid in studying the subject Forensic Medicine—a compulsory course of undergraduate medical curricula in the study programs General Medicine and Dental Medicine, as well as in postgraduate education in the field of Forensic Medicine.

The publication was developed with the financial support of the Cultural and Educational Grant Agency (KEGA) of the Ministry of Education, Youth and Sports of the Slovak Republic—project KEGA No. 009UPJŠ-4/2024: Innovation of teaching forensic medicine with an electronic atlas of autopsy findings.

Special thanks to colleagues at the Forensic Medicine and Pathological Anatomy Unit of Health Care Surveillance Authority in Košice for the teamwork, collaboration, and positive attitude that enrich our workdays.

Dorota Sopková, 2025

1 Postmortem Changes

1A | Early postmortem changes

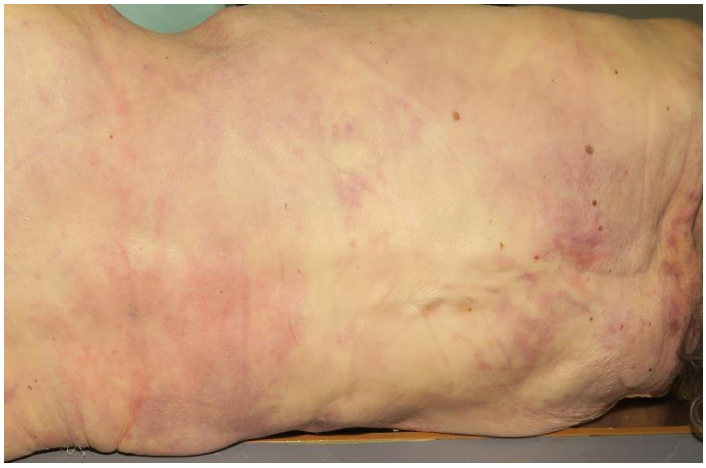

Fig. 1A.1 **Postmortem lividity**

Initial stage of manifestation characterized by reddish-purple patchy discoloration on the back.

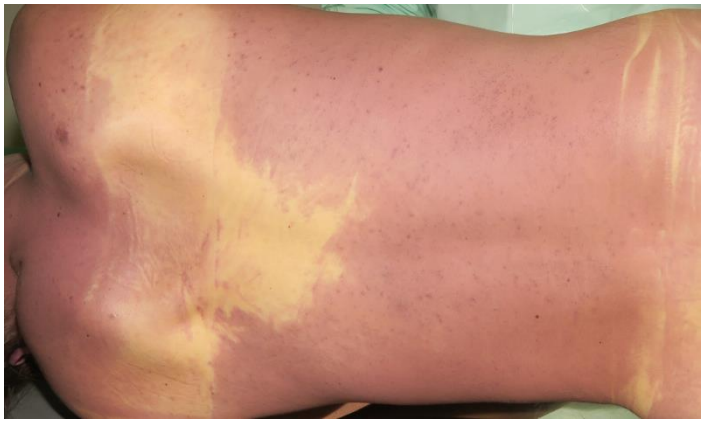

Fig. 1A.2 **Postmortem lividity**

Confluent reddish-purple discoloration on the back with contact flattening (contact pallor) over the scapular region.

Fig. 1A.3 **Postmortem lividity**

Confluent reddish-purple discoloration on the back with contact flattening produced by clothing and other objects.

Fig. 1A.4 **Postmortem drying of the lips**

Lips are dark-red and stiff.

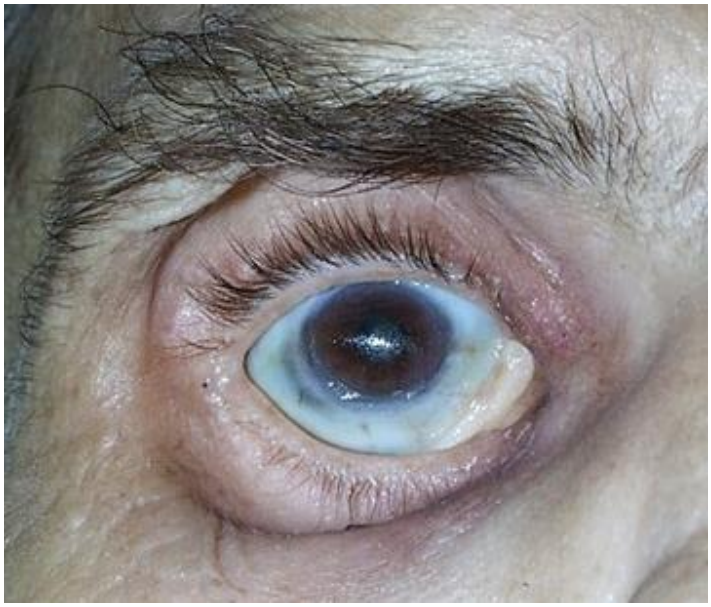

Fig. 1A.5 ***Tache noir* in the sclera**

Linear, brown discoloration of the sclera resulting from incomplete occlusion after death.

Fig. 1B.1 **Putrefaction**

Early manifestation is greenish discoloration of the skin of the anterior abdominal wall beginning at the lower right quadrant.

Fig. 1B.2 **Putrefaction**

More pronounced greenish discoloration of the skin of the anterior abdominal wall.

Fig. 1B.3 **Putrefaction**

Outlining of the superficial veins resulting from bacteria-induced hemolysis. It is referred to as marbling of the skin.

Fig. 1B.4 **Putrefaction**

Advanced putrefaction with skin discoloration, marbling and skin slippage.

Fig. 1B.5 **Mummification**

The skin is dry, hard, and leatherlike. Its color changes to blackish-brown.

Fig. 1B.6 **Mummification**

Mummification of the hand.

Fig. 1B.7 **Saponification**

Subcutaneous and intra-abdominal fat is replaced by grayish white soap-like waxy substance (adipocere).

Fig. 1C.1 **Animal predation**

Postmortem bite injury of the right foot.

Fig. 1C.2 **Insect predation**

Multiple fly eggs in an open wound on the left shin.

Fig. 1C.3 **Insect predation**

Extensive maggot activity on the limb of a decomposing corpse.

Fig. 1C.4 **Molds**

Multiple fungal colonies growing on the face.

2 Injuries

2A | Blunt force injuries

Fig. 2A.1 **Abrasion**

Abrasion on the head characterized by the disruption and loss of superficial layers of the skin.

Fig. 2A.2 **Linear abrasions**

Multiple linear abrasions (scratches) on the abdomen produced by horizontal or tangential friction by a pointed end of an object.

Fig. 2A.3 **Brush abrasion**

Brush abrasion on the right hand of a traffic accident victim resulting from the body moving/being dragged against the road (road rash).

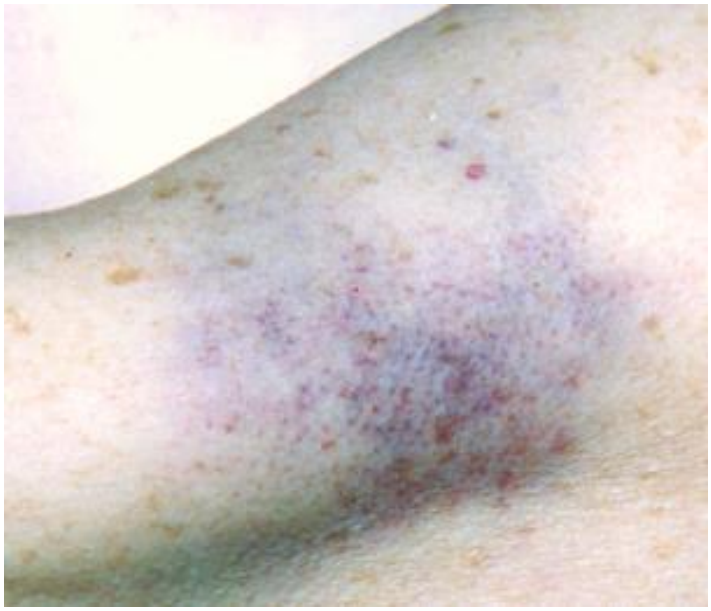

Fig. 2A.4 **Bruise**

Bruise on the left arm resulting from a rupture of small vessels within the tissue as a result of blunt trauma.

Fig. 2A.5 **Bruises**

Larger area of bruising on the abdomen. Extensive bruising in this region is often associated with damage to the intra-abdominal structures and hemoperitoneum.

Fig. 2A.6 **Patterned bruising**

Bruises produced by a stick-like object with a characteristic appearance of two parallel lines with space between them (tram-line).

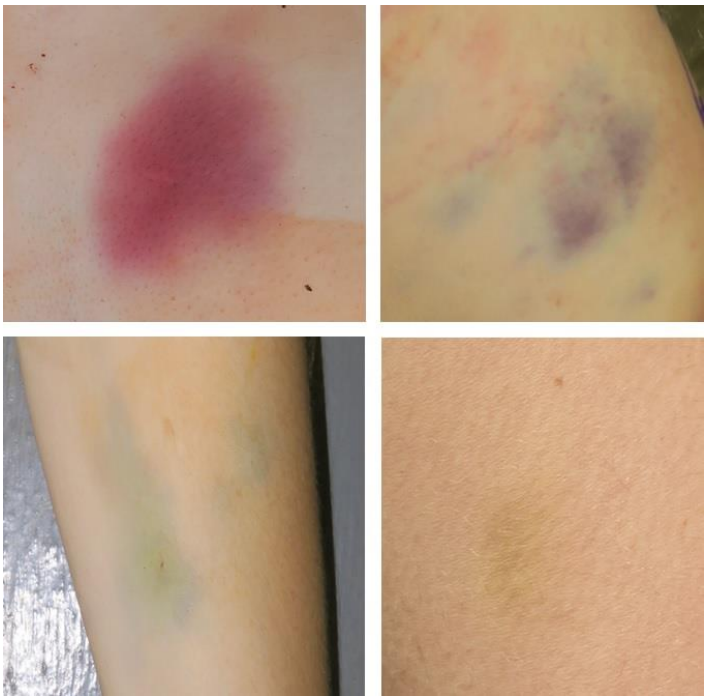

Fig. 2A.7 **Color progression of bruises**

Different color variations of bruises are caused by a chemical degradation of hemoglobin during the healing process. The sequence is red, blue, green, yellow, and brown.

Fig. 2A.8 **Bruise**

Multicolored bruise with color changes proceeding from periphery towards the center, indicating that it occurred a few days prior to death.

Fig. 2A.9 **Laceration**

Laceration of the scalp with minimal associated abrasion.

Fig. 2A.10 **Laceration**

Linear laceration of the forehead with jagged margins and tissue bridging.

Fig. 2A.11 **Laceration**

Laceration of the scalp with extensive associated abrasions and tissue bridging.

Fig. 2A.12 **Laceration**

Irregularly shaped laceration of the scalp extending through to the surface of the skull without tissue bridging—typical in areas where the skin is close to the bone.

Fig. 2B.1 **Cut (incised wound)**

Spindle-shaped incised wound that is longer on the skin surface than it is deep.

Fig. 2B.2 **Hesitation marks**

Self-inflicted superficial cuts oriented parallel to each other located on the forearm.

Fig. 2B.3 **Cuts (incised wounds)**

Two irregular incised wounds on the head produced by a knife.

Fig. 2B.4 **Cut (incised wound)**

Deep incised wound on the neck produced by a knife.

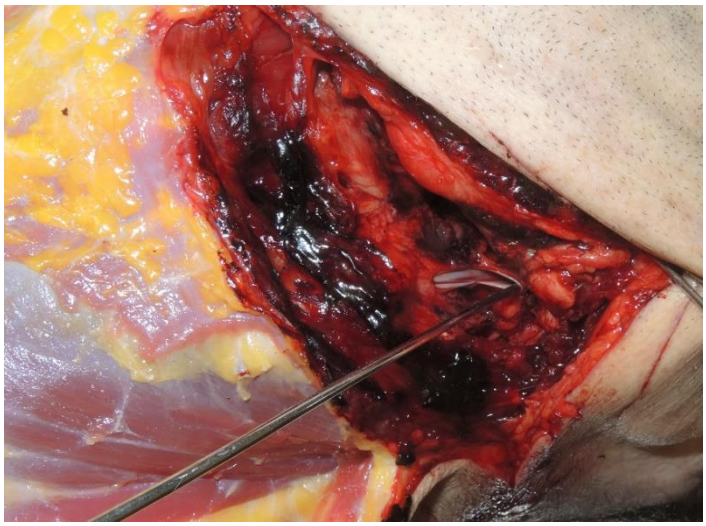

Fig. 2B.5 **Cut wound**

Probe entering the transected vessel within the incised wound of the neck.

Fig. 2B.6 **Stab wound**

Stab wound with clearly defined edges and no tissue bridges; the wound is deeper than it is wide. The left angle comes to a point (sharp angle) and the right angle has a squared-off appearance (blunt angle) indicating a single-edged knife.

Fig. 2B.7 **Stab wound**

Stab wound with a fish-tailing on the left angle.

Fig. 2B.8 **Stab wounds**

Cluster of stab wounds on the chest produced by a knife.

Fig. 2B.9 **Slash (chop wound)**

Chop wound on the head with an underlying skull fracture.

Fig. 2B.10 **Slash (chop wound)**

Chop wound on the head with an underlying skull fracture.

Fig. 2B.11 **Slash (chop wound)**

Chop wounds with digital amputations.

Fig. 2C.1 **Rifled entrance wound**

Contact entrance wound characterized by a central round defect with a surrounding greasy rim and marginal abrasion adjacent to it. A muzzle imprint mark characterized by a patterned abrasion is present around the defect.

Fig. 2C.2 **Rifled entrance wound**

Contact entrance wound with a surrounding greasy rim and marginal abrasion. Only a partial muzzle imprint mark is present at the right lower area of the skin surrounding the central defect.

Fig. 2C.3 **Rifled entrance wound**

Contact entrance wound of the scalp showing characteristic stellate appearance due to splitting of the skin because of gases being reflected back by the underlying bone, dissecting beneath the skin and causing it to expand outward.

Fig. 2C.4 **Rifled entrance wound**

Medium (intermediate) range contact entrance wound characterized by gunpowder tattooing and absence of soot around the defect.

Fig. 2C.5 **Entrance wound produced by a captive bolt gun**

Round defect with surrounding soot deposition.

Fig. 2C.6 **Penetrating gunshot wound**

Bruising of the skin underlying the end of the wound channel in a penetrating gunshot wound the where projectile lacks the energy to produce an exit wound.

Fig. 2C.7 **Rifled exit wound**

Irregularly shaped defect with slightly abraded margins; it may resemble ordinary laceration.

Fig. 2C.8 **Rifled exit wound**

Irregularly shaped defect with everted margins.

Fig. 2C.9 **Shot gun entrance wound**

Contact shotgun wound of the head with massive destruction.

Fig. 2D.1 **Dog bite injuries**

Multiple lacerations on the head and back with adjacent bruising.

Fig. 2D.2 **Dog bite injury**

Two opposing lacerations (on the left) and one deep laceration with protrusion of the subcutaneous fat (on the right) on the upper limb.

Fig. 2E.1 **Frost bites**

Frost bites on toes presenting with edema and bluish skin discoloration.

Fig. 2E.2 **Scald**

Irregularly shaped area of reddening.

Fig. 2E.3 **Burns**

Third-degree burns on the trunk treated with a surgical incision on the right lateral side (escharotomy).

Fig. 2E.4 **Burns**

Third-degree burns with wound infection on the trunk and two surgical incisions perpendicular to each other.

Fig. 2E.5 **Burns**

Third-degree burns with wound infection on the trunk and the right upper limb.

Fig. 2F.1 **Electrical injury**

Electric mark/burn on the palm of the hand representing a point where a low-voltage electric current entered the body. It has a characteristic appearance of a collapsed blister with raised edges.

Fig. 2F.2 **Electrical injury**

Electric burn on the hand with extensive charring.

Fig. 2F.3 **Electrical injury**

High-voltage electric burn on the chest. Typically, it is characterized by a central dried area surrounded by pale skin and a peripheral rim of red discoloration.

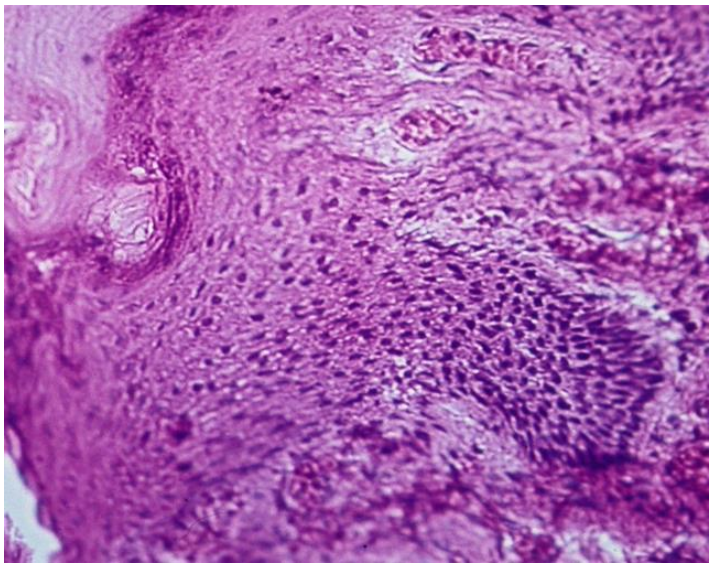

Fig. 2F.4 **Electrical injury**

Microscopic image of an electric mark characterized by a palisade arrangement of epidermal basal cells and nuclear elongation (H&E).

Fig. 2F.5 **Lightning injury**

Singed hair on the head.

Fig. 2F.6 **Lightning injury**

Singed eyebrow hair and eyelashes.

3 Cardiovascular System

3A | Disorders affecting great vessels and coronary arteries

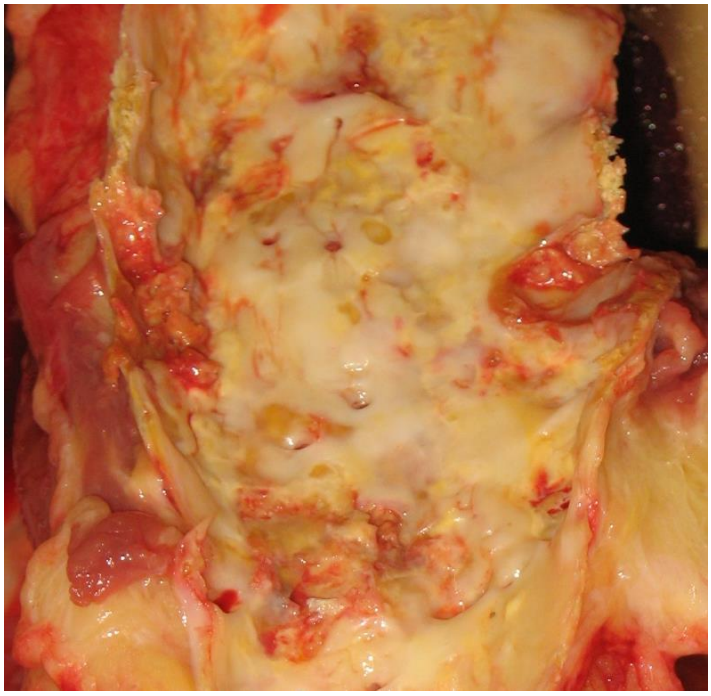

Fig. 3A.1 **Atherosclerosis**

Calcified and ulcerated atheromas in the abdominal aorta.

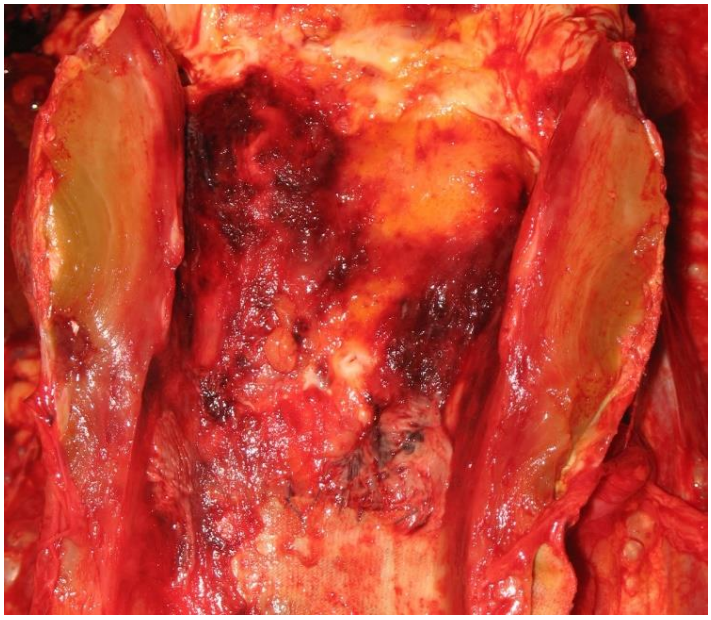

Fig. 3A.2 **Atherosclerosis**

Mural thrombus overlaying an atheromatous plaque in the abdominal aorta.

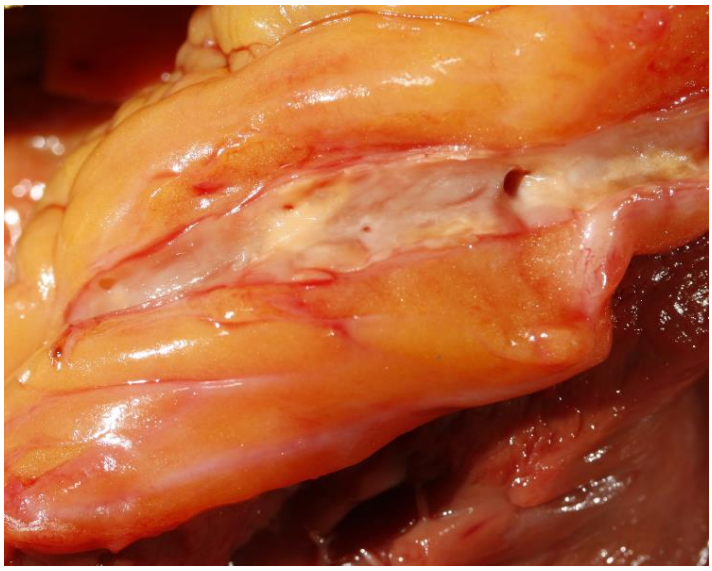

Fig. 3A.3 **Atherosclerosis**

Calcified atheromas in the left anterior descending artery.

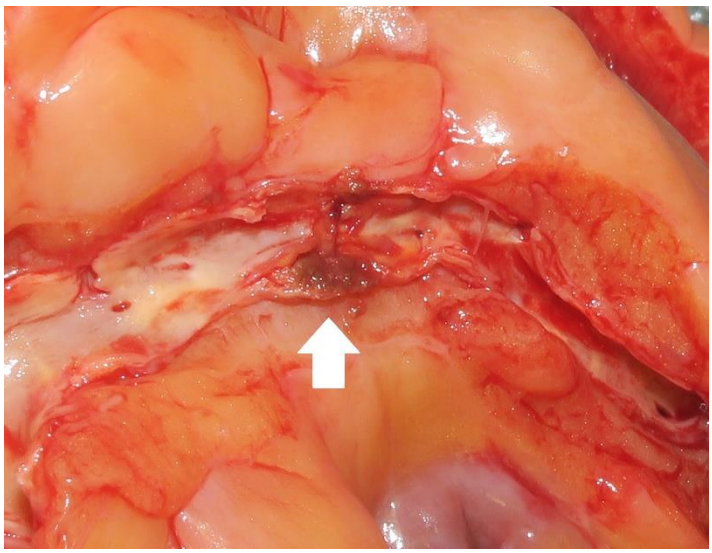

Fig. 3A.4 **Atherosclerosis**

Intraplaque hemorrhage in the atherosclerotic coronary lesion.

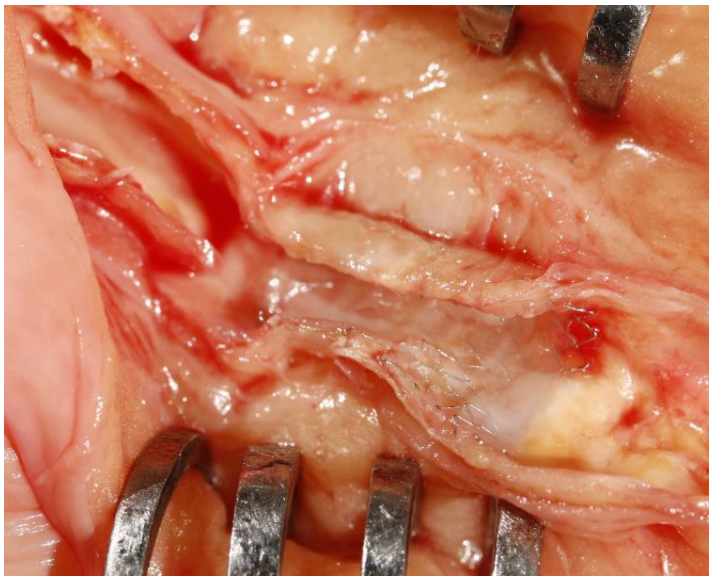

Fig. 3A.5 **Atherosclerosis**

Left anterior descending artery containing metallic stent.

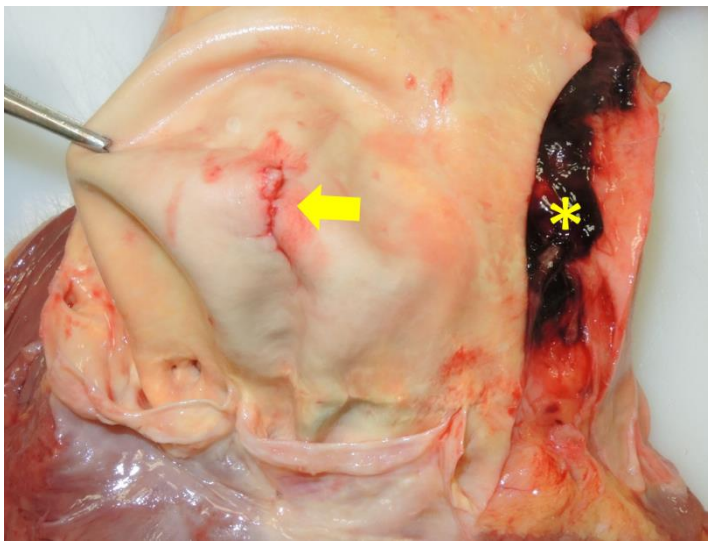

Fig. 3A.6 **Dissection**

Intimal tear in the ascending thoracic aorta (arrow) and the exposed false lumen (asterisk).

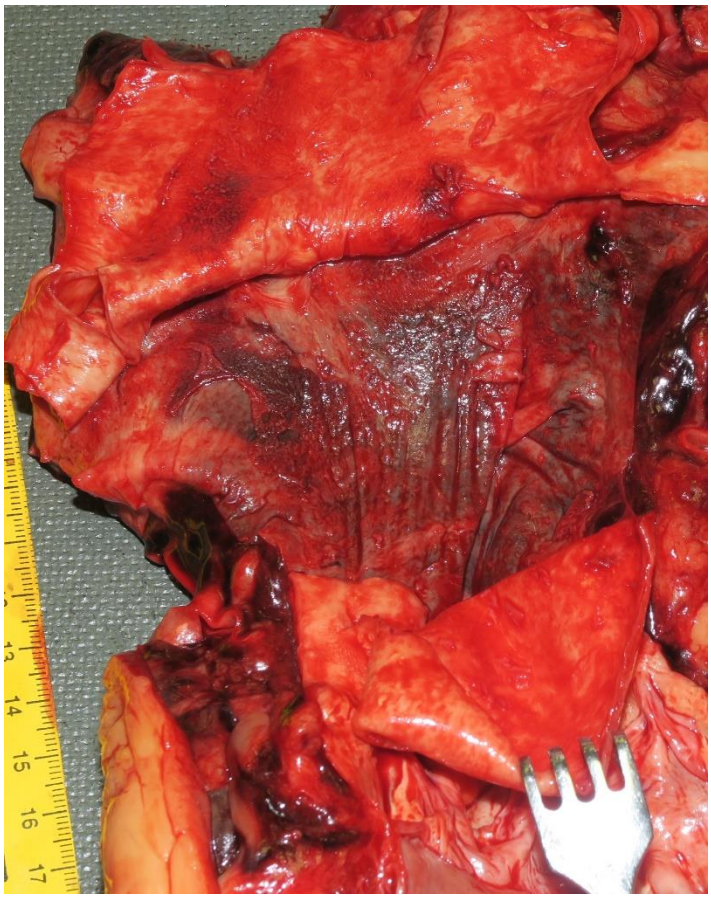

Fig. 3A.7 **Dissection**

The inner layers of the aortic wall are flipped over to expose the false lumen and the outer layers.

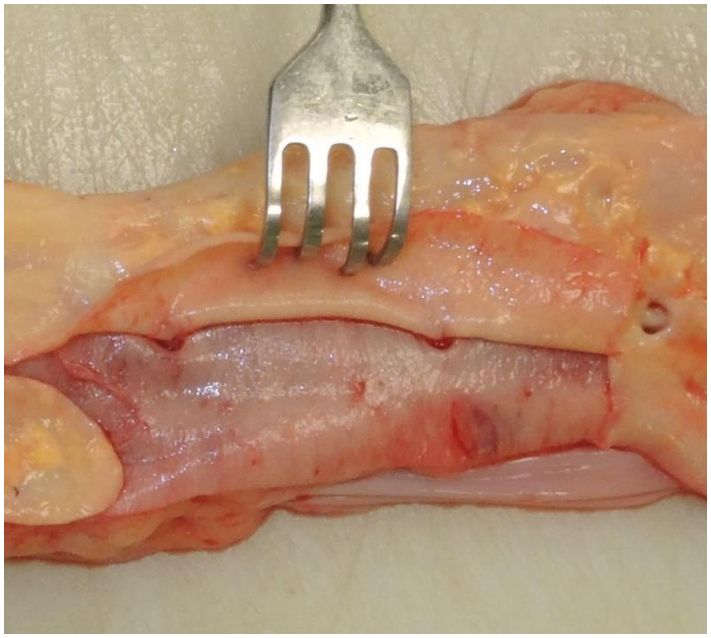

Fig. 3A.8 **Dissection**

The hook is used to lift the layer of the aortic wall to expose a false lumen.

Fig. 3A.9 **Dissection**

Cross sections of the formalin-fixed thoracic aorta showing separation of the layers of the vessel's wall and a false lumen (asterisk on the left, arrow on the right).

Fig. 3A.10 **Dissection**

Microscopic image of the cross section of the left anterior descending artery affected by dissection. Hemorrhage is present in the false lumen (asterisk); the original lumen is compressed (H&E).

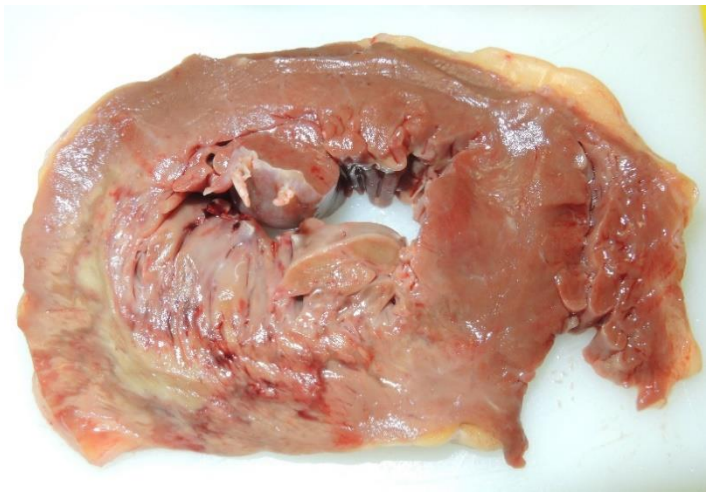

Fig. 3B.1 **Acute myocardial infarction**

Transverse (short-axis) sections of the left ventricle showing tan yellow, irregular area with intermittent hemorrhages affecting the entire thickness of the ventricle's wall.

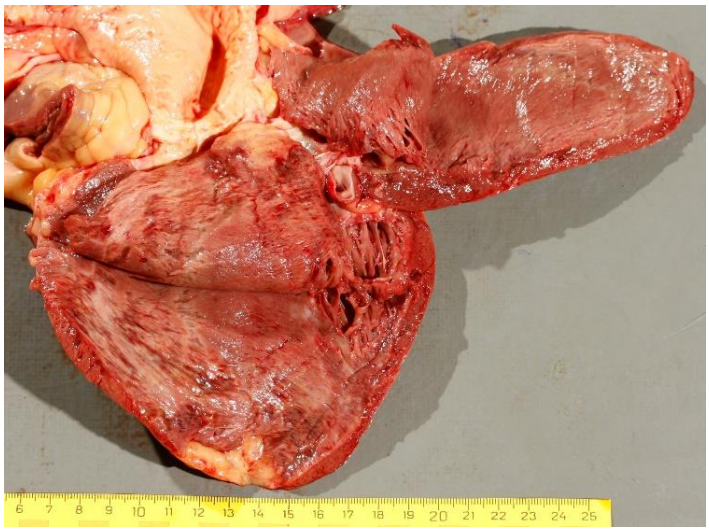

Fig. 3B.2 **Acute myocardial infarction**

Tan yellow, irregular area with intermittent hemorrhage on the cut surface of the left ventricle after a slice made parallel to the endo-epicardial surface.

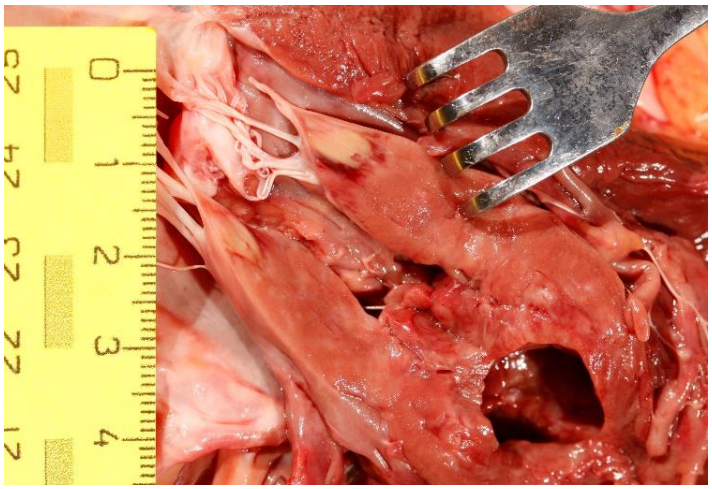

Fig. 3B.3 **Acute myocardial infarction**

Tan yellow area with a rim of hyperemia on the cut surface of the anterolateral papillary muscle.

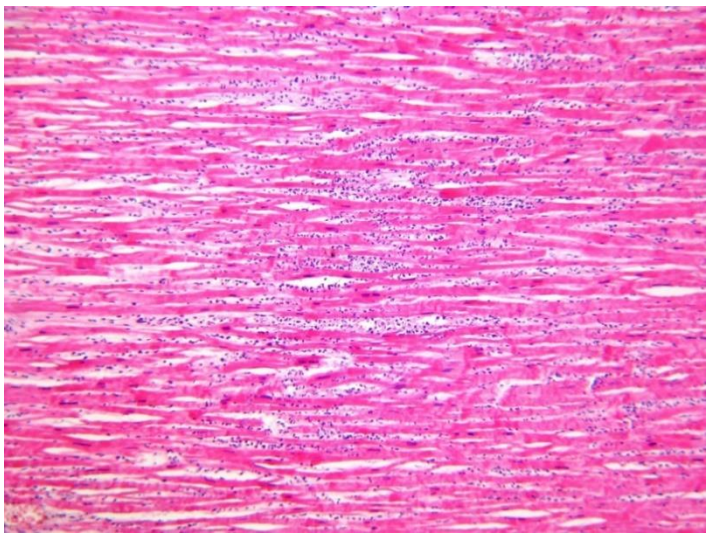

Fig. 3B.4 **Acute myocardial infarction**

Microscopic appearance characterized by neutrophil infiltration, and loss of nuclei in the infarcted myocardium (H&E).

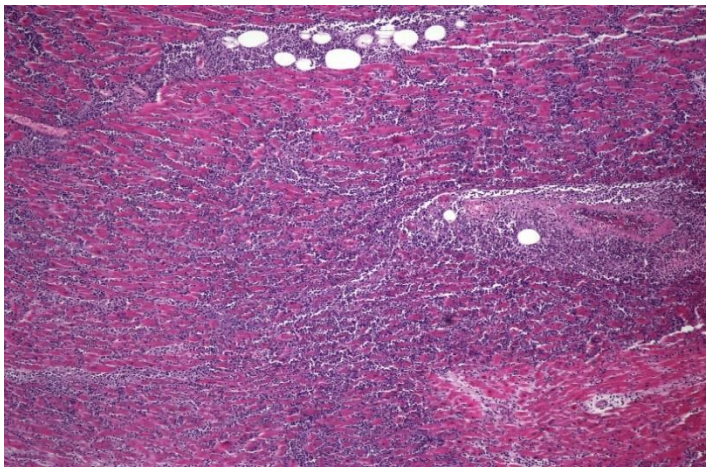

Fig. 3B.5 **Acute myocardial infarction**

Heavy neutrophil infiltration within the infarcted myocardium (H&E).

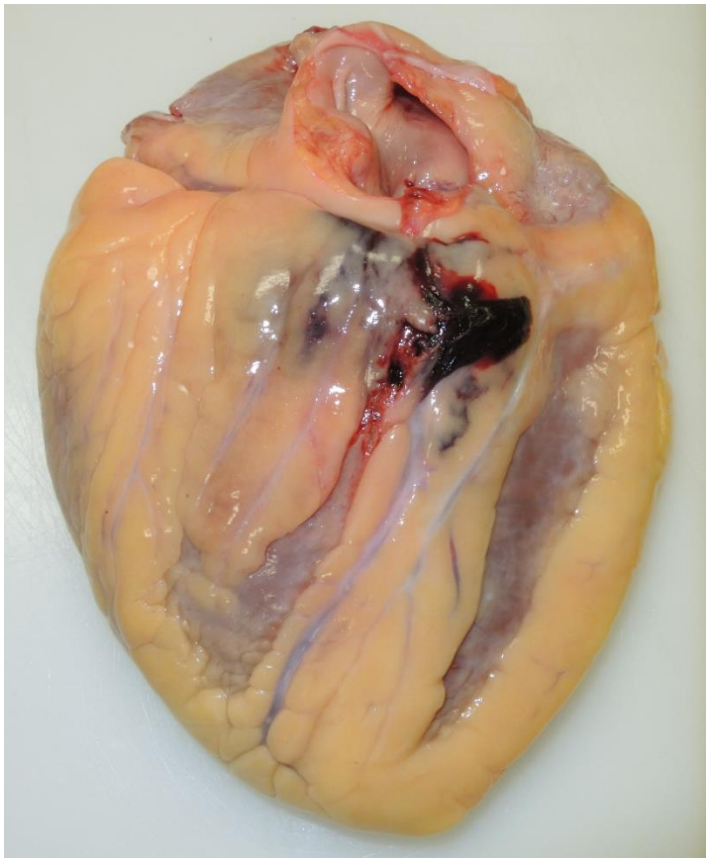

Fig. 3B.6 **Cardiac rupture in acute myocardial infarction**

Area of rupture visible on the posterior surface of the left ventricle.

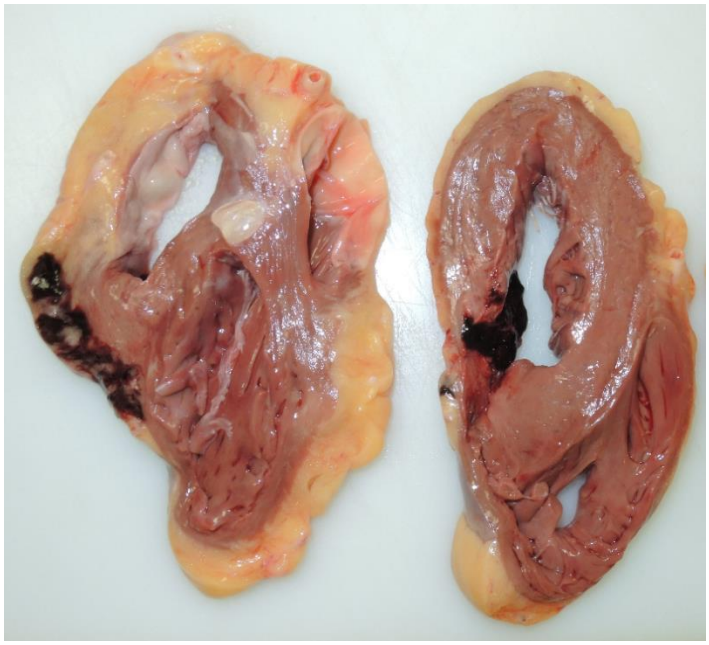

Fig. 3B.7 **Cardiac rupture in acute myocardial infarction**

Transverse section of the left ventricle showing rupture and hemorrhage on the posterior surface of the left ventricle.

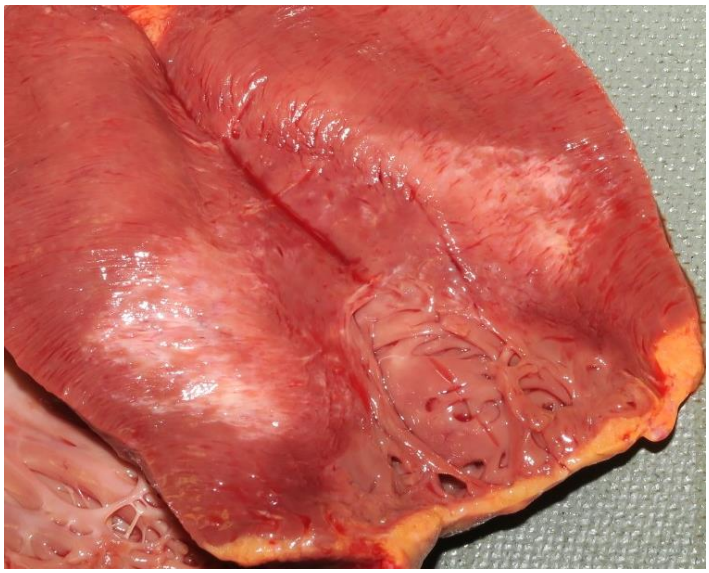

Fig. 3B.8 **Myocardial scar**

Pale, irregular area representing fibrotic scar on the cut surface of the left ventricle.

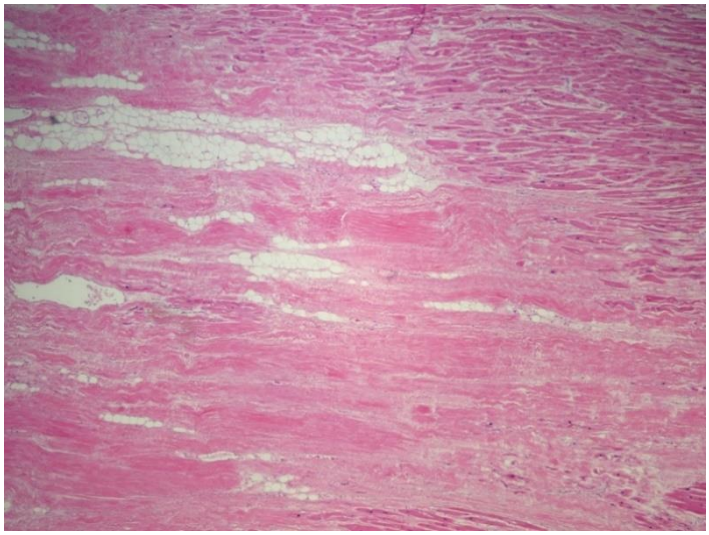

Fig. 3B.9 **Myocardial scar**

Microscopic image of the myocardial scar showing myocardium replaced with fibrotic tissue (H&E).

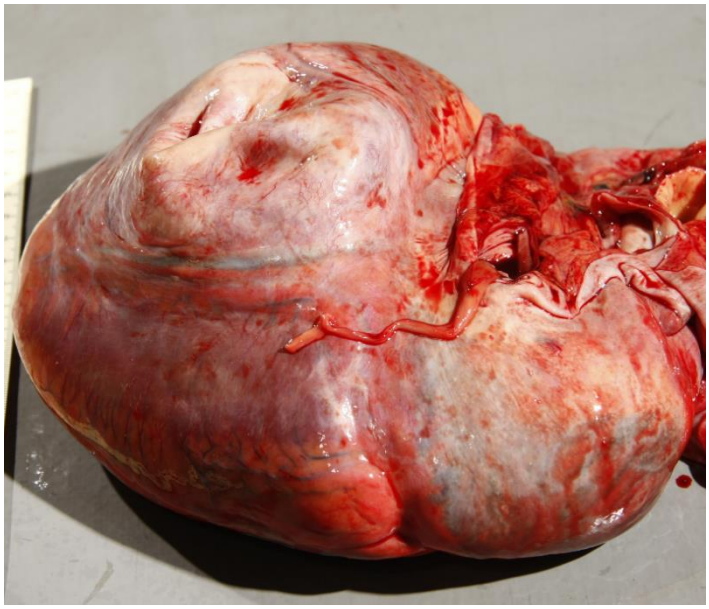

Fig. 3B.10 **Ventricular aneurysm**

Outward bulging of the posterior wall of the left ventricle, at the site of a healed transmural myocardial infarction where the myocardium is pale and fibrotic.

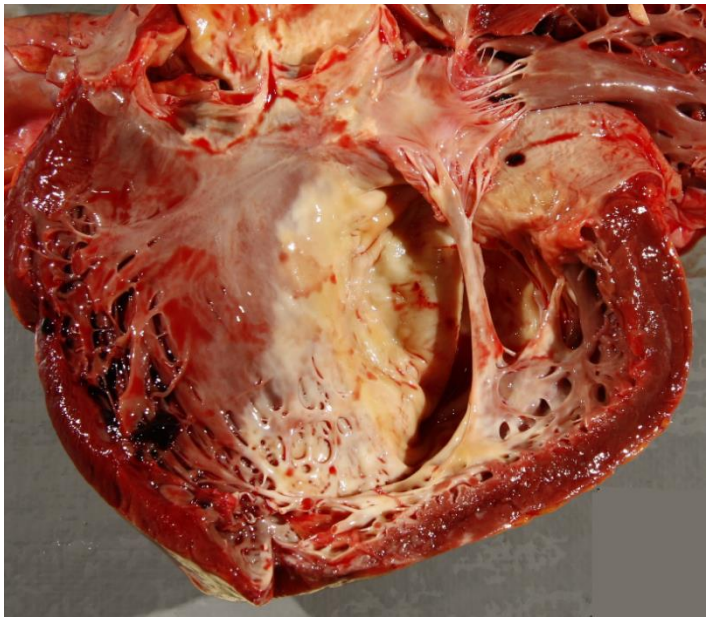

Fig. 3B.11 **Ventricular aneurysm**

Endocardium of the left ventricle showing extensive scarring of the posterior surface and thinning of the ventricle's wall resulting in an aneurysm formation.

Fig. 3C.1 **Ventricular hypertrophy**

Significant thickening of the left ventricular wall demonstrated on the transverse sections of the heart.

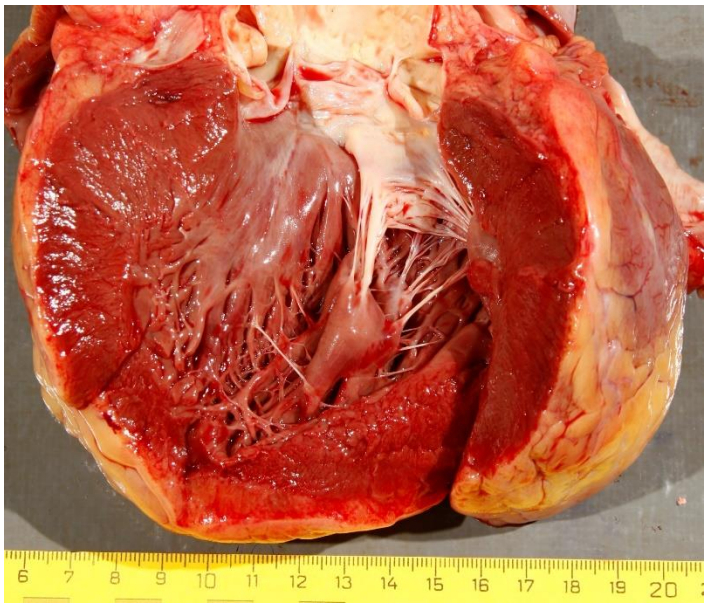

Fig. 3C.2 **Ventricular hypertrophy**

Significant thickening of the left ventricular wall demonstrated on the heart dissected by a blow flow method.

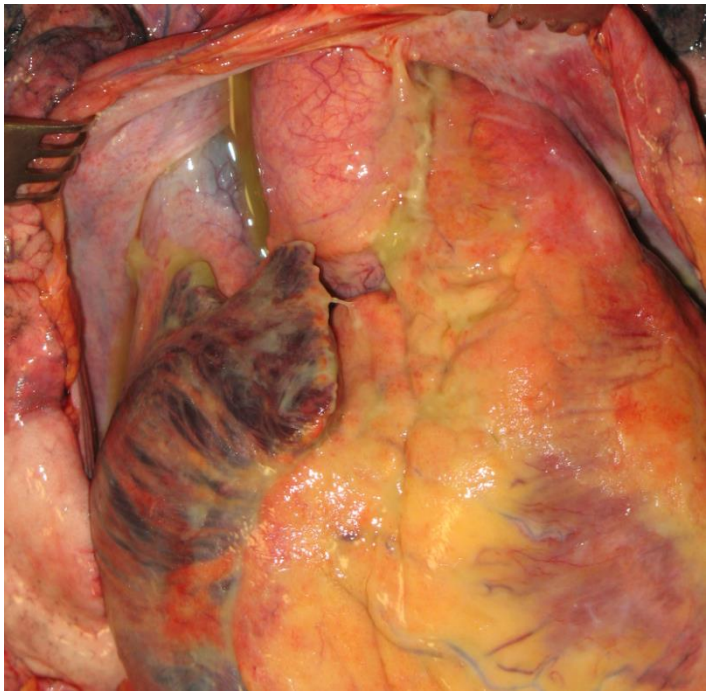

Fig. 3D.1 **Purulent pericarditis**

Accumulation of pus in the pericardial sac around the thoracic aorta.

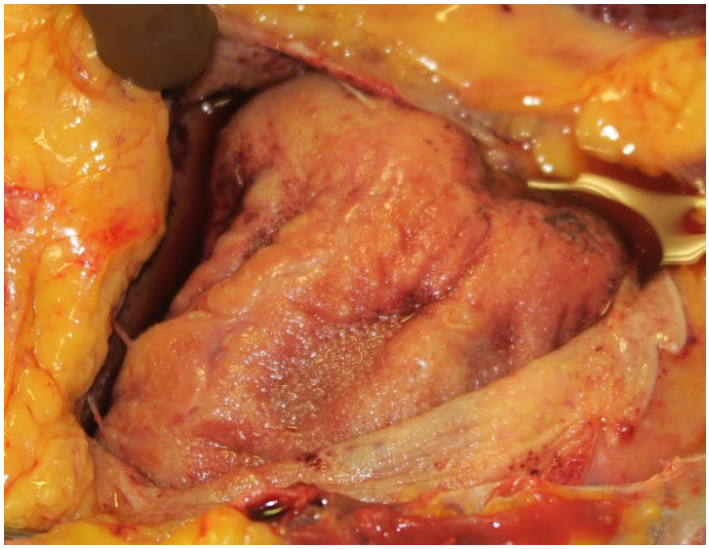

Fig. 3D.2 **Fibrinous pericarditis**

Clear serous exudate is present in the pericardial sac; epicardium is covered with fibrin strands, and there are focal adhesions between pericardial surfaces.

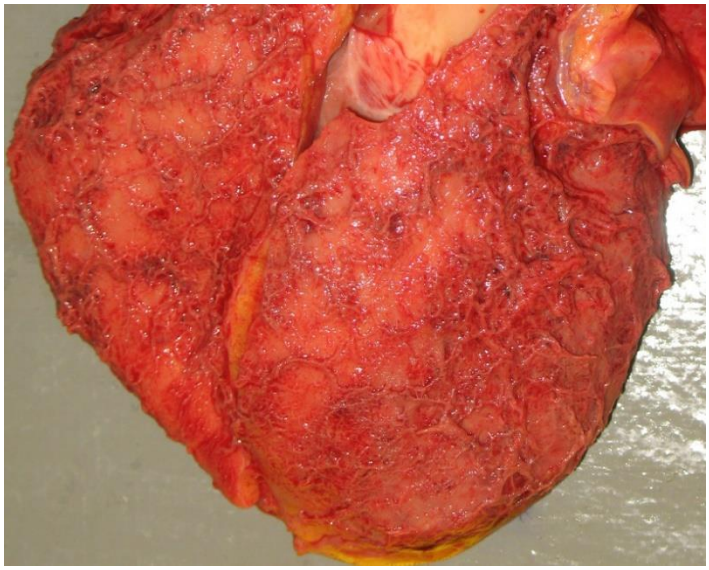

Fig. 3D.3 **Fibrinous pericarditis**

Inflamed pericardium is erythematous and granular due to the presence of fibrin strands. This gross appearance is referred to as ''bread and butter'', because it resembles two pieces of buttered bread pressed together then pulled apart.

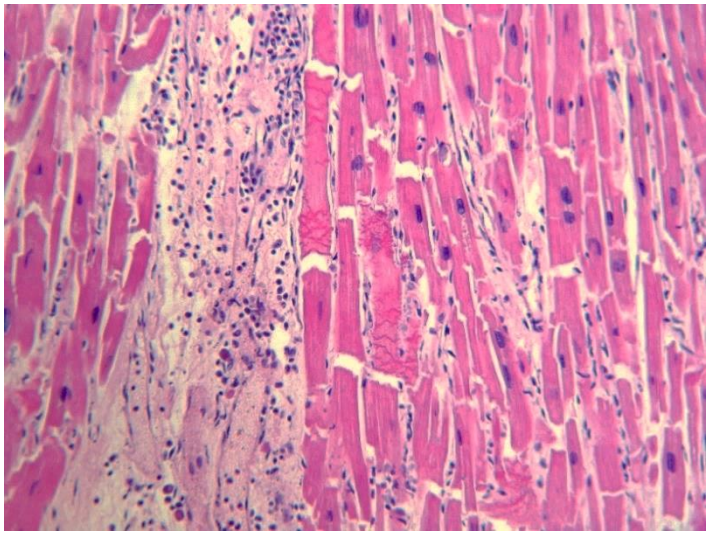

Fig. 3D.4 **Myocarditis**

Microscopic image characterized by the presence of inflammatory infiltrates with associated myocyte necrosis (H&E).

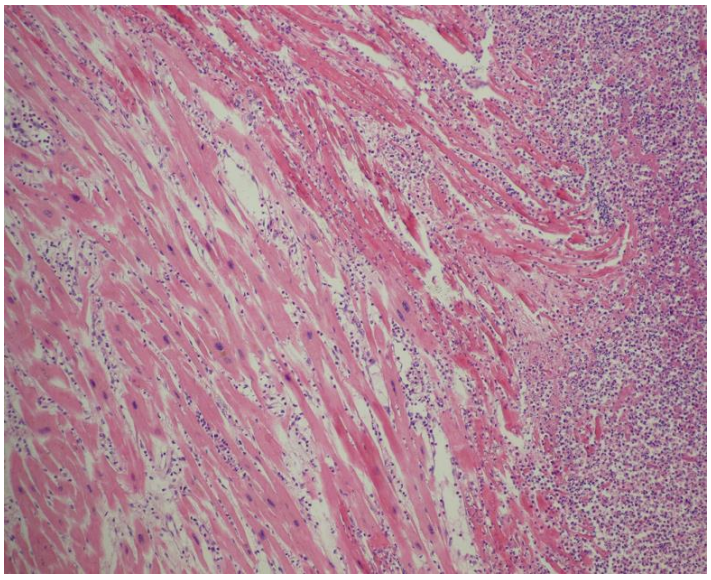

Fig. 3D.5 **Myocarditis**

Severe myocarditis with extensive neutrophil infiltration (H&E).

Fig. 3E.1 **Arrhythmogenic ventricular cardiomyopathy**

The sections of the right ventricle demonstrating almost complete replacement of myocardium with fat.

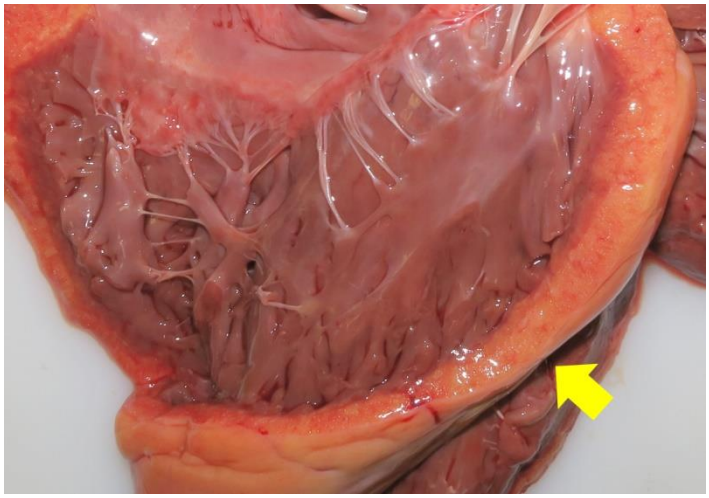

Fig. 3E.2 **Arrhythmogenic ventricular cardiomyopathy**

Opened right ventricle showing almost complete replacement of myocardium with fat (arrow).

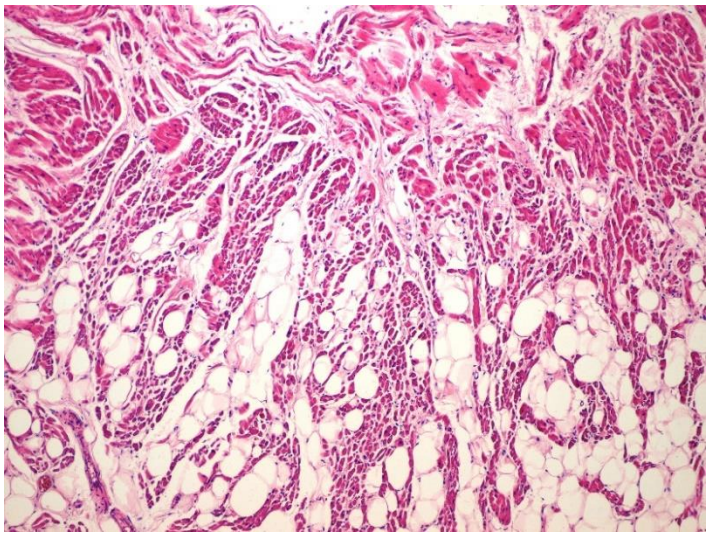

Fig. 3E.3 **Arrhythmogenic ventricular cardiomyopathy**

Microscopic image characterized by fibrofatty replacement of the right ventricular myocardium (H&E).

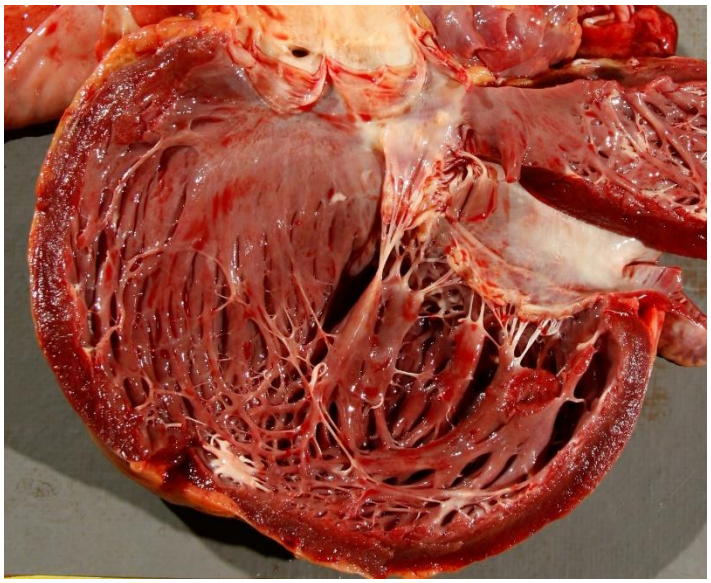

Fig. 3E.4 **Dilated cardiomyopathy**

The heart is of globular shape with a pronounced dilation of the left ventricular chamber and thinning of the myocardium.

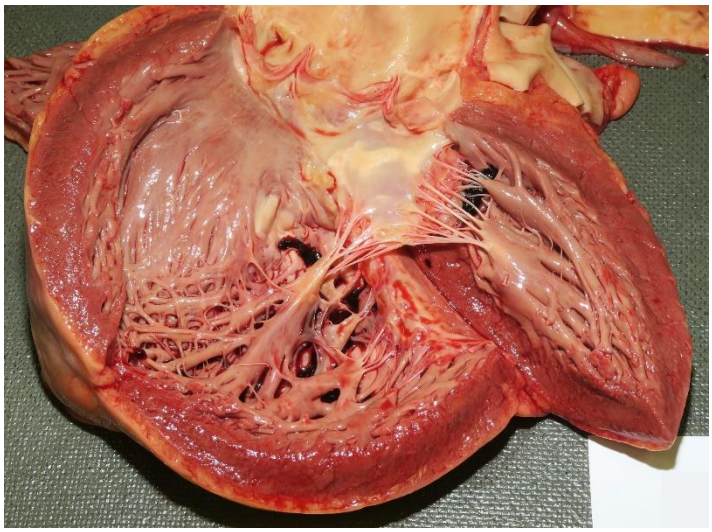

Fig. 3E.5 **Dilated cardiomyopathy**

Another example of the heart of a globular shape and visible dilation of the left ventricular chamber.

Fig. 3F.1 **Cardiac tamponade**

Blood beneath the visceral pericardium creates a characteristic bluish appearance (blue dome sign).

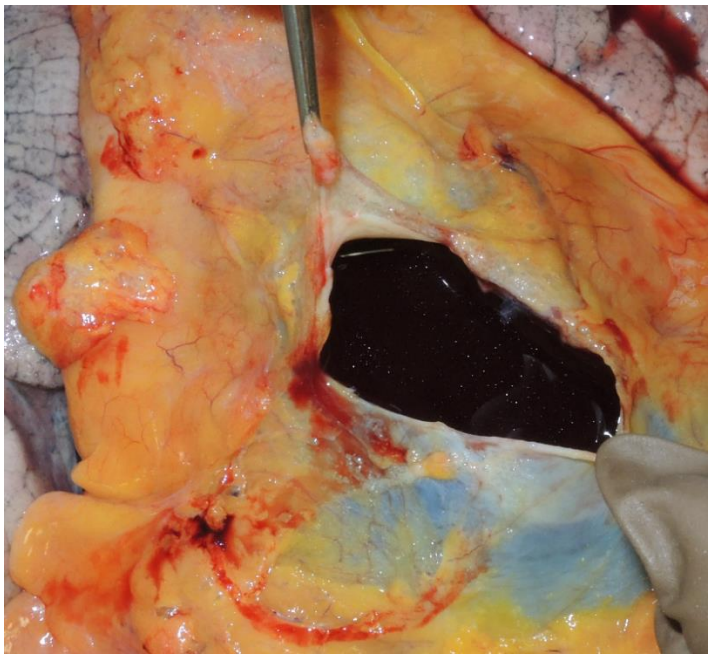

Fig. 3F.2 **Cardiac tamponade**

Opened pericardial sac showing accumulation of blood within.

Fig. 3G.1 **Cardiac laceration**

Laceration with associated superior subpericardial hemorrhage on the posterior surface of the left ventricle.

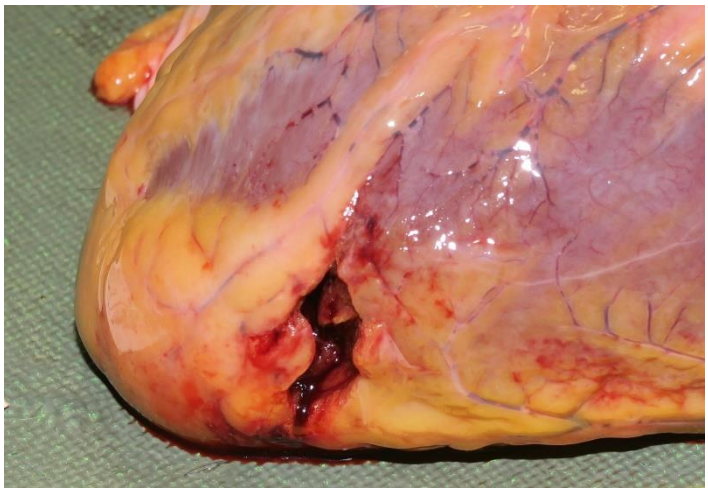

Fig. 3G.2 **Cardiac laceration**

Deep laceration at the apex of the heart.

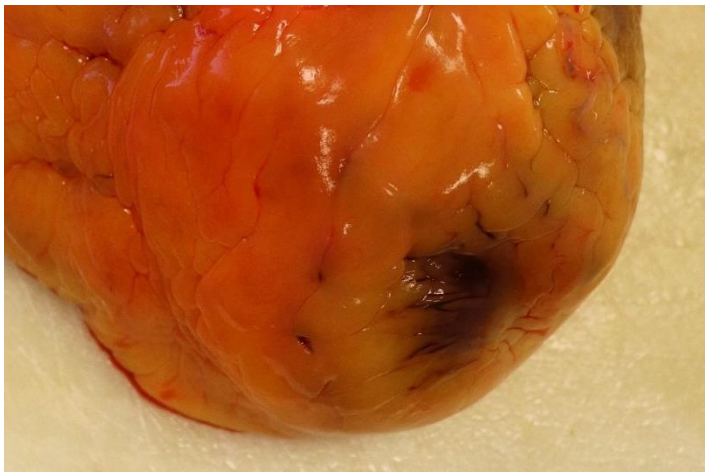

Fig. 3G.3 **Cardiac contusion**

Focal hemorrhage at the apex of the heart.

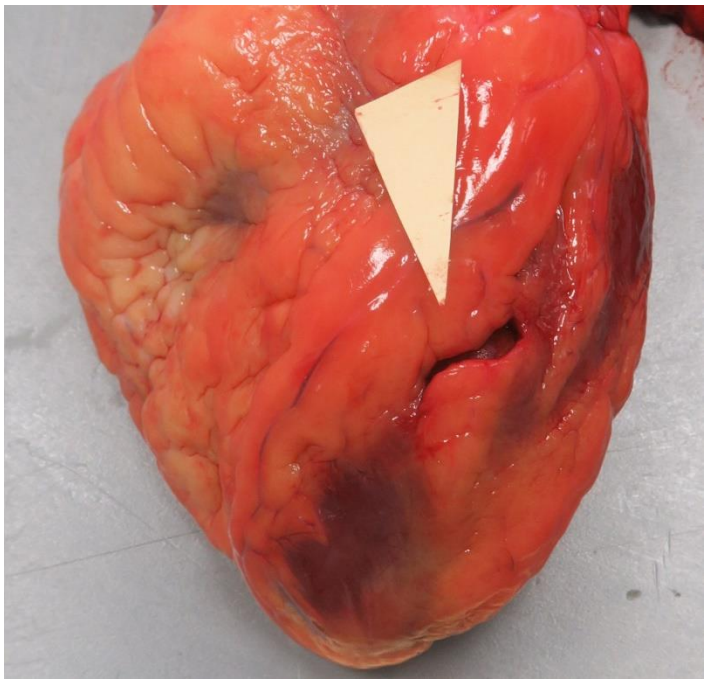

Fig. 3G.4 **Stab wound of the heart**

Stab wound at the anterior surface of the heart (arrow).

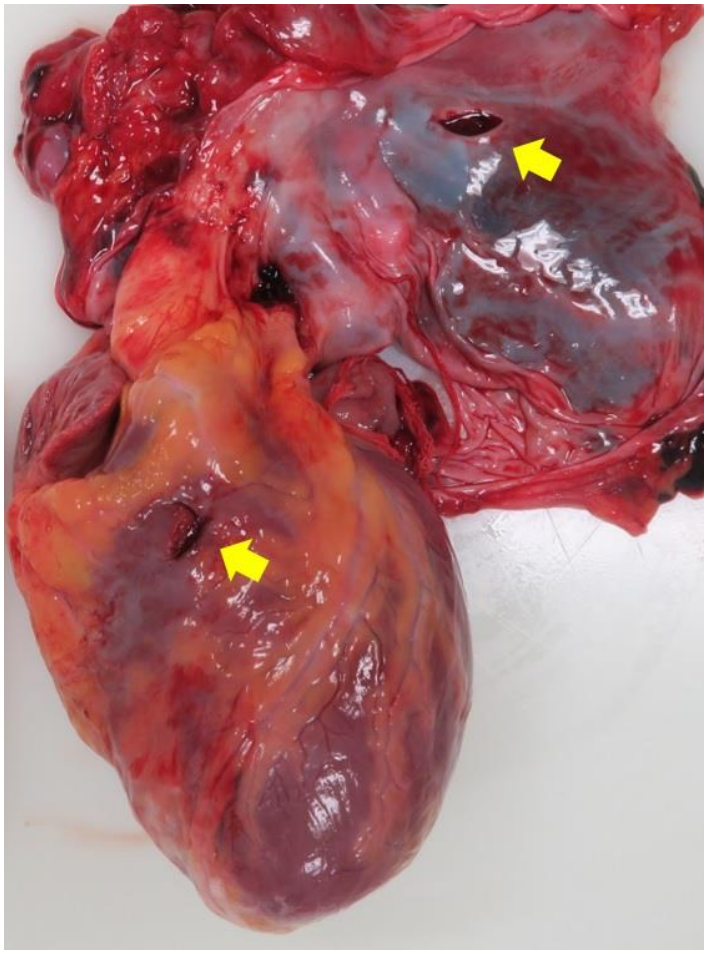

Fig. 3G.5 **Stab wound of the heart**

Heart with a layer of visceral pericardium attached to it. The upper arrow points to the stab wound in the pericardium; lower arrow points to the stab wound at the anterior surface of the heart.

4 Respiratory System

4A | Vascular diseases

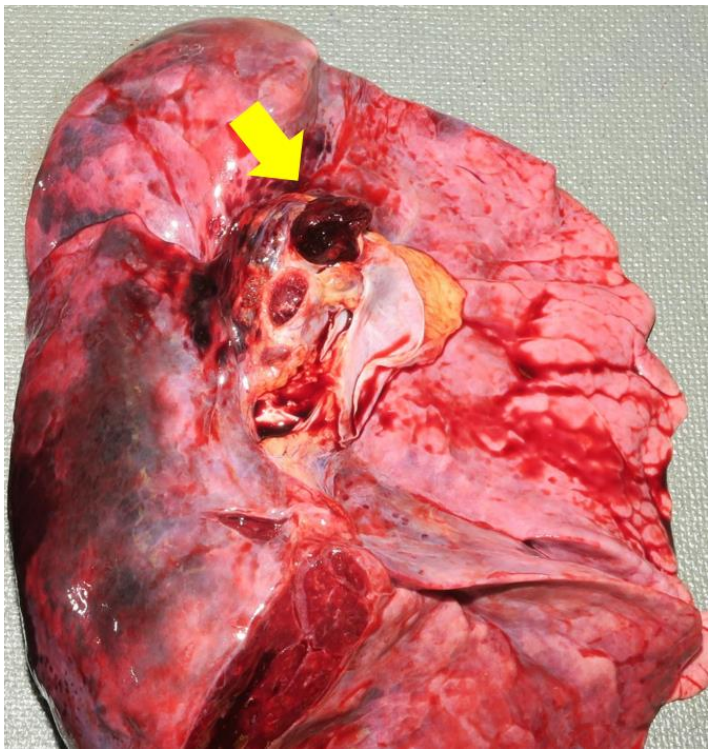

Fig. 4A.1 **Pulmonary thromboembolism**

Solid mass obturating the lumen of the left pulmonary artery.

Fig. 4A.2 **Pulmonary thromboembolism**

Close-up view on solid mass within the left pulmonary artery.

Fig. 4A.3 **Thrombus vs. postmortem coagulum**

Thrombus (left) has a granular matte surface that shows layering of the blood and fibrin (lines of Zahn). It attaches to the vessel wall and can organize over time. Postmortem clots (right) are gelatinous, have a smooth and shiny surface without a laminated structure, and are readily removed.

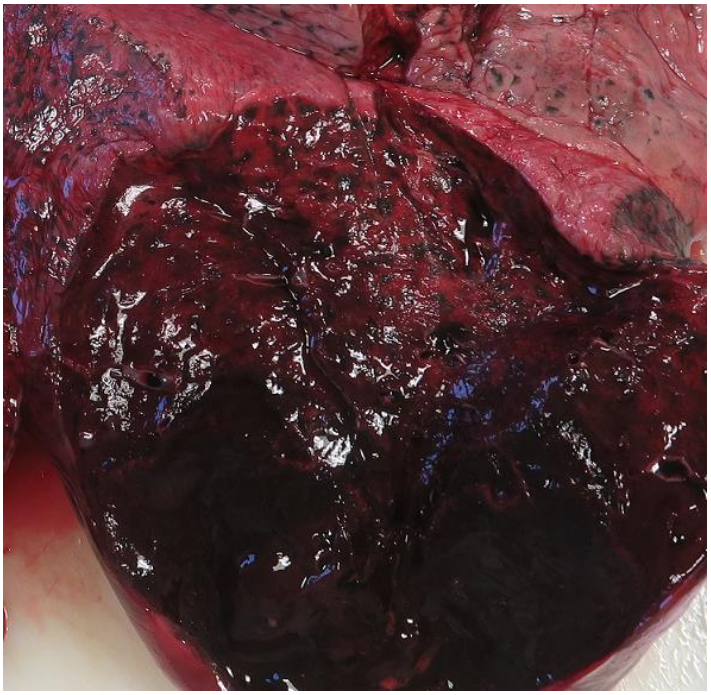

Fig. 4A.4 **Pulmonary infarction**

Pulmonary infarction as a result of pulmonary thromboembolism. It appears as a wedge-shaped, dark red area located on the periphery.

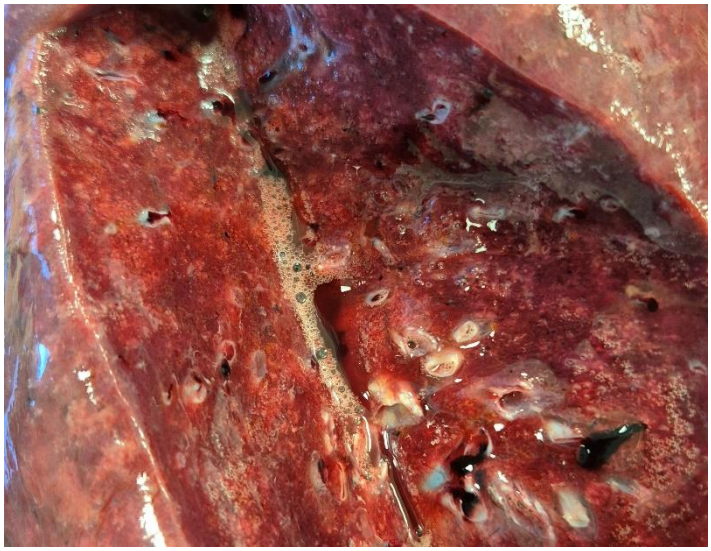

Fig. 4B.1 **Lung edema**

Cut surface of the lung showing frothy fluid oozing from the alveolar spaces.

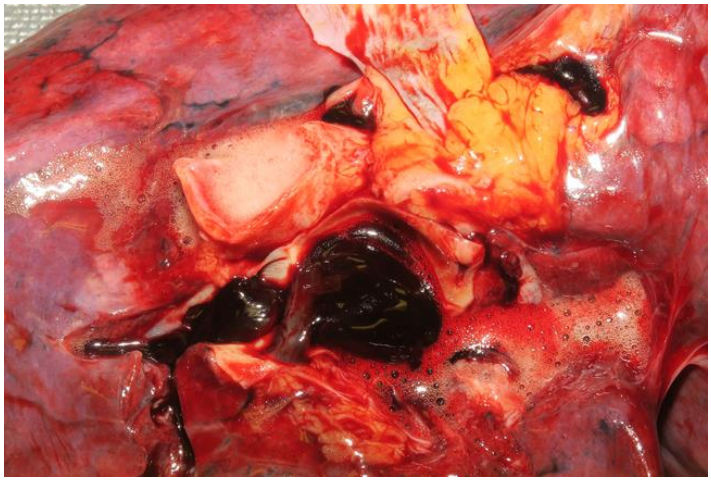

Fig. 4B.2 **Lung edema**

Frothy fluid oozing from the bronchi at the lung hilum.

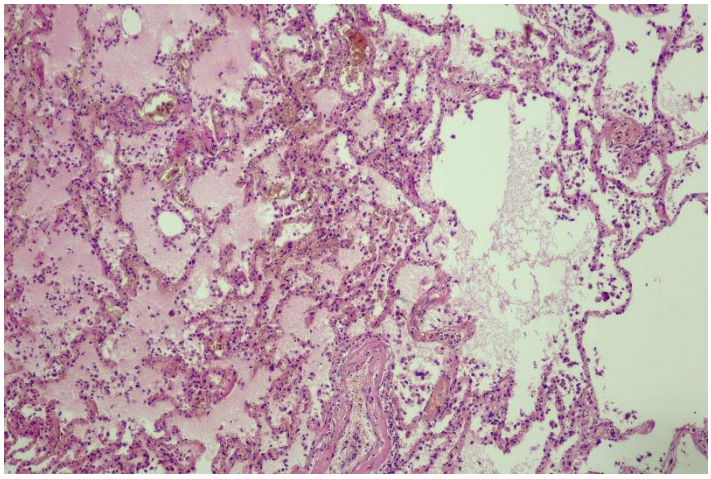

Fig. 4B.3 **Lung edema**

Alveoli filled with eosinophilic amorphous fluid (H&E).

Fig. 4C.1 **Bacterial pneumonia**

The cut surface of the affected lung tissue is dark red, firm and airless. Consistency of the lung is comparable to the liver tissue (red hepatization).

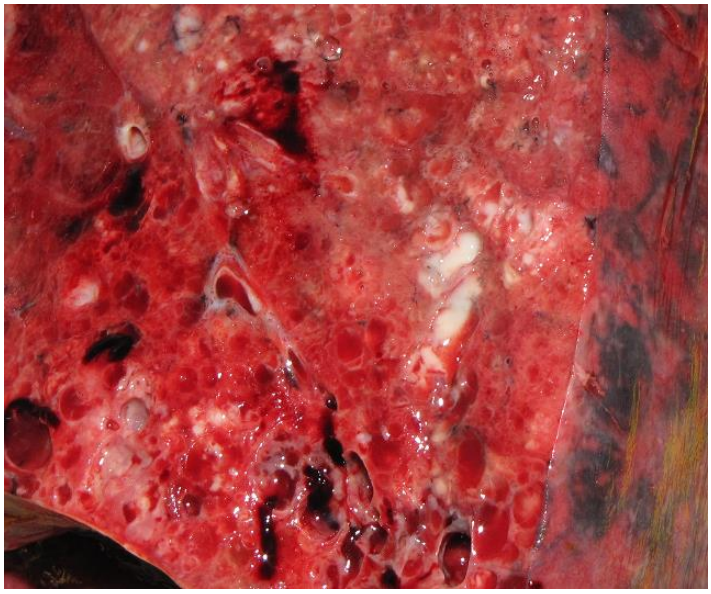

Fig. 4C.2 **Bacterial pneumonia**

Purulent exudate is expressed from the bronchi on the cut surface of lung.

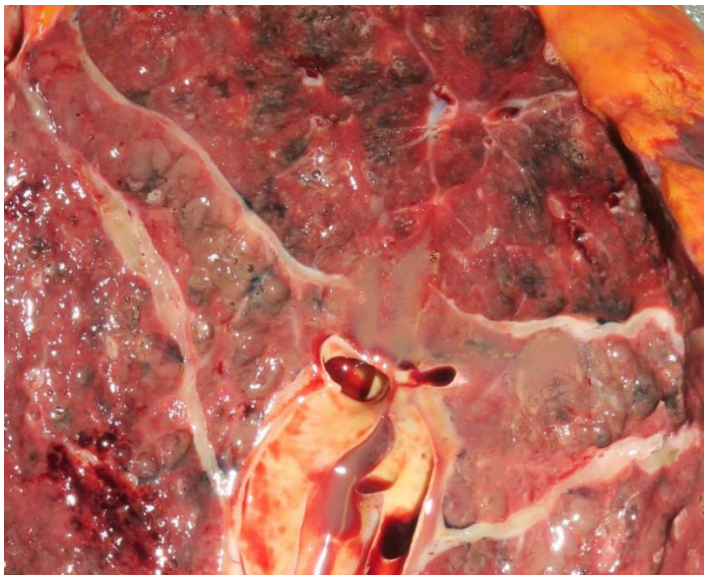

Fig. 4C.3 **Bacterial pneumonia**

Following red hepatization affected lung tissue appears gray/grayish brown on the cut surface due to fibrinopurulent exudate, and it resumes liver-like consistency (gray hepatization).

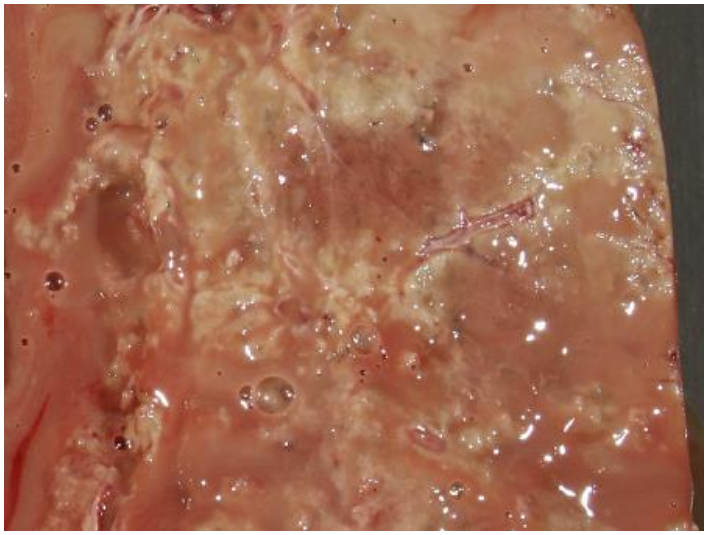

Fig. 4C.4 **Bacterial pneumonia**

Sever alar pneumonia in the stage of gray hepatization.

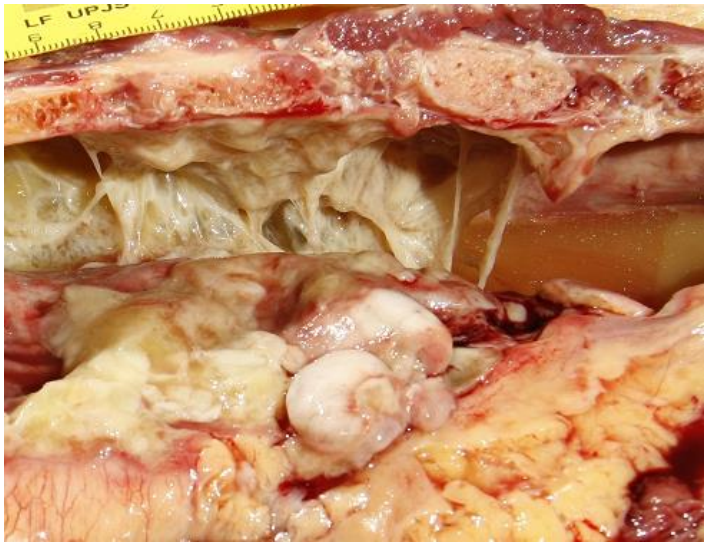

Fig. 4C.5 **Bacterial pneumonia**

Pleural serofibrinous exudate and adhesions associated with alar pneumonia.

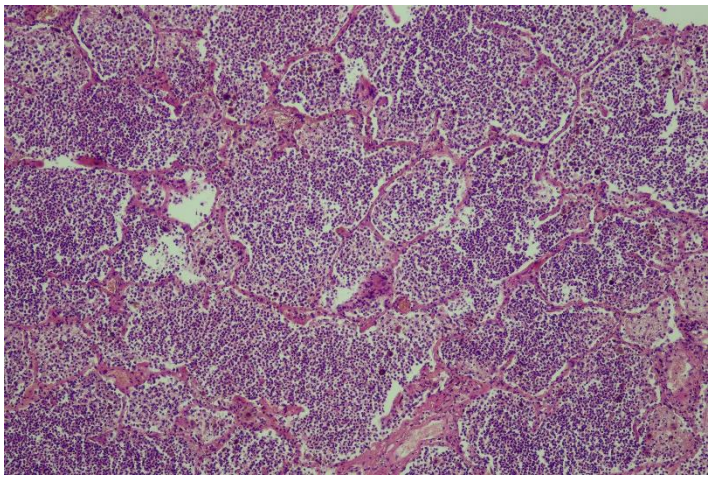

Fig. 4C.6 **Bacterial pneumonia**

Microscopic appearance of bacterial pneumonia showing dense infiltration by neutrophils mixed with fibrin nets (H&E).

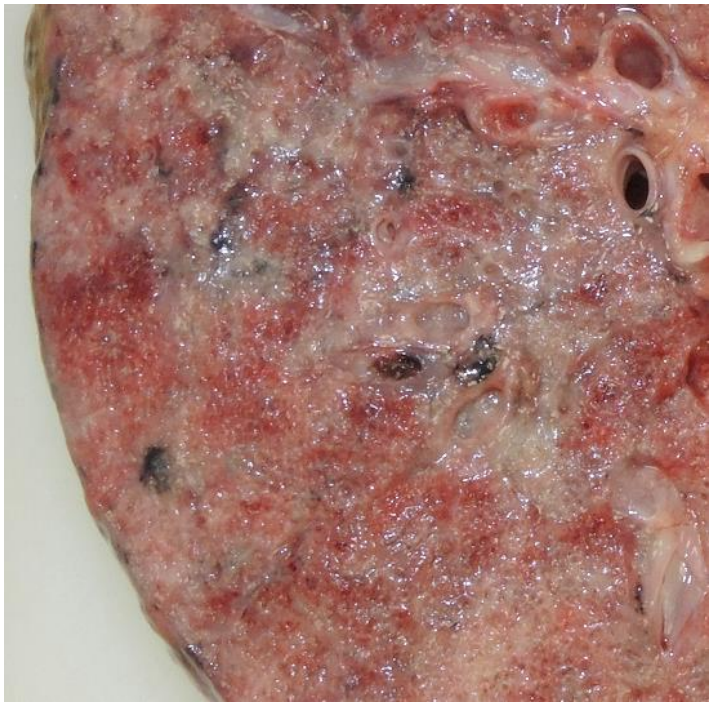

Fig. 4C.7 **Interstitial pneumonia**

The cut surface of the lung showing consolidation changes.

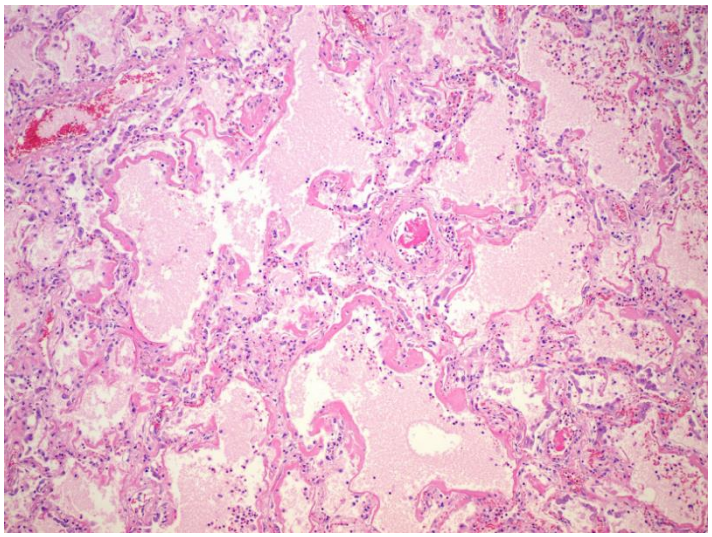

Fig. 4C.8 **Interstitial pneumonia**

Diffuse alveolar damage characterized by the presence of hyaline membranes along alveolar walls (H&E).

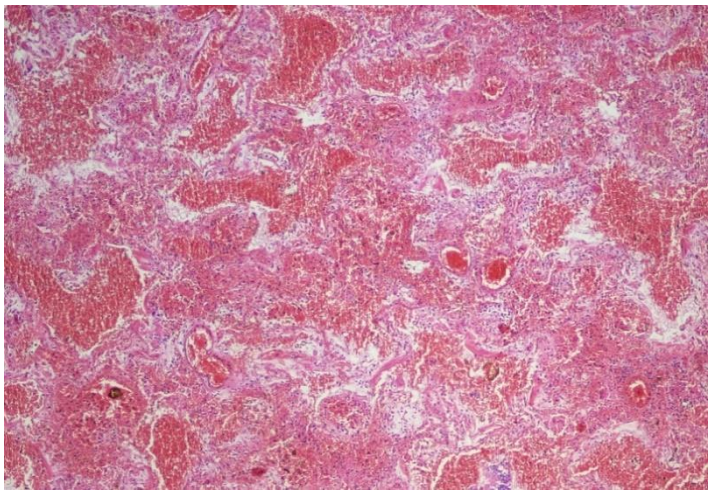

Fig. 4C.9 **Interstitial pneumonia**

Diffuse alveolar hemorrhage characterized by alveoli filled with extravasated erythrocytes (H&E).

Fig. 4C.10 **Tuberculosis**

The cut surface of the lung showing irregularly sized rounded firm tan nodules – granulomas (tuberculomas).

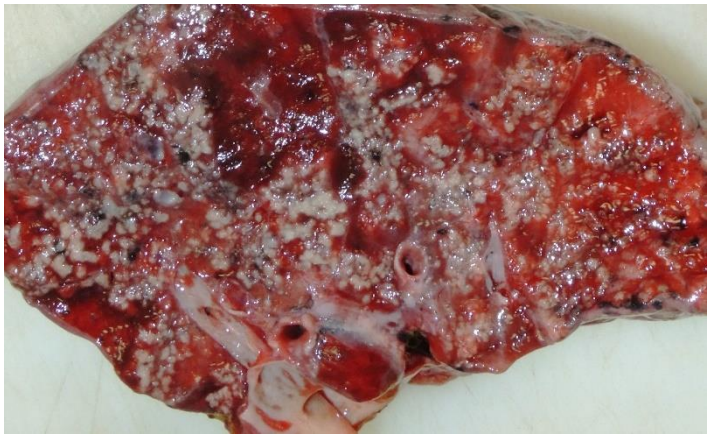

Fig. 4C.11 **Miliary tuberculosis**

The cut surface of the lung showing numerous small nodules.

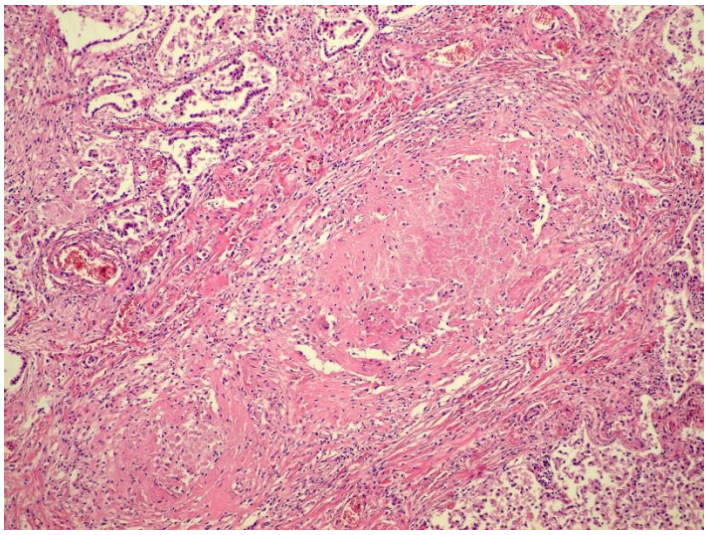

Fig. 4C.12 **Tuberculosis**

Microscopic image of the lung in tuberculosis showing necrotizing granuloma (H&E).

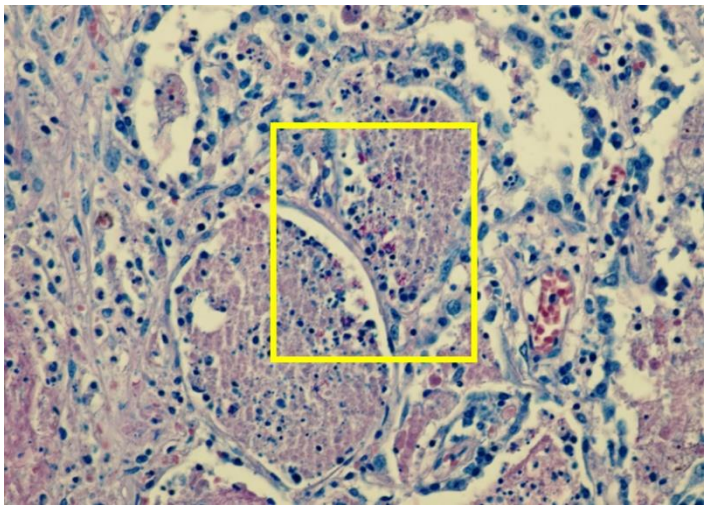

Fig. 4C.13 **Tuberculosis**

Rod-shaped bacilli of dark pink color—Mycobacterium tuberculosis (Ziehl-Neelsen staining).

Fig. 4D.1 **Primary lung cancer**

Adenocarcinoma arising from the right bronchus as a solitary yellow-white firm lesion.

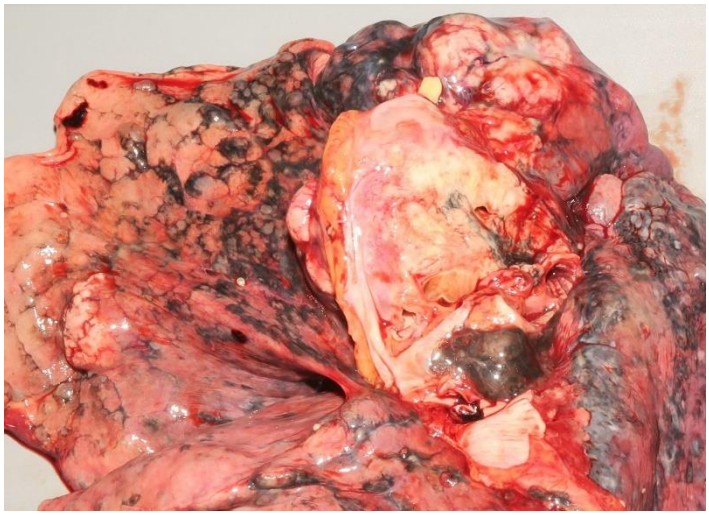

Fig. 4D.2 **Primary lung cancer**

A yellow-white form lesion arising from the bronchus at the hilum of the left lung.

Fig. 4D.3 **Lung metastases**

Multiple irregular white masses of different sizes on both lungs.

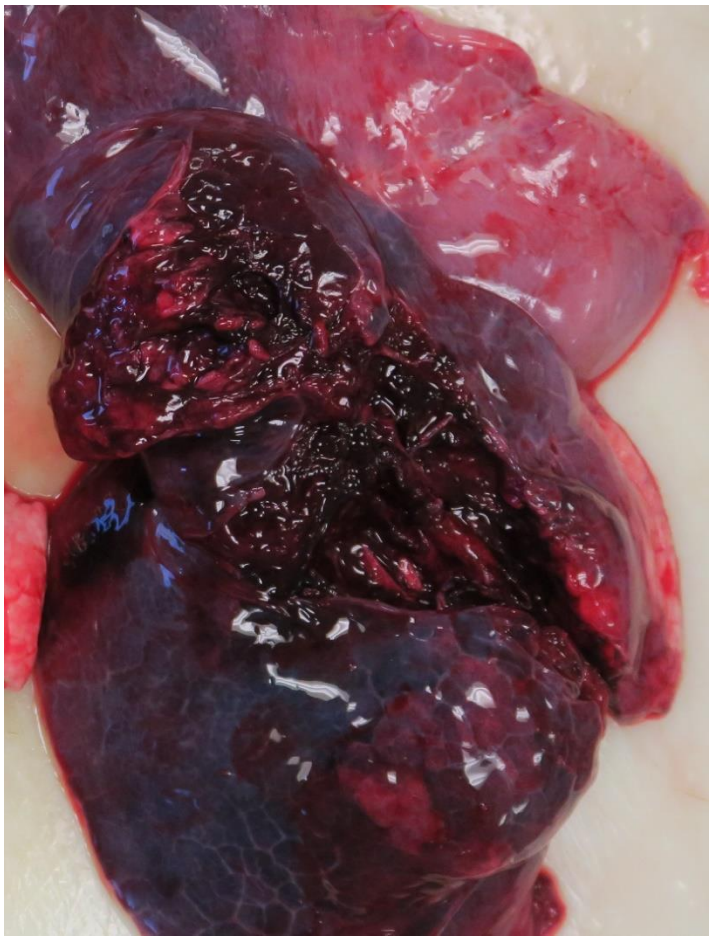

Fig. 4E.1 **Lung laceration**

Extensive laceration of the left lung affecting both lobes.

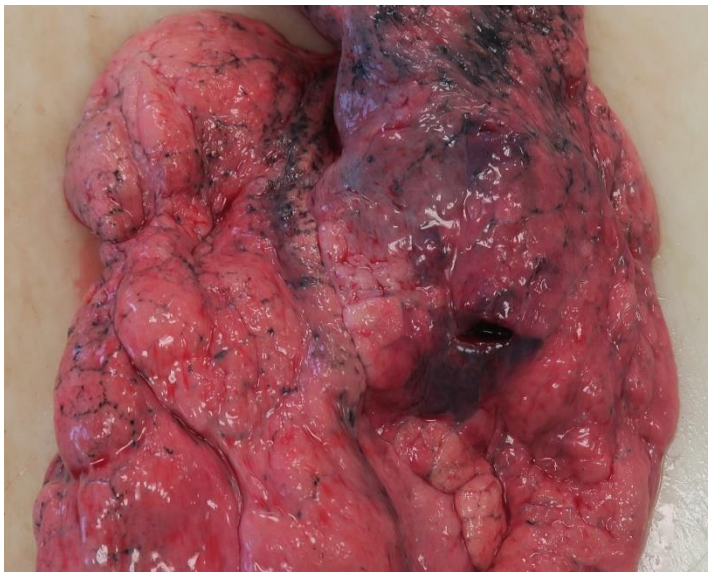

Fig. 4E.2 **Stab wound of the lung**

Stab wound of the upper lobe of the left lung.

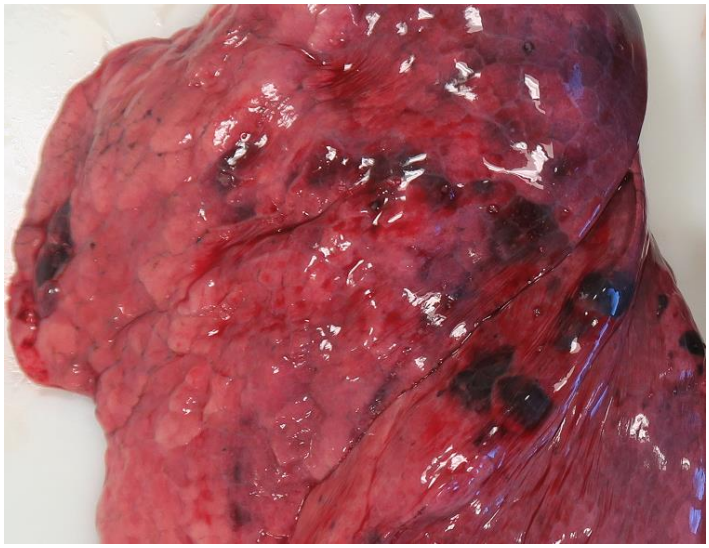

Fig. 4E.3 **Pulmonary contusion**

Foci of hemorrhages on the costal surfaces of both lobes of the left lung.

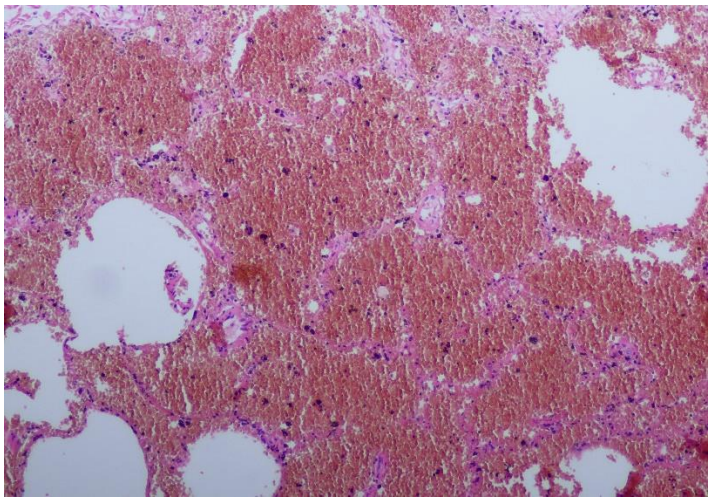

Fig. 4E.4 **Pulmonary contusion**

Parenchymal hemorrhage affecting both interstitium and alveoli (H&E).

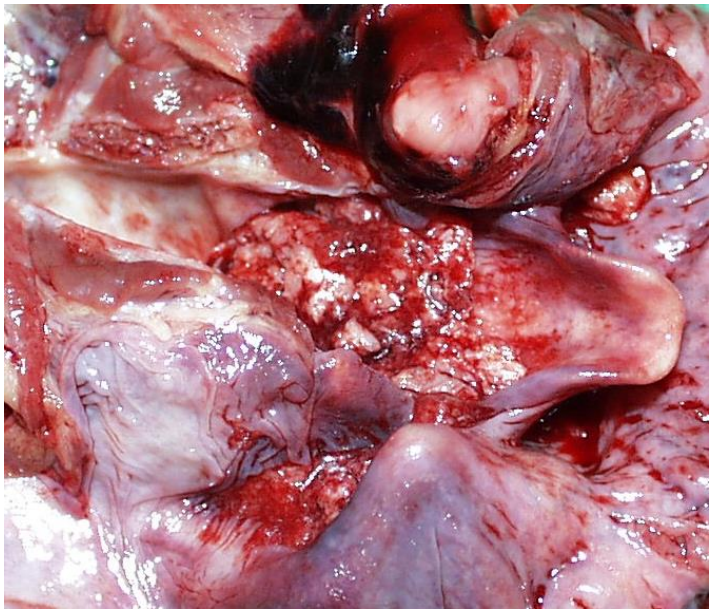

Fig. 4F.1 **Choking – bolus death**

Fragment of under-chewed food lodged in the glottis completely obstructing the airways.

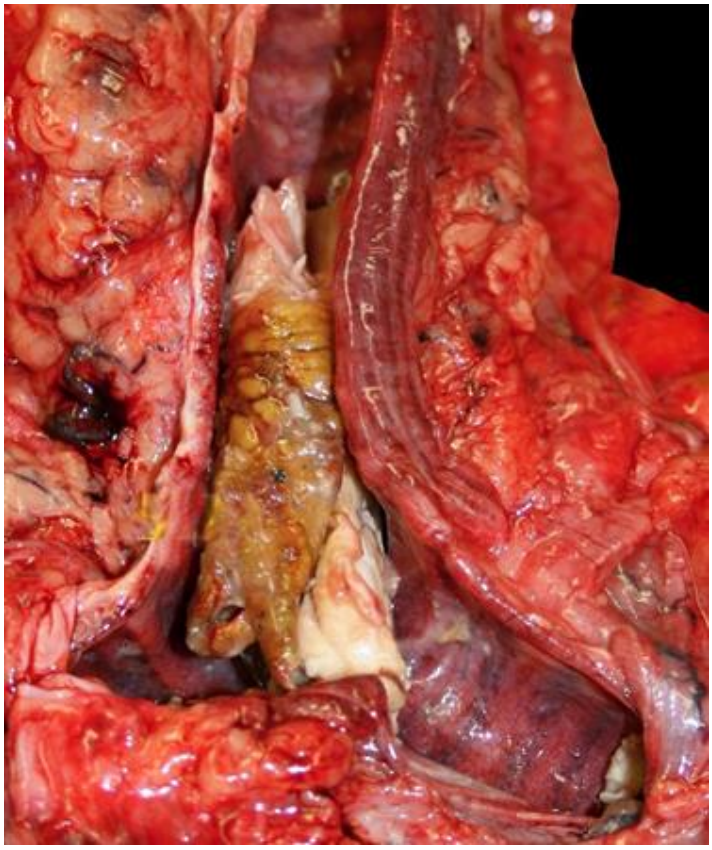

Fig. 4F.2 **Choking**

Obstruction of trachea and main bronchi by a fragment of food.

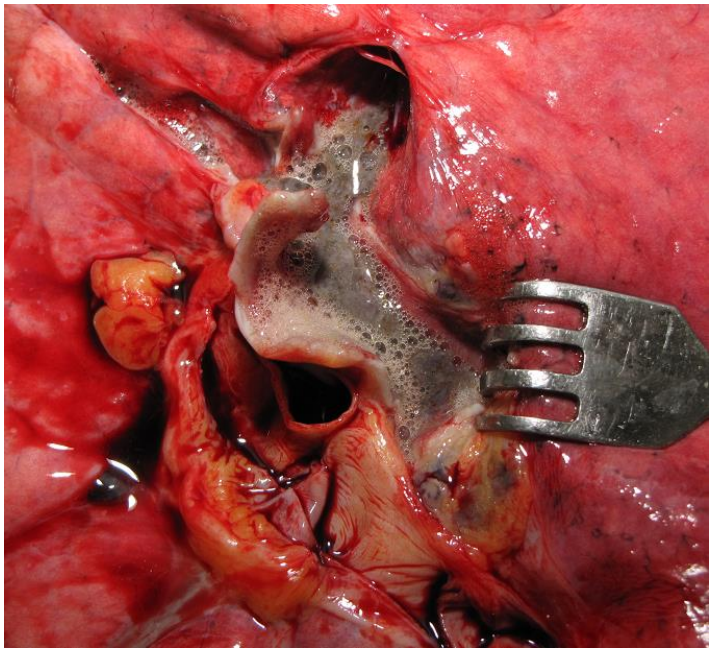

Fig. 4F.3 **Aspiration**

Close-up view of the lung hilum showing greyish, frothy liquid oozing from the bronchi in a case of aspiration of vomit.

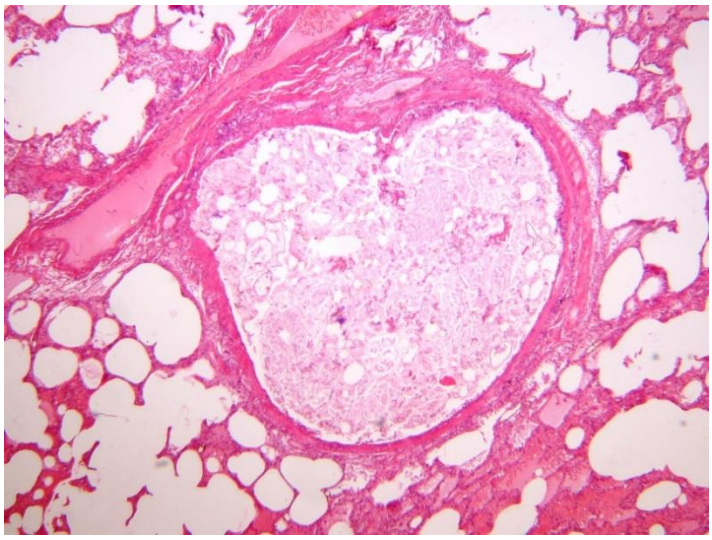

Fig. 4F.4 **Aspiration**

Microscopic image of the lung tissue showing gastric content in a bronchiole (H&E).

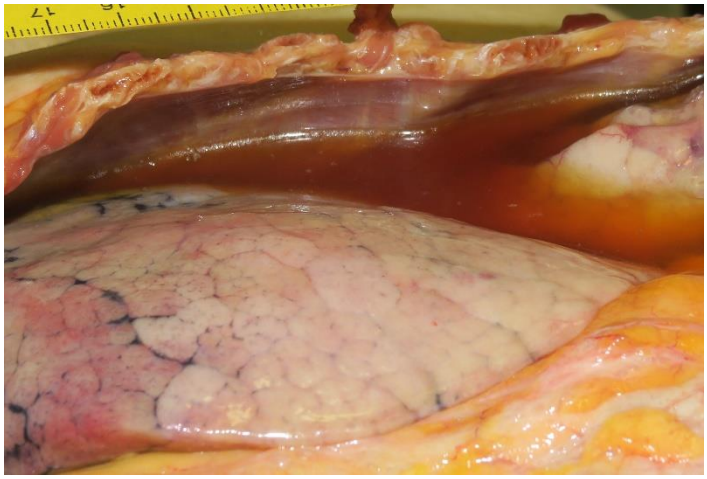

Fig. 4G.1 **Hydrothorax**

Serous liquid of yellow-brown color within the left thoracic cavity.

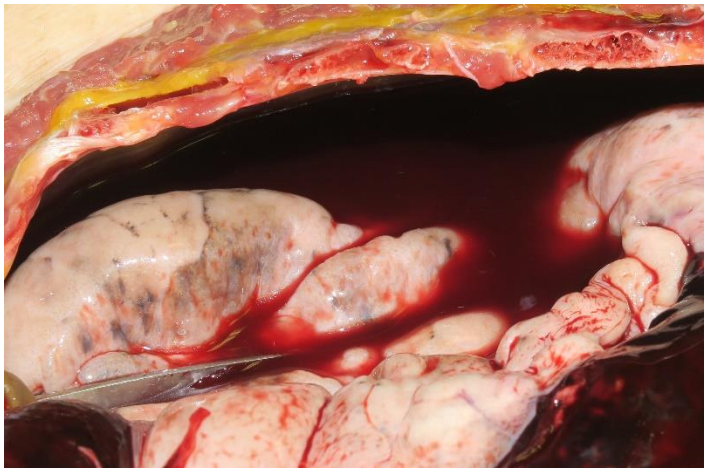

Fig. 4G.2 **Hemothorax**

Liquid blood within the right thoracic cavity.

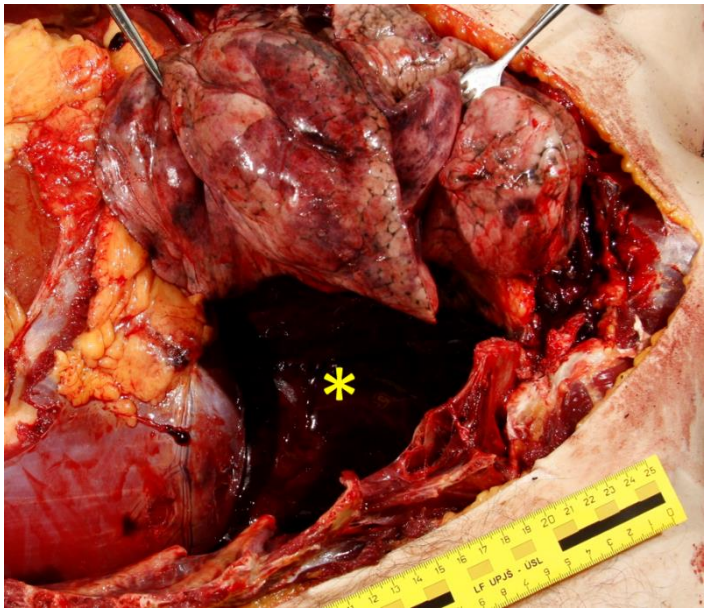

Fig. 4G.3 **Hemothorax**

The left lung is lifted off of the thoracic cavity to expose the blood within it (asterisk).

5 Digestive System

5A | Lithiasis

Fig. 5A.1 **Cholecystolithiasis**

Multiple square-shaped stones
of different sizes filling the gallbladder.

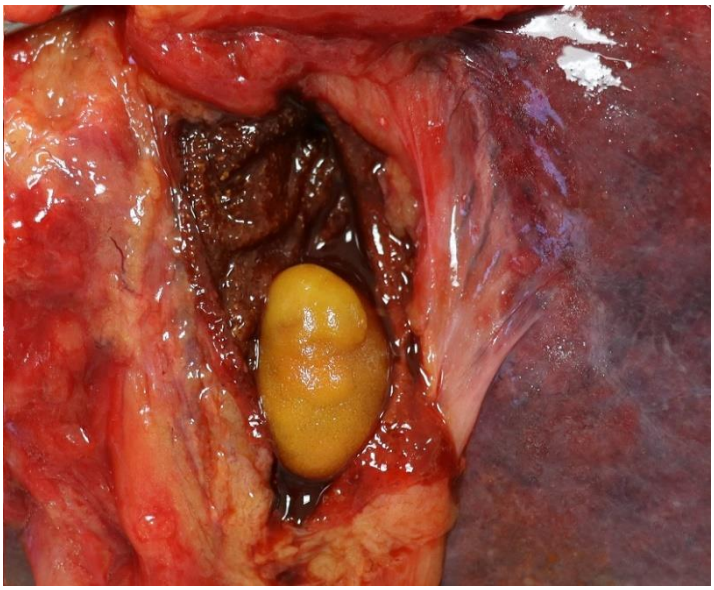

Fig. 5A.2 **Cholecystolithiasis**

Large oval-shaped stone present
at the base (fundus) of the gallbladder.

Fig. 5B.1 **Esophageal varices**

Dilated veins in the submucosa of the lower part of the esophagus.

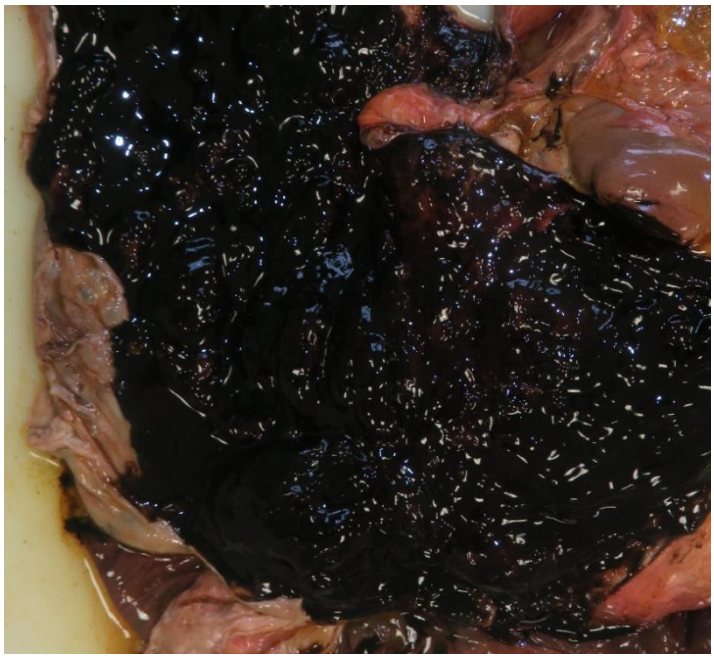

Fig. 5B.2 **Esophageal varices**

Blood in the stomach from ruptured esophageal varices.

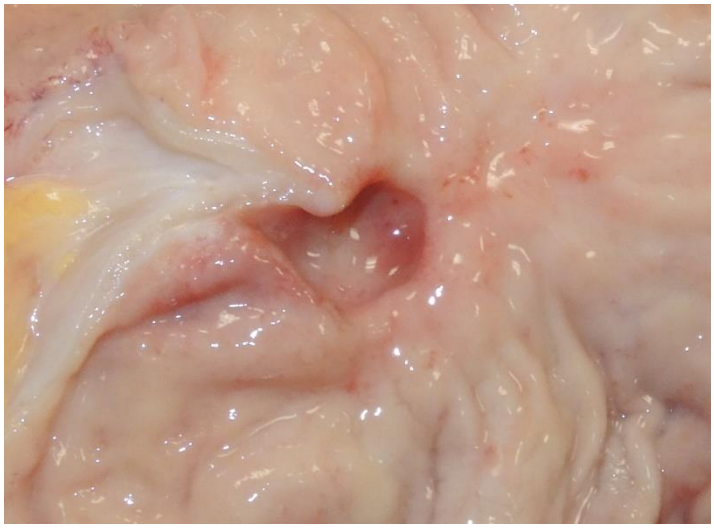

Fig. 5C.1 **Gastric ulcer**

Chronic ulcer in the gastric mucosa is typically round/oval shaped, deep, with slightly elevated (overhanging) margins.

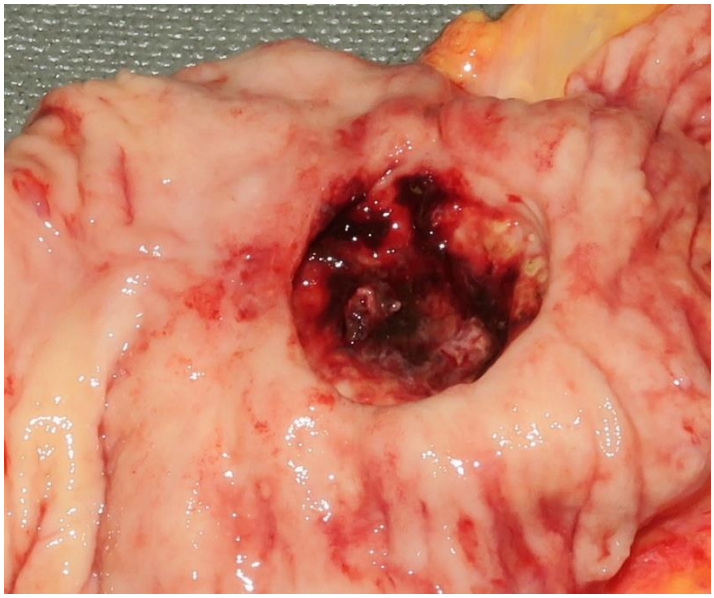

Fig. 5C.2 **Duodenal ulcer**

Duodenal ulcer with hemorrhage from eroded vessels at the ulcer base.

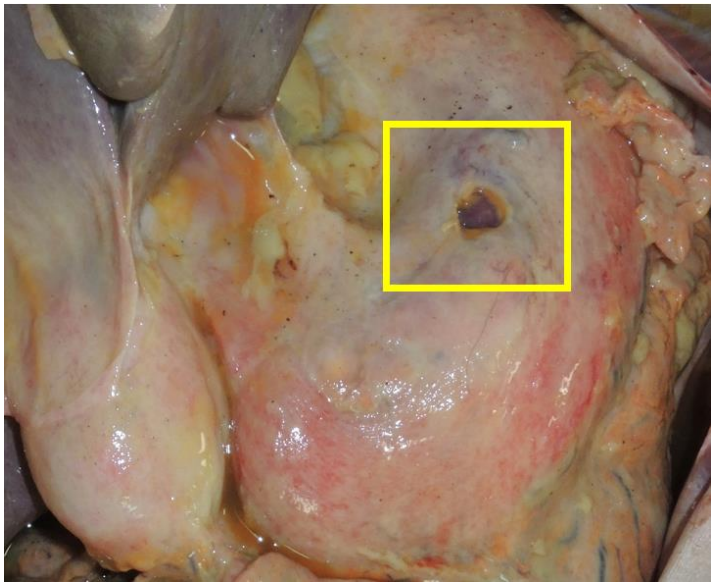

Fig. 5C.3 **Perforated gastric ulcer**

Stomach in situ with a marked defect in the wall.

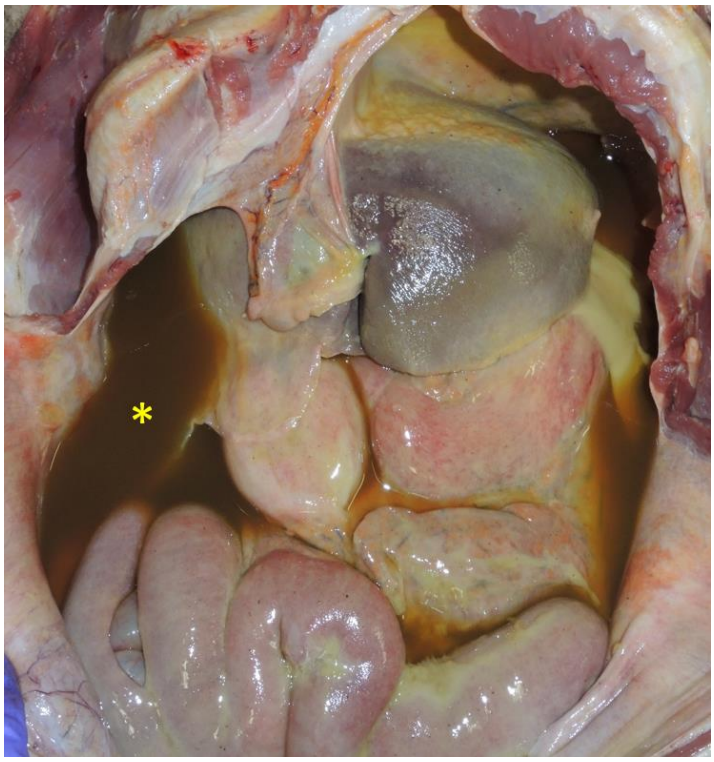

Fig. 5C.4 **Perforated gastric ulcer**

Gastric content in the abdominal cavity (asterisk).

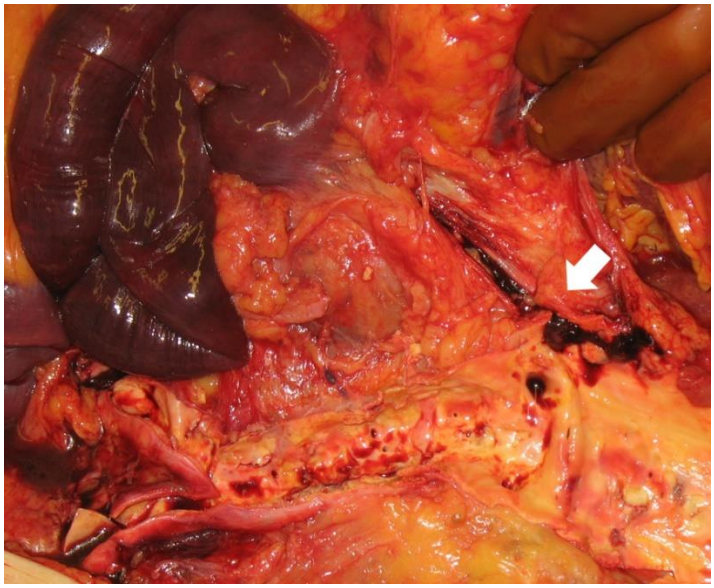

Fig. 5D.1 **Mesenteric infarction**

Thrombosis of the superior mesenteric artery (white arrow), resulting in a mesenteric infarction.

Fig. 5D.2 **Mesenteric infarction**

Infarction (necrosis) of the small intestine characterized by dark red discoloration.

Fig. 5D.3 **Mesenteric infarction**

Small intestine mucosa showing dark red discoloration due to necrosis.

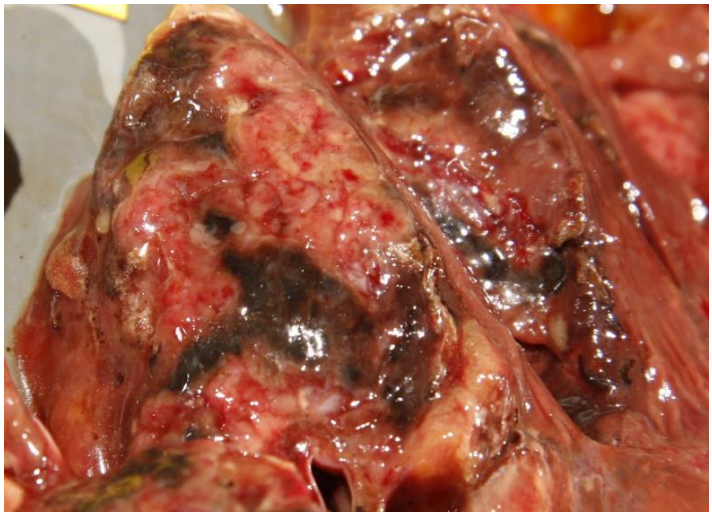

Fig. 5D.4 **Acute hemorrhagic (necrotizing) pancreatitis**

Areas of hemorrhages on the cut surface of the pancreatic tail.

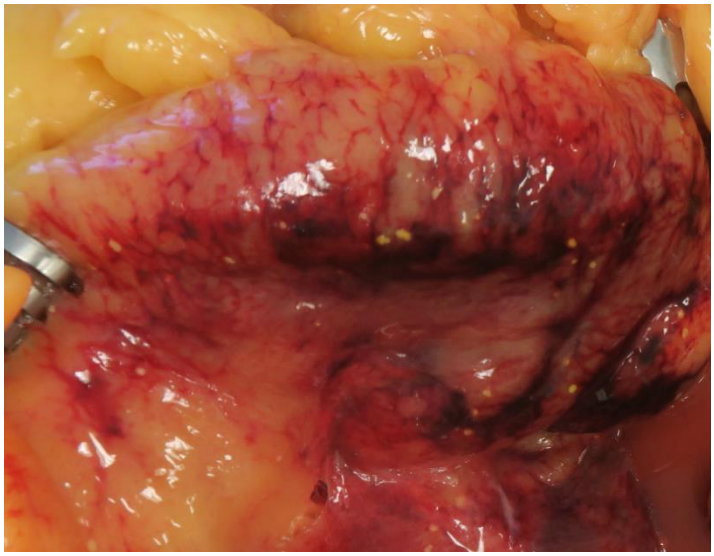

Fig. 5D.5 **Fat necrosis**

Necrosis of the adipose tissue of the intestinal mesentery associated with pancreatitis appears as yellow-white flecks.

Fig. 5E.1 **Ulcerous colitis**

Transversally oriented part of the intestine at the upper part of the image that continues downward on the left is large intestine (asterisk). It shows mucosal erythema and granularity with superficial ulcerations. Small intestine mucosa is diffusely erythematous.

Fig. 5E.2 **Pseudomembranous colitis**

Colorectal mucosa is covered with yellow-green pseudomembranes in forms of plaques 2 to 10 mm in diameter. In some parts, the plaques are confluent.

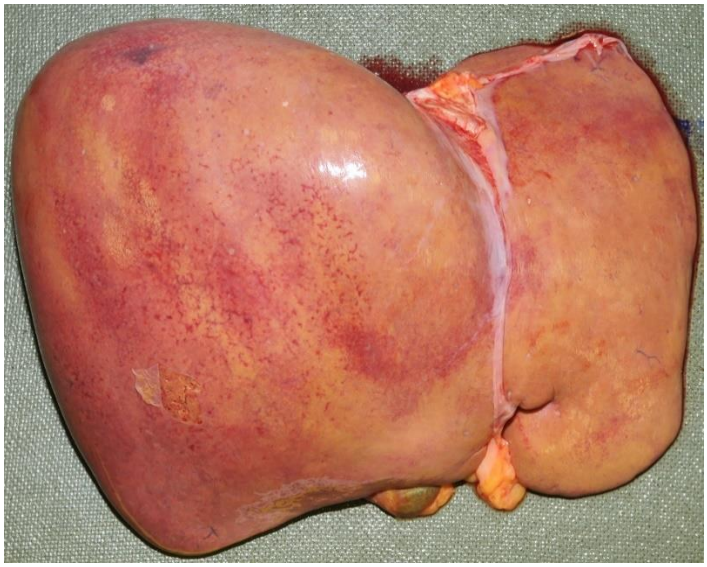

Fig. 5F.1 **Steatosis (fatty liver)**

The liver is enlarged and has a pale yellow appearance.

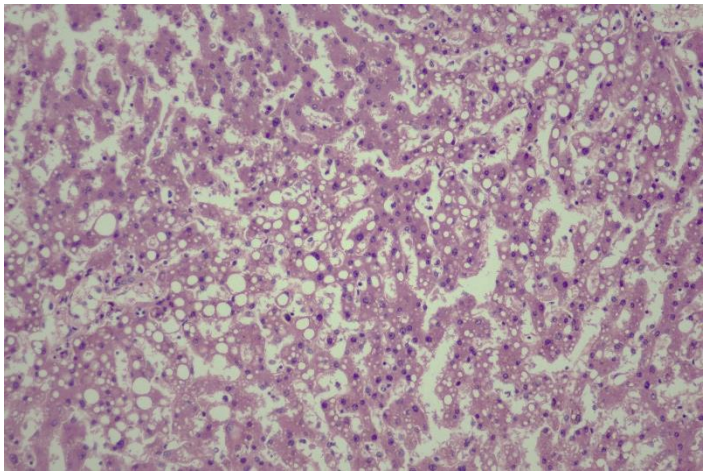

Fig. 5F.2 **Steatosis**

Fatty tissue deposits visible as intracytoplasmic vacuoles displacing the nucleus to the periphery of the cells (H&E).

Fig. 5F.3 **Cirhosis**

Cirrhotic liver showing nodular texture and yellow-brown discoloration. The nodules are of varying sizes.

Fig. 5F.4 **Cirhosis**

Cut surface of the liver showing nodular architecture.

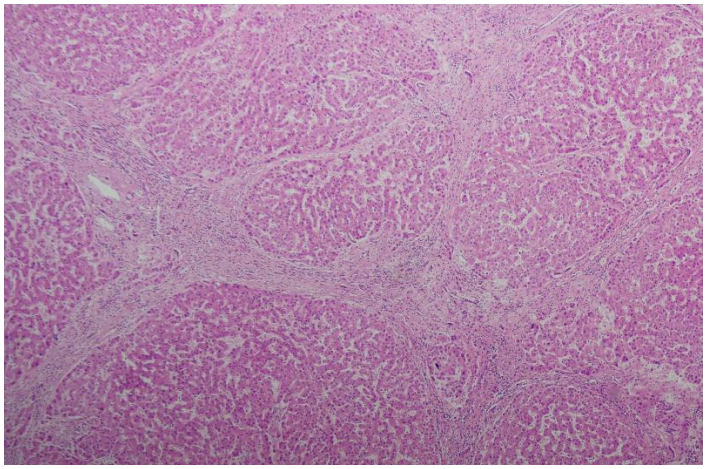

Fig. 5F.5 **Cirhosis**

Microscopic image characterized by rounded parenchymal nodules and bridging fibrous septa (H&E).

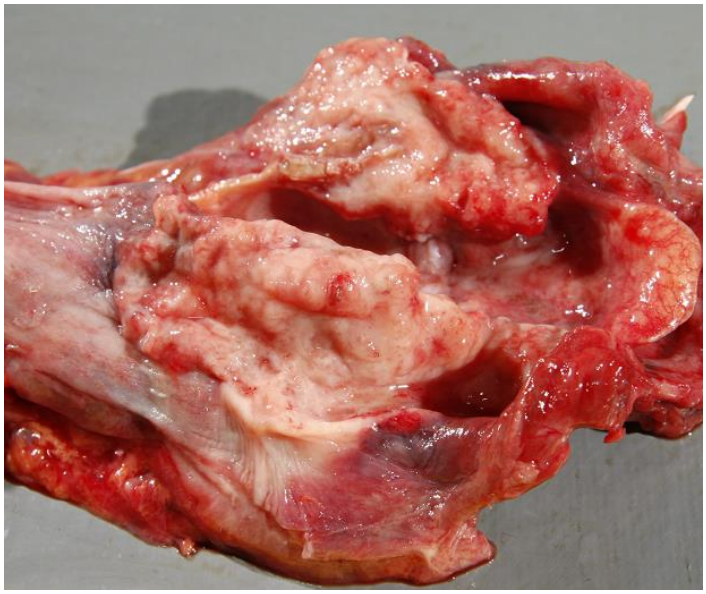

Fig. 5G.1 **Esophageal carcinoma**

Squamous cell carcinoma appearing as cauliflower-like exophytic mass of gray-white color at the upper part of esophagus.

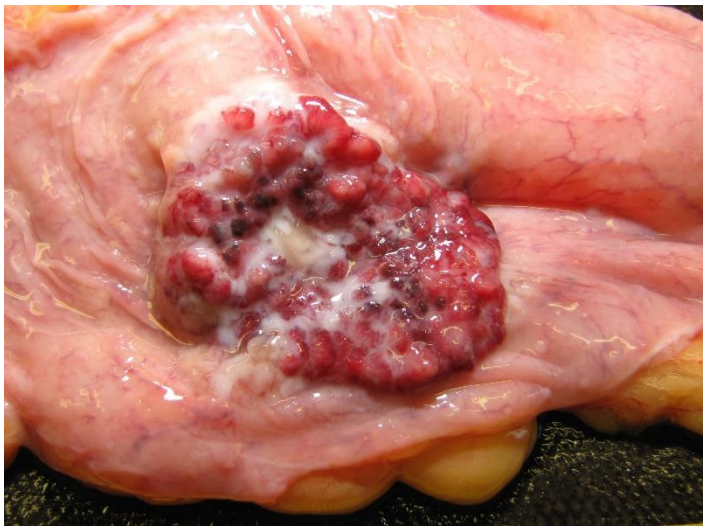

Fig. 5G.2 **Large intestine carcinoma**

Intestinal mucosa affected by adenocarcinoma characterized by a firm exophytic mass of gray-pink color with a sunken center.

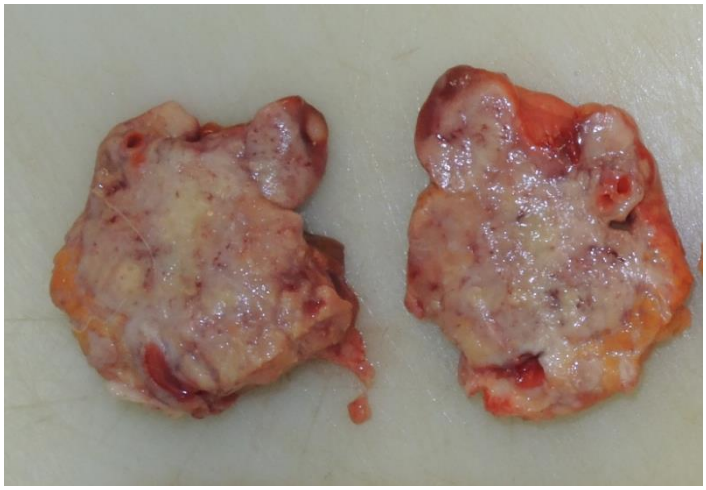

Fig. 5G.3 **Pancreatic cancer**

Cut surface of the pancreas showing ductal adenocarcinoma. It appears as a firm, white, solid mass with irregular margins.

Fig. 5G.4 **Liver hemangioma**

Solitary mass of blackish-red color on the capsular surface of left lobe.

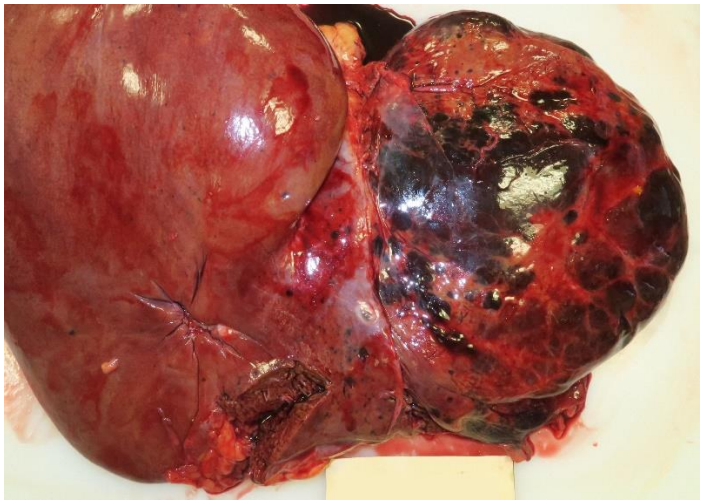

Fig. 5G.5 **Giant liver hemangioma**

Huge blackish-red mass with a "honeycomb" appearance completely affecting the left lobe.

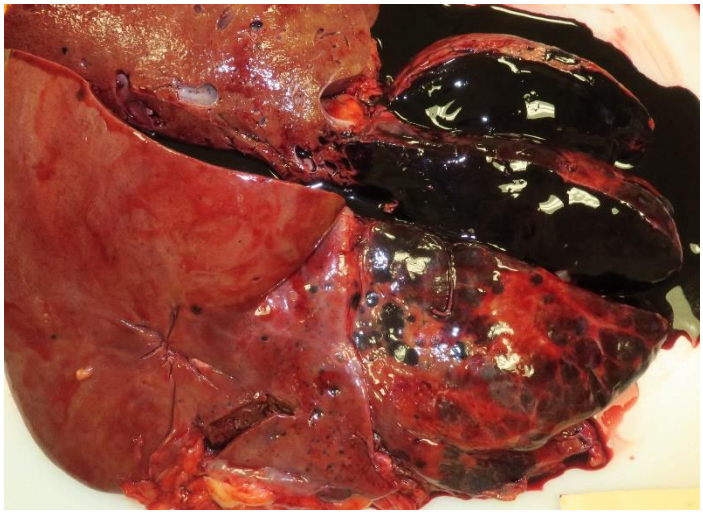

Fig. 5G.6 **Giant liver hemangioma**

Transverse section of the mass from the previous image shows rich hemorrhagic content.

Fig. 5G.7 **Liver metastases**

Multiple gray-white masses of different sizes on the capsular surface of the liver.

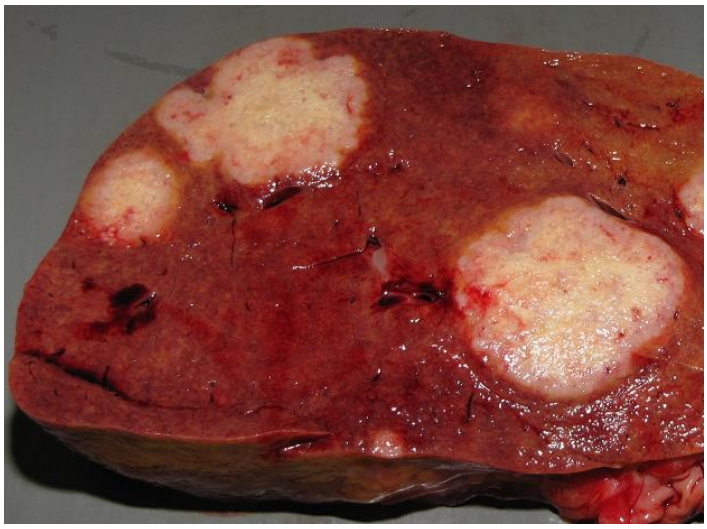

Fig. 5G.8 **Liver metastases**

Cut surface of the liver showing marginated firm gray-white tumor deposits of different size.

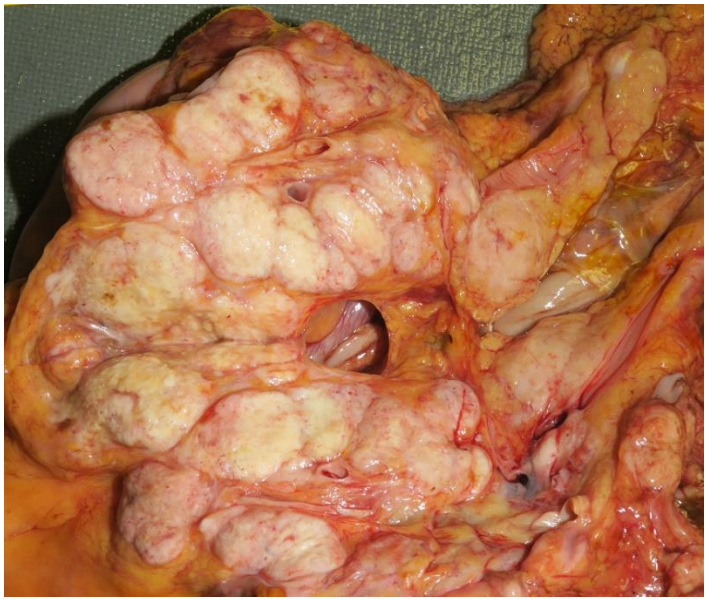

Fig. 5G.9 **Pancreatic cancer**

Cut surface of the pancreatic tail showing a complete replacement of the parenchyma with tumor deposits.

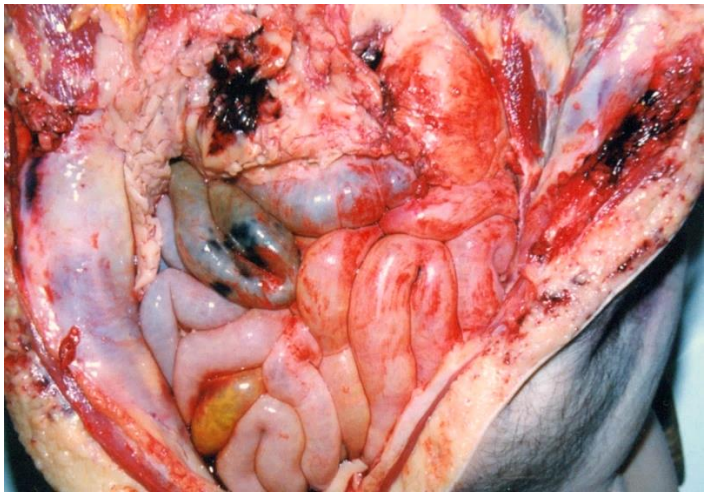

Fig. 5H.1 **Intestinal injury**

Focal wall hemorrhages in the small intestines and in the greater omentum situated above. There is hemorrhage within the subcutaneous soft tissues on the right.

Fig. 5H.2 **Liver laceration**

Multiple liver lacerations on the diaphragmatic surface.

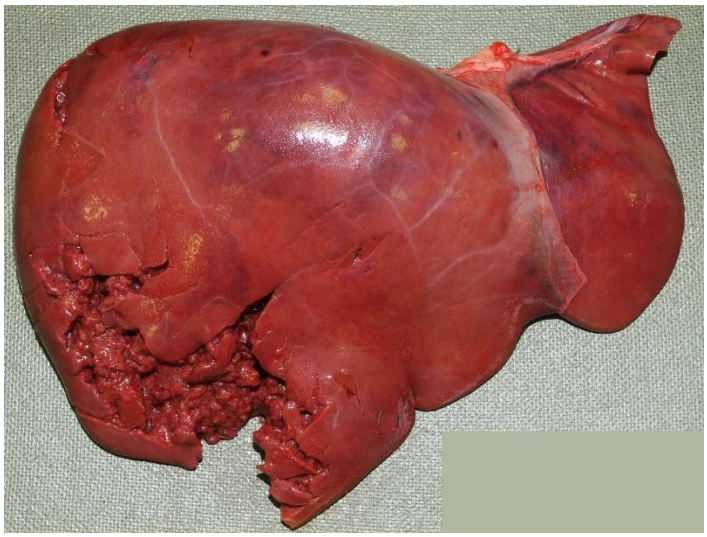

Fig. 5H.3 **Liver laceration**

Liver laceration with avulsion of the parenchyma of the right lobe.

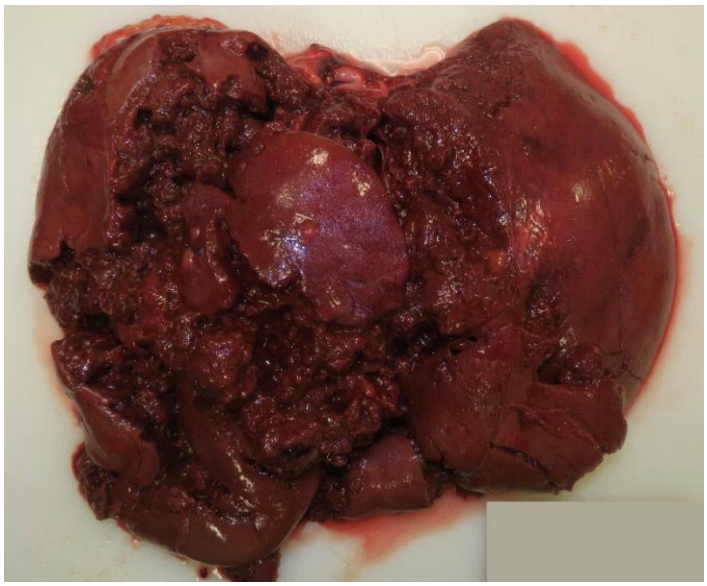

Fig. 5H.4 **Liver laceration**

Liver lacerations with extensive parenchymal disruption.

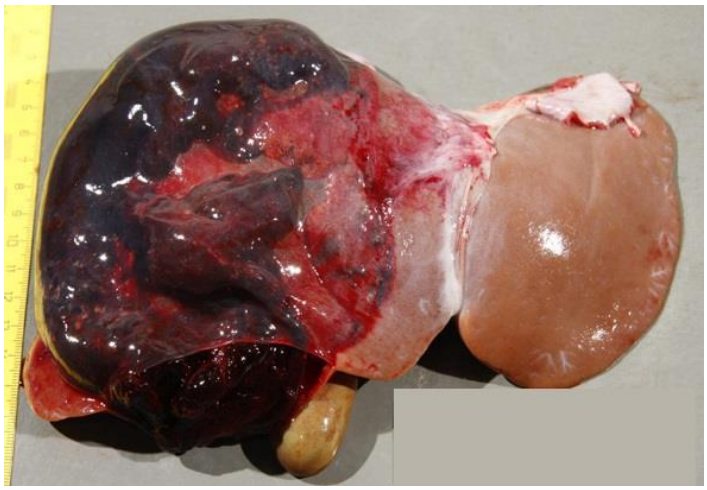

Fig. 5H.5 **Subcapsular liver hematoma**

Collections of blood under the capsule of the whole right lobe.

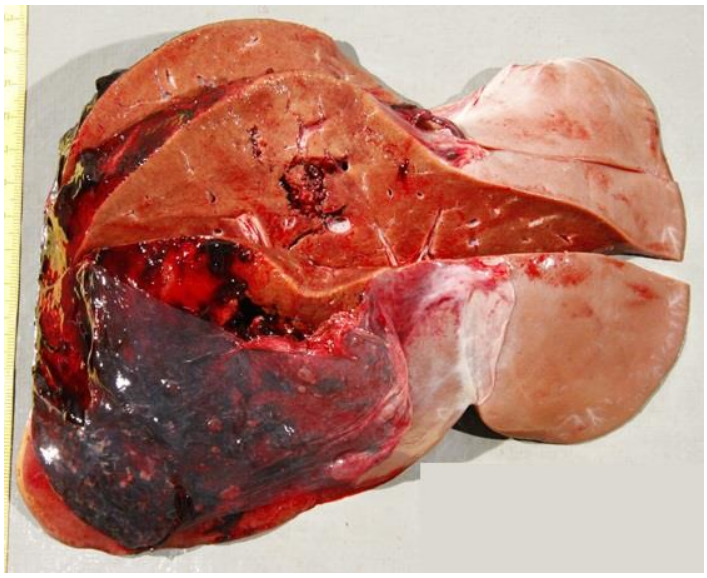

Fig. 5H.6 **Subcapsular liver hematoma**

Transverse sections of the liver from the previous image shows underlying contusion of the parenchyma in some areas.

Fig. 5I.1 **Sulfuric acid poisoning**

Esophageal mucosa affected by coagulative necrosis.

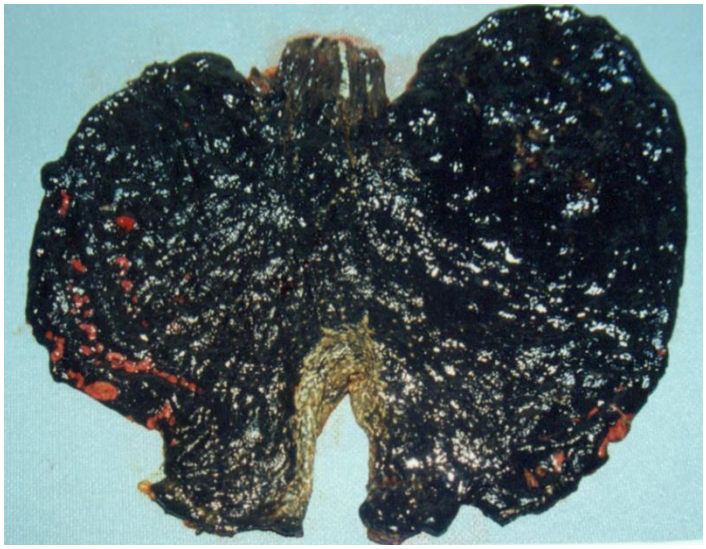

Fig. 5I.2 **Sulfuric acid poisoning**

Gastric mucosa showing black-green discoloration and extensive corrosion.

Fig. 5I.3 **Sulfuric acid poisoning**

Duodenum mucosa showing grayish green discoloration.

Fig. 5I.4 **Amanita phalloides poisoning**

Cut surface of the liver showing foci of necrosis presenting as pale, tan-yellow lesions.

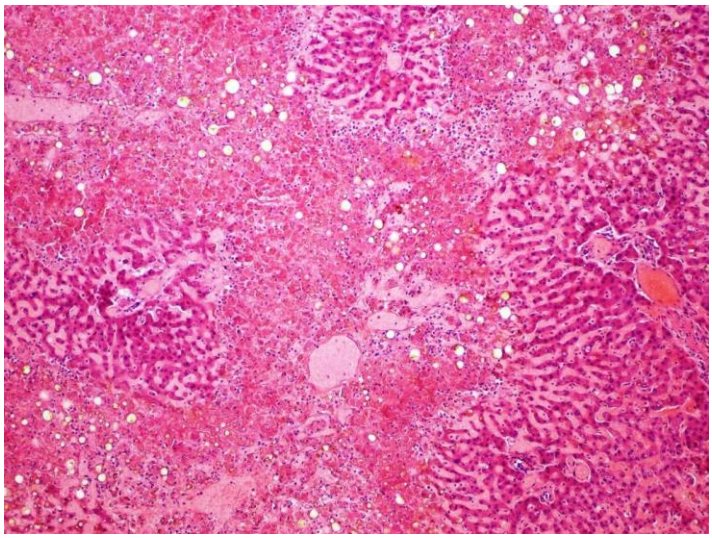

Fig. 5I.5 **Amanita phalloides poisoning**

Microscopic image of the liver showing patchy necrosis and hemorrhages (H&E).

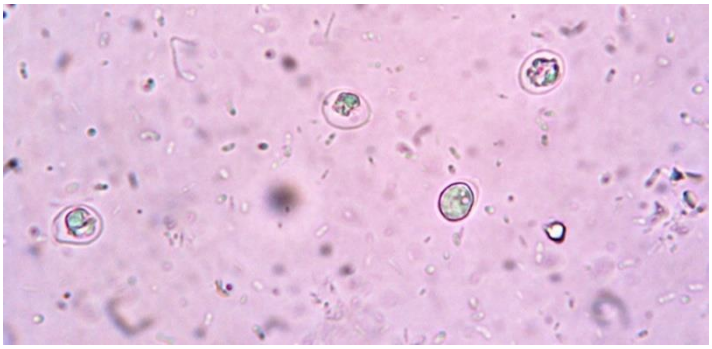

Fig. 5I.6 **Amanita phalloides poisoning**

The spore of *Amanita phalloides* confirmed microscopically in the gastrointestinal content (without staining).

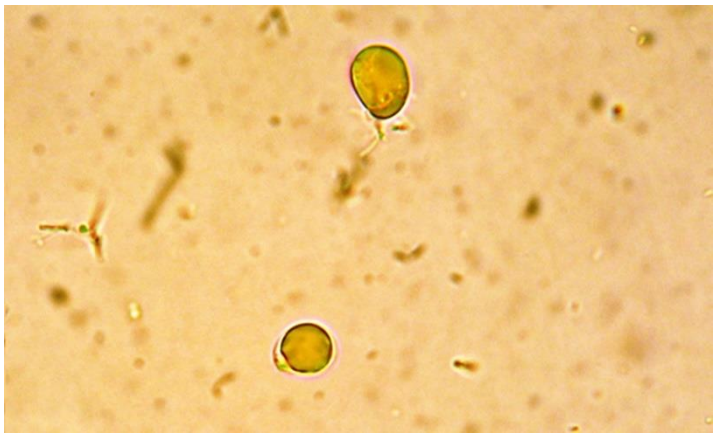

Fig. 5I.7 **Amanita phalloides poisoning**

The spore of *Amanita phalloides* confirmed microscopically in the gastrointestinal content (Melzer's reagent).

Fig. 5J.1 **Ascites**

Serous liquid present in the peritoneal cavity.

Fig. 5J.2 **Hemoperitoneum**

Liquid and coagulated blood within the peritoneal cavity.

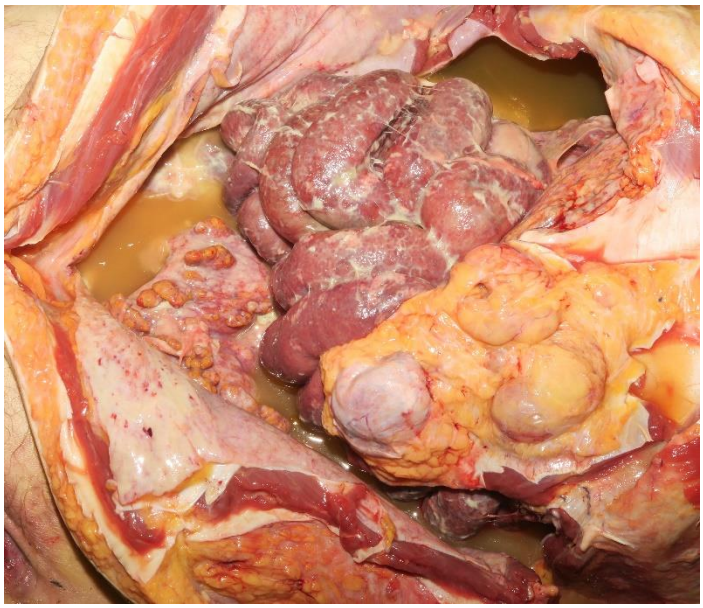

Fig. 5J.3 **Fibrinopurulent peritonitis**

Purulent exudate in the abdominal cavity and fibrin depositions on the serosa of the small intestine.

6 Genitourinary System

6A | Lithiasis

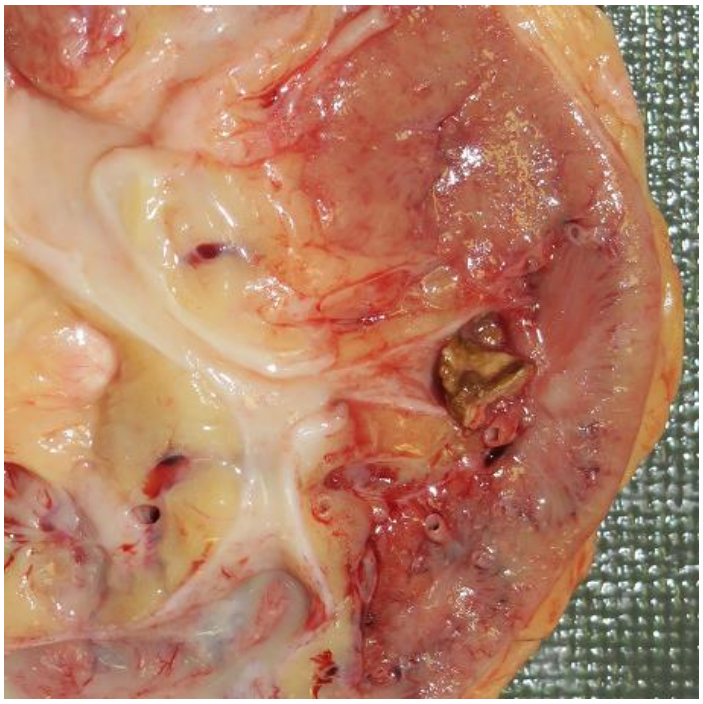

Fig. 6A.1 **Nephrolithiasis (renal calculi)**

Irregularly shaped stone (calculus) within the renal calyx.

Fig. 6A.2 **Ureterolithiasis**

Irregularly shaped stone attached to the mucosa of the ureter.

Fig. 6B.1 **Renal cysts**

Kidney with multiple simple cortical cysts. These have thin walls that are easily punctured, and they contain yellowish serous fluid.

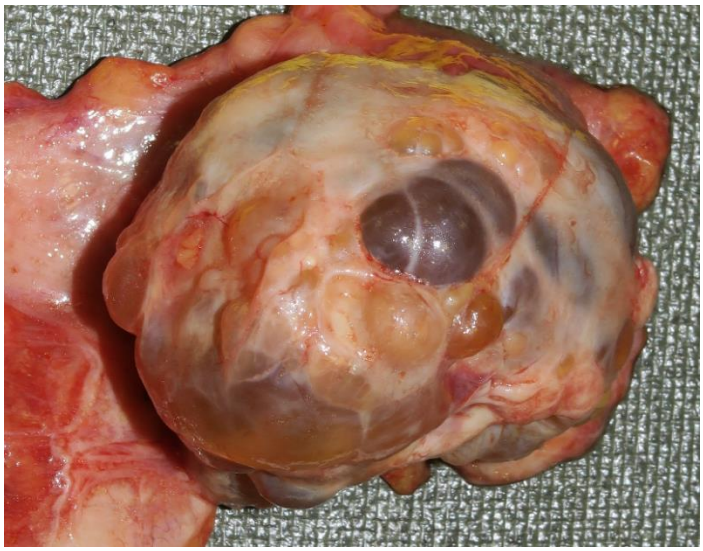

Fig. 6B.2 **Ovarian cysts**

Multiple fluid-filled sacs visible on the ovarian surface.

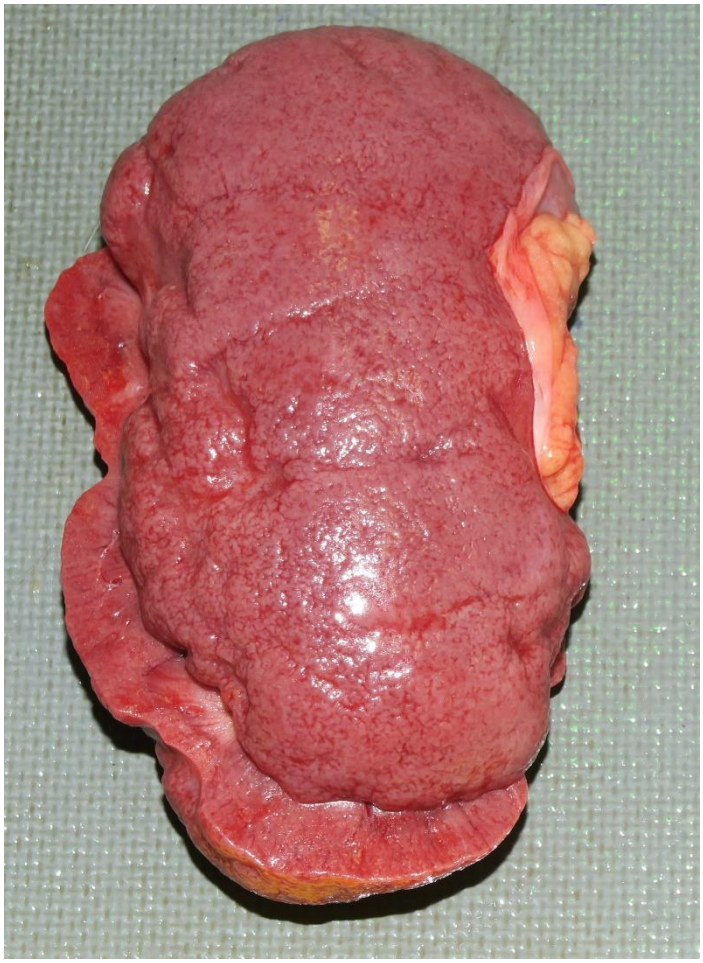

Fig. 6C.1 **Benign nephrosclerosis**

Surface of the kidney is granular and contains scars.

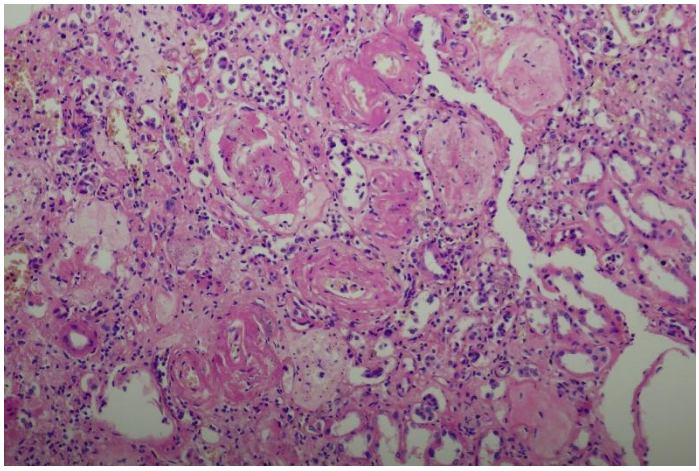

Fig. 6C.2 **Benign nephrosclerosis**

Microscopic image characterized by glomerular turfs being replaced by collagen (glomerulosclerosis) and thickening of the arteriolar wall due to the accumulation of pink homogeneous material (hyaline arteriolosclerosis).

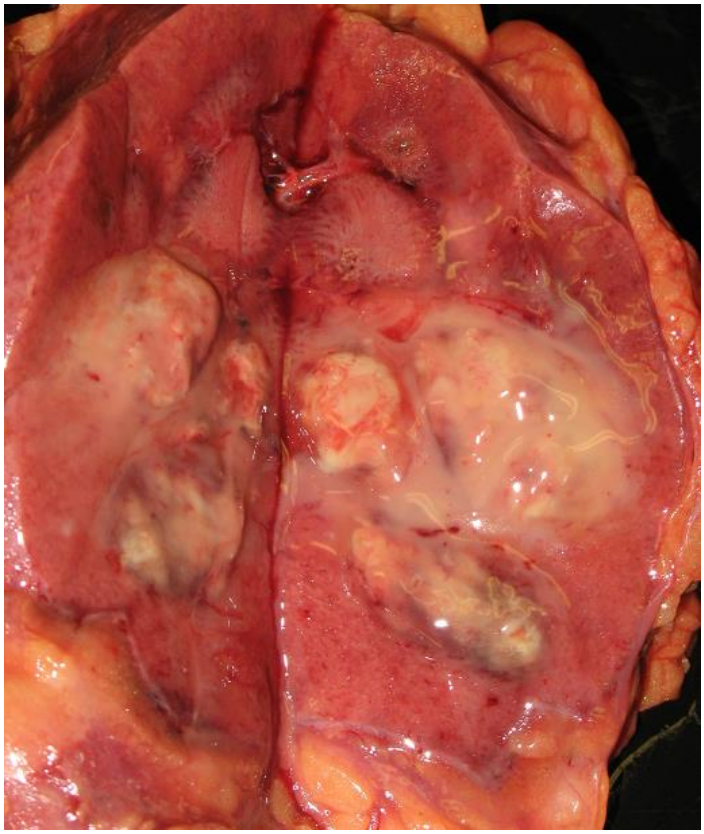

Fig. 6D.1 **Pyelonephritis**

Cut surface of the kidney showing accumulation purulent exudate in the renal pelvis.

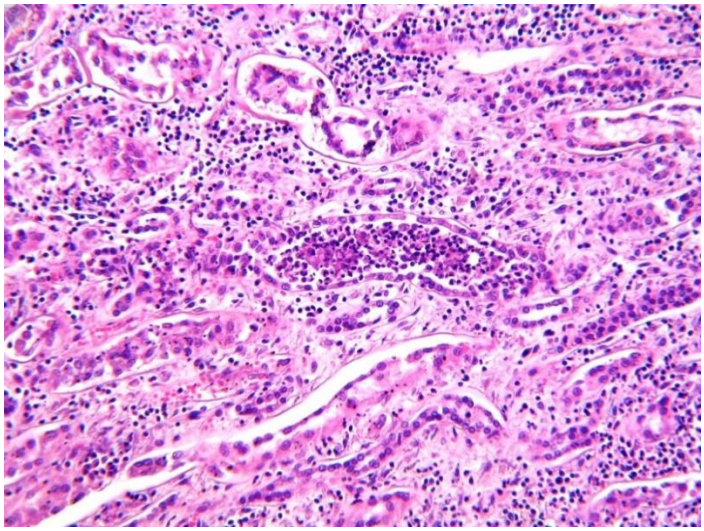

Fig. 6D.2 **Pyelonephritis**

Microscopic image of the kidney showing neutrophil-rich interstitial inflammatory infiltrate (H&E).

Fig. 6E.1 **Kidney cancer**

Cut surface of the kidney showing solitary marginated solid mass, yellow on cut surface with focal necrosis.

Fig. 6E.2 **Kidney metastases**

Multiple small irregular yellow masses on the surface, some showing central indentations due to necrosis.

Fig. 6E.3 **Prostate cancer**

Serial sections of the prostate show poorly circumscribed scattered lesions of pink-gray color.

Fig. 6E.4 **Cervical cancer**

Longitudinal section of the cervix shows diffuse enlargement caused by tumor infiltration (asterisk).

Fig. 6F.1 **Acute tubular necrosis**

On the cut surface of the kidney, an abnormally pale cortex is visible, and there may be linear hemorrhages in the cortex, medulla, and papillae.

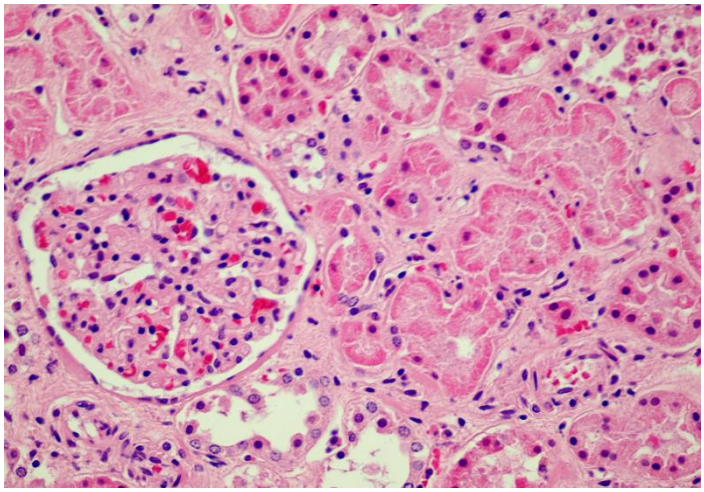

Fig. 6F.2 **Acute tubular necrosis**

Microscopic image characterized by necrosis of tubular epithelium with soughing of cells into the lumen. The glomeruli are preserved (H&E).

7 Lymphoreticular System

7A | Various spleen pathology

Fig. 7A.1 **Icing sugar spleen (*perisplenitis cartilaginea*)**

Creamy yellow to white plaques on the capsular surface of the spleen.

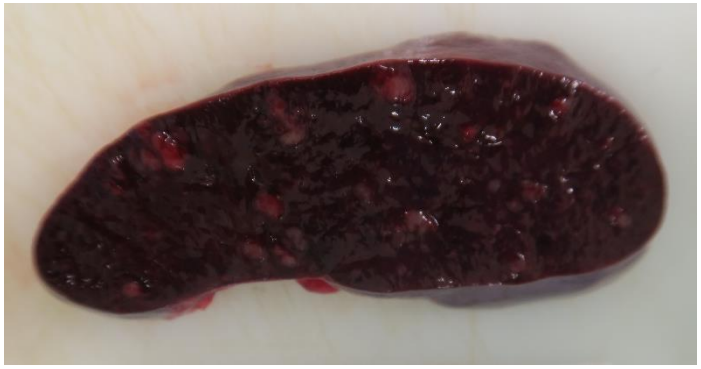

Fig. 7A.2 **Splenic metastases**

Multiple small pale nodules on the cut surface of the spleen of a child with Hodgkin lymphoma.

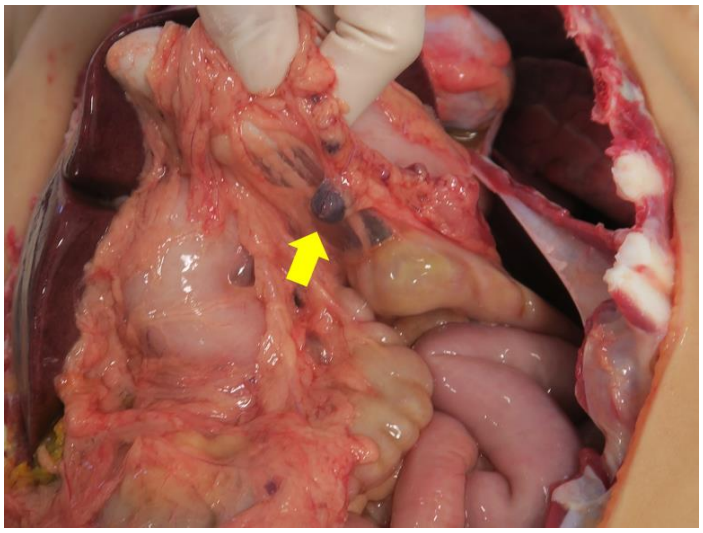

Fig. 7A.3 **Accessory spleen**

Small isolated nodule of spleen attached to the adipose tissue.

Fig. 7A.4 **Accessory spleen**

Eviscerated spleen and accessory spleen.

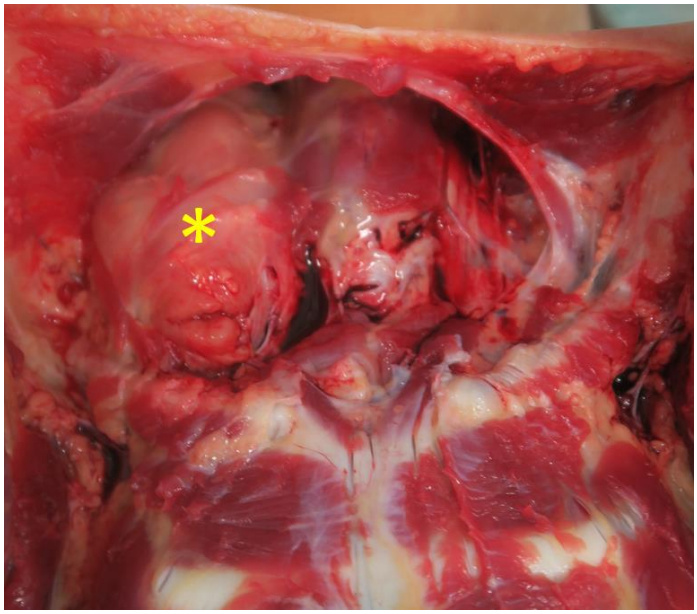

Fig. 7B.1 **Lymphadenomegaly**

Unilateral enlargement of the cervical lymph node (asterisk).

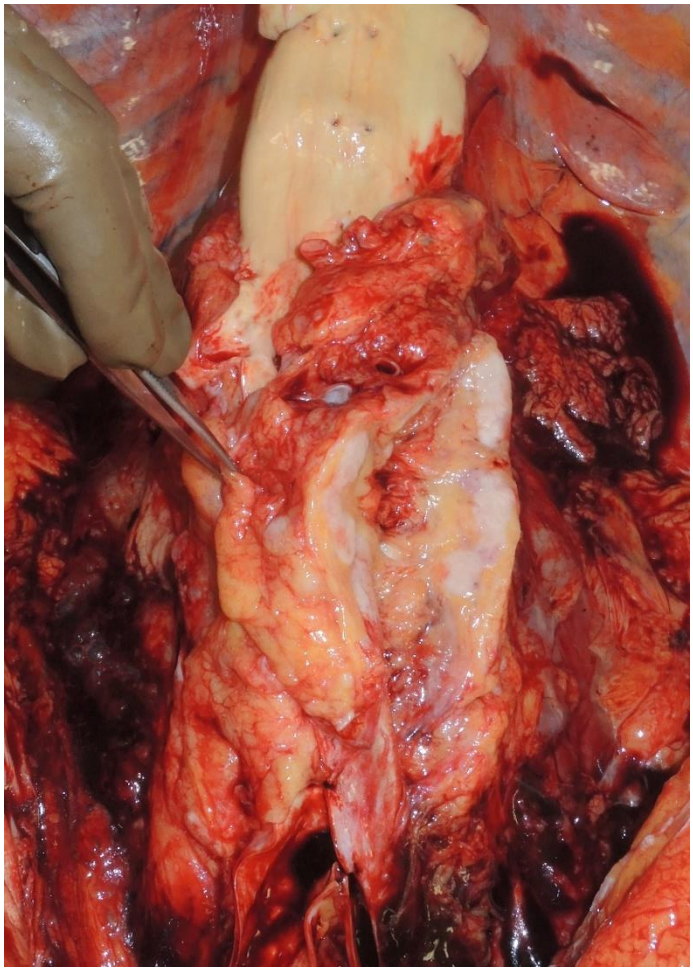

Fig. 7B.2 **Lymphadenomegaly**

Transversally cut enlarged lower paraaortic lymph nodes.

Fig. 7C.1 **Spleen rupture**

Diaphragmatic surface of the spleen showing multiple lacerations of the capsule and the parenchyma.

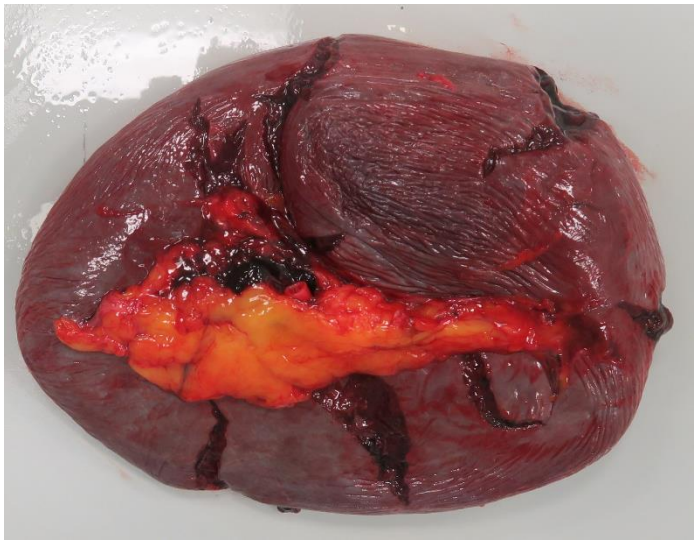

Fig. 7C.2 **Spleen rupture**

Visceral surface of the spleen from the previous image showing the same finding of multiple lacerations.

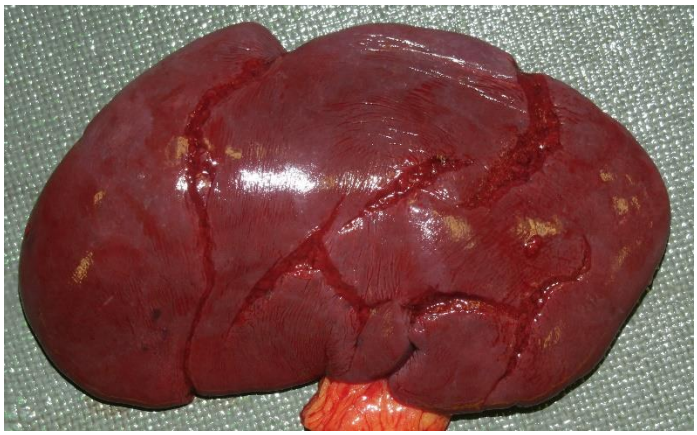

Fig. 7C.3 **Spleen rupture**

Another example of a spleen with multiple lacerations.

Fig. 7C.4 **Subcapsular splenic hematoma**

Diaphragmatic surface of the spleen showing the unruptured subcapsular hematoma. It is characterized by spleen enlargement and a purplish discoloration of the surface.

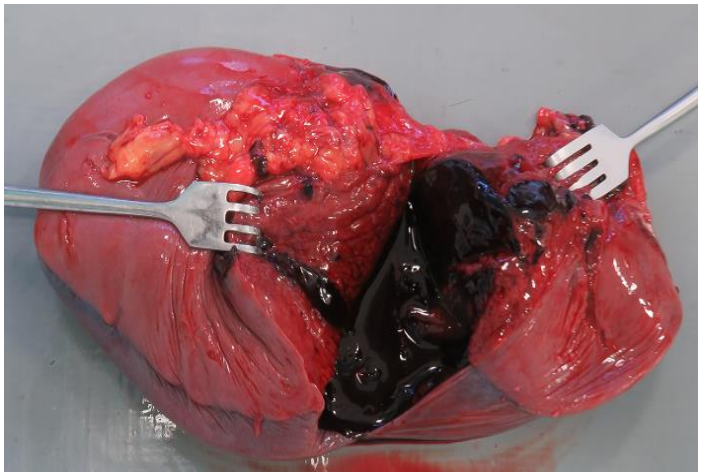

Fig. 7C.5 **Subcapsular splenic hematoma**

Transverse cut to the spleen showing subcapsular hematoma resulting from a tear in the parenchyma in the presence of an intact capsule.

8 Central Nervous System

8A | Inflammation

Fig. 8A.1 **Meningitis**

Bacterial (purulent) meningitis characterized by the presence of opaque, creamy exudate over the frontal lobes.

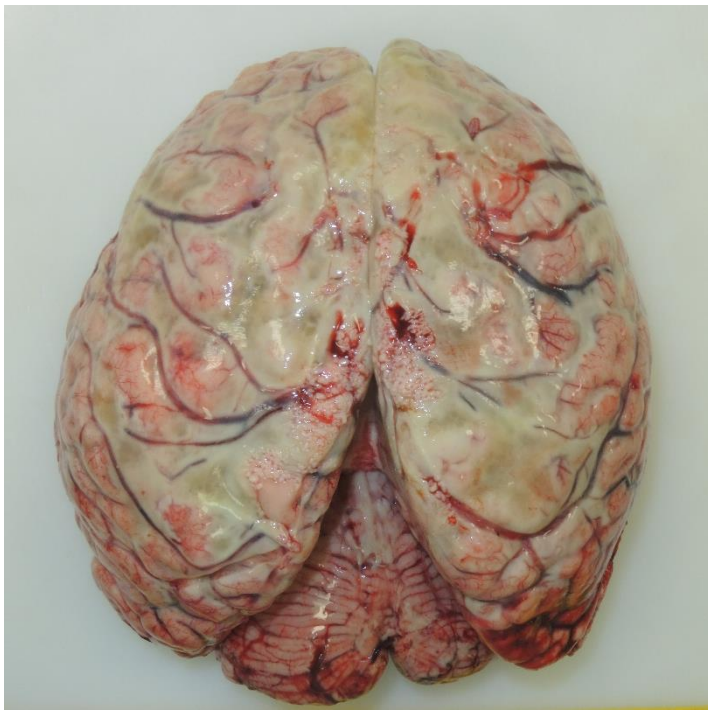

Fig. 8A.2 **Meningitis**

Extensive bacterial meningitis with purulent exudate covering both cerebral hemispheres.

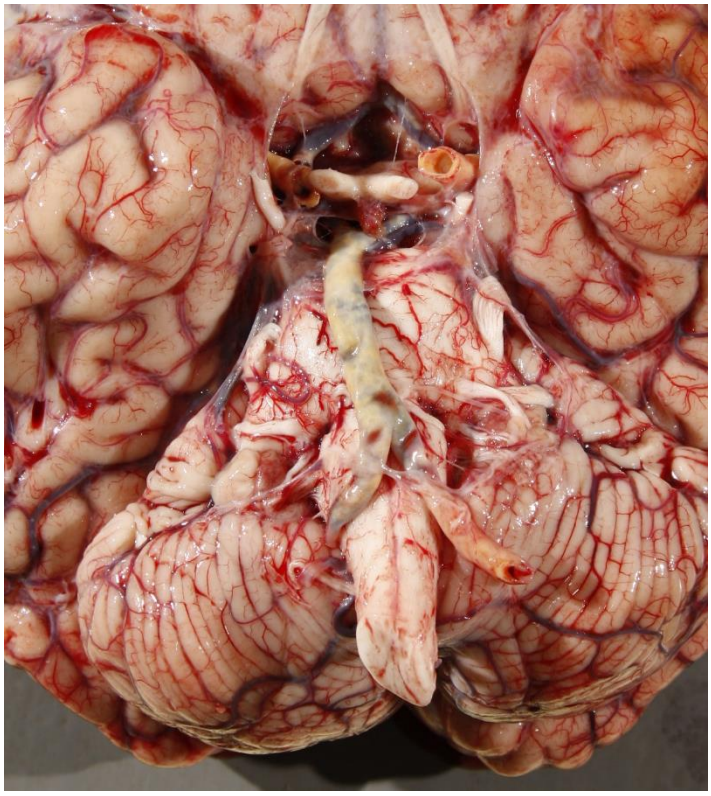

Fig. 8B.1 **Atherosclerosis**

Arteries in the circle of Willis affected by atherosclerosis characterized by yellow discoloration of the arteries' walls.

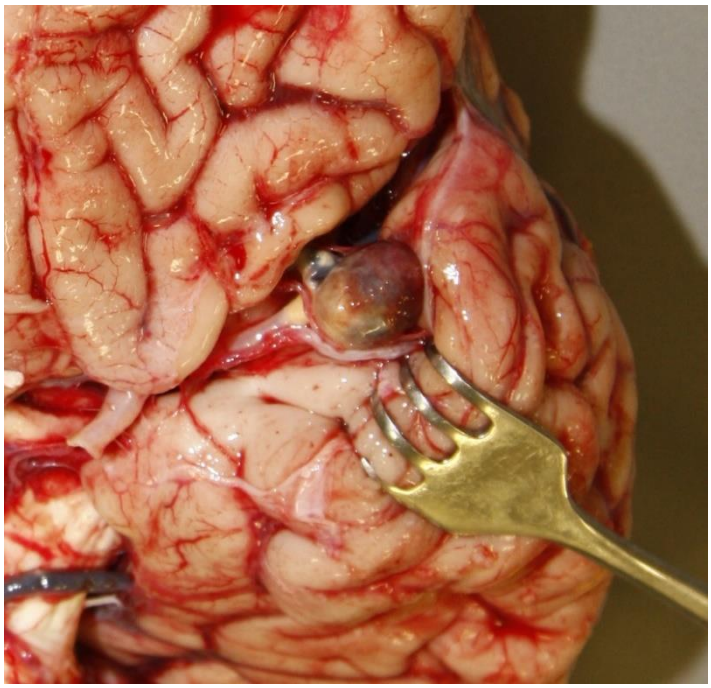

Fig. 8B.2 **Berry aneurysm**

Unruptured berry (saccular) aneurysm of the left middle cerebral artery.

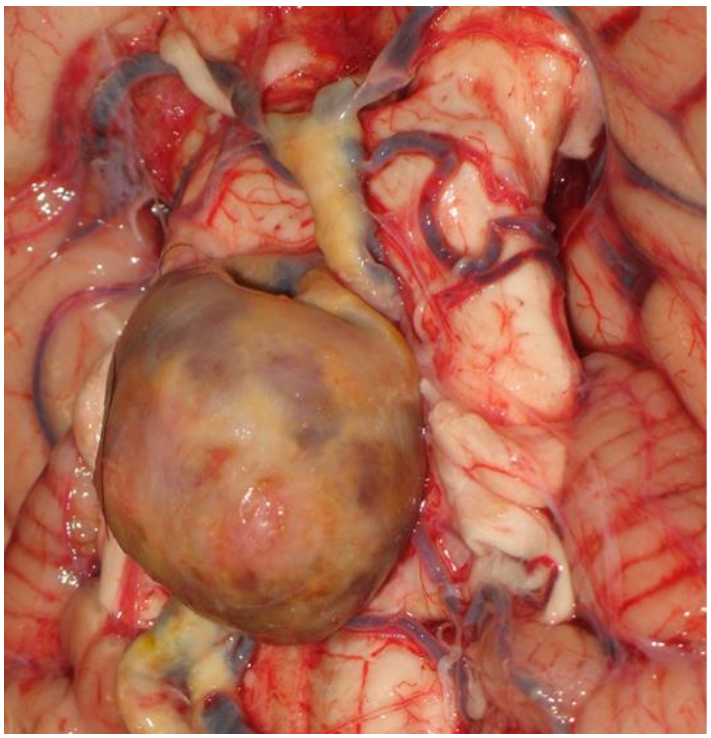

Fig. 8B.3 **Berry aneurysm**

Circle of Willis atherosclerosis and a large berry aneurysm of the basilar artery.

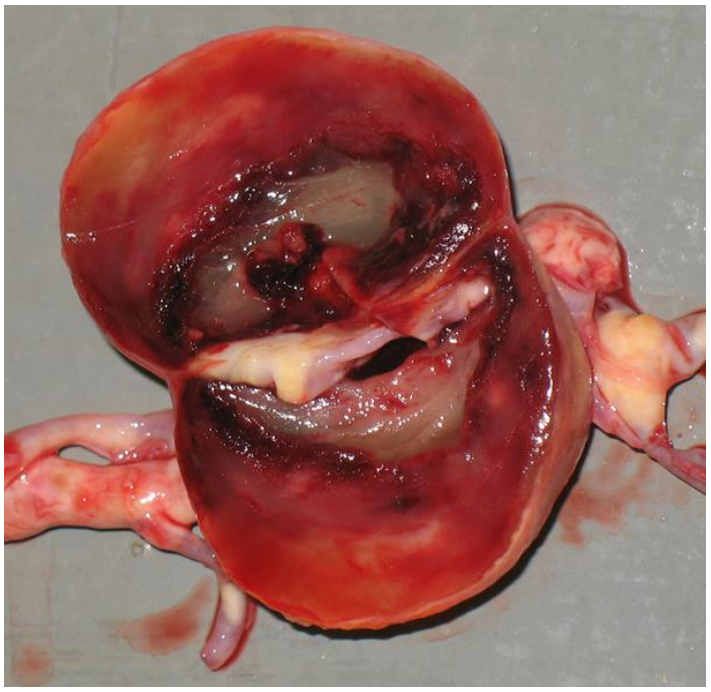

Fig. 8B.4 **Berry aneurysm**

Cut surface of the large berry aneurysm showing mural thrombus.

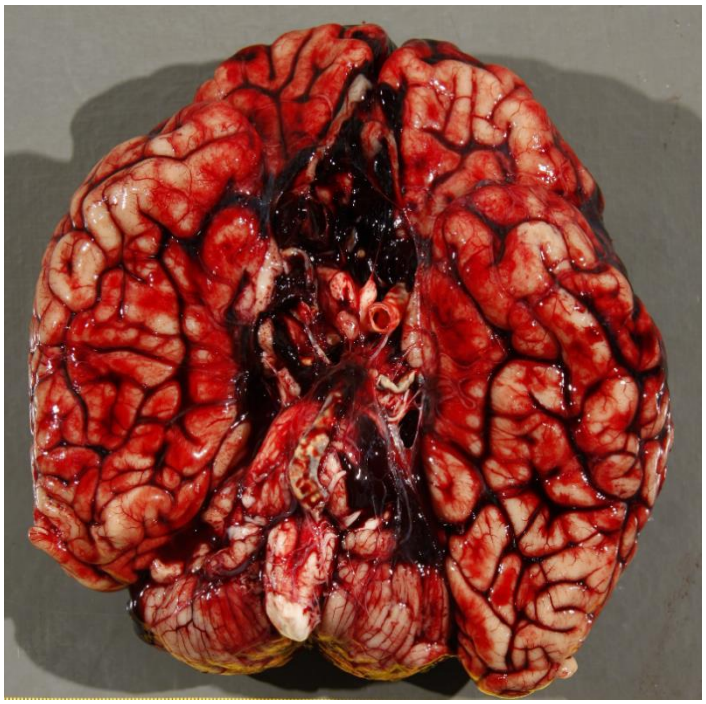

Fig. 8B.5 **Ruptured berry aneurysm**

Subarachnoid hemorrhage at the base of the brain caused by a ruptured aneurysm of the right internal carotid artery.

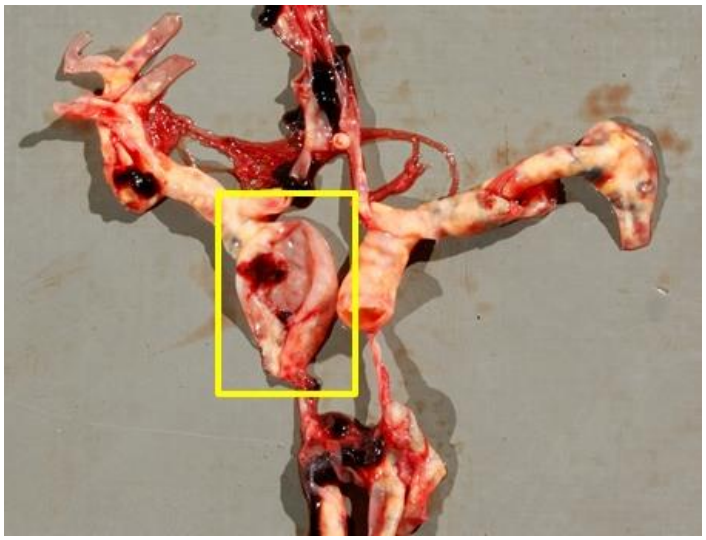

Fig. 8B.6 **Ruptured berry aneurysm**

Ruptured aneurysm of the right internal carotid artery.

Fig. 8B.7 **Hemorrhagic stroke**

Devastating intraparenchymal hemorrhage into the left hemisphere.

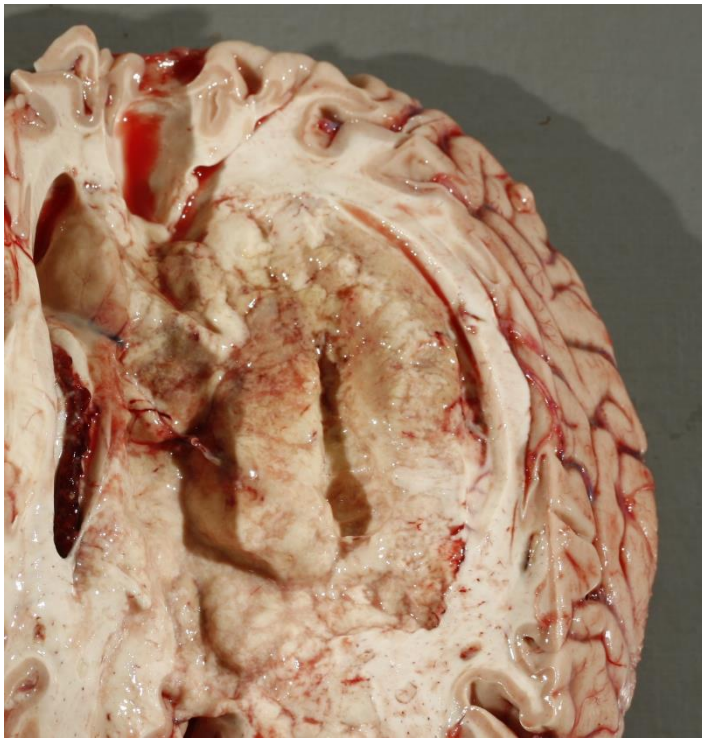

Fig. 8B.8 **Ischemic stroke**

Ischemic stroke in the right basal ganglia characterized by poorly demarcated area of softening and discoloration.

Fig. 8C.1 **Epidural hematoma**

Collection of blood outside the dura over the left brain hemisphere.
A portion of the dura over the frontal lobes is reflected, exposing the underlying brain.

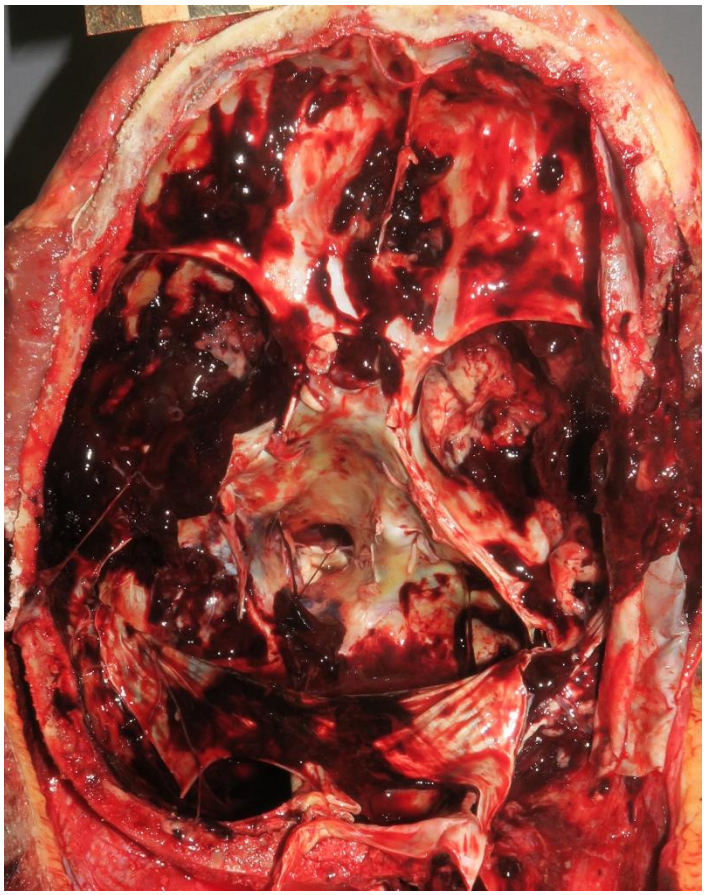

Fig. 8C.2 **Subdural hematoma**

Base of the skull after removal of the brain showing collections of clotted blood. The dura has remained adherent to the inner aspect of the skull base.

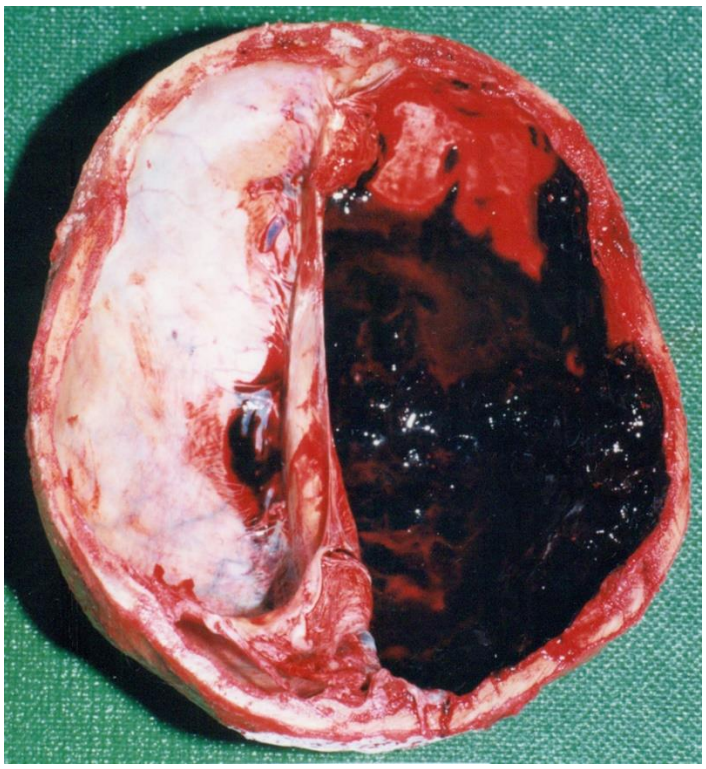

Fig. 8C.3 **Subdural hematoma**

Scalp showing left-sided subdural hematoma.

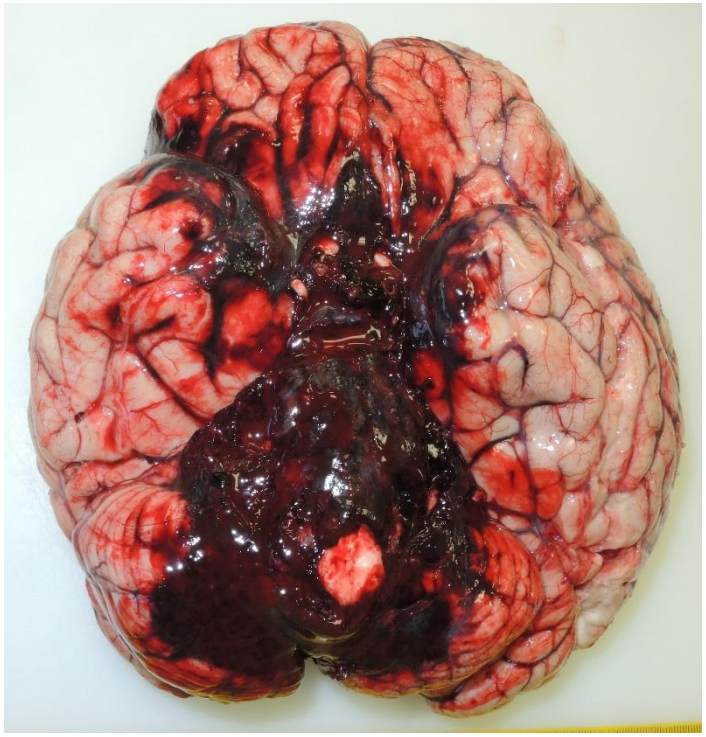

Fig. 8C.4 **Subarachnoid hemorrhage**

Focal collections of blood between the arachnoid and the pia mater surrounding the base of the brain and cerebellum.

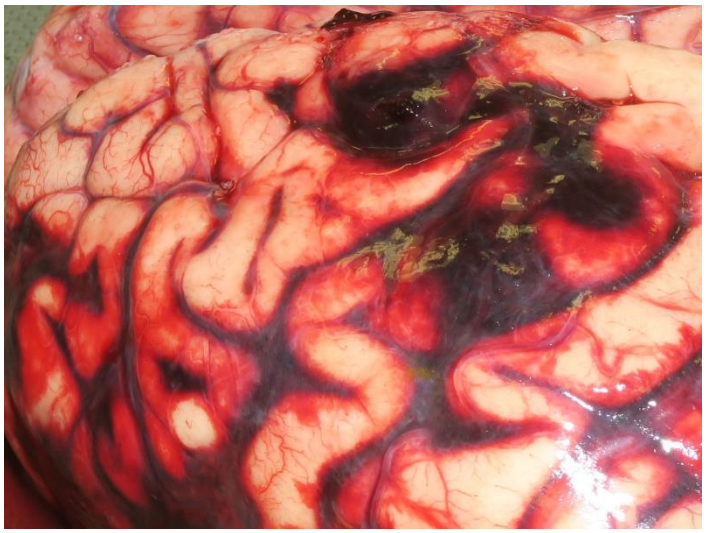

Fig. 8C.5 **Subarachnoid hemorrhage**

Close-up view of subarachnoid hemorrhage over the left frontal lobe.

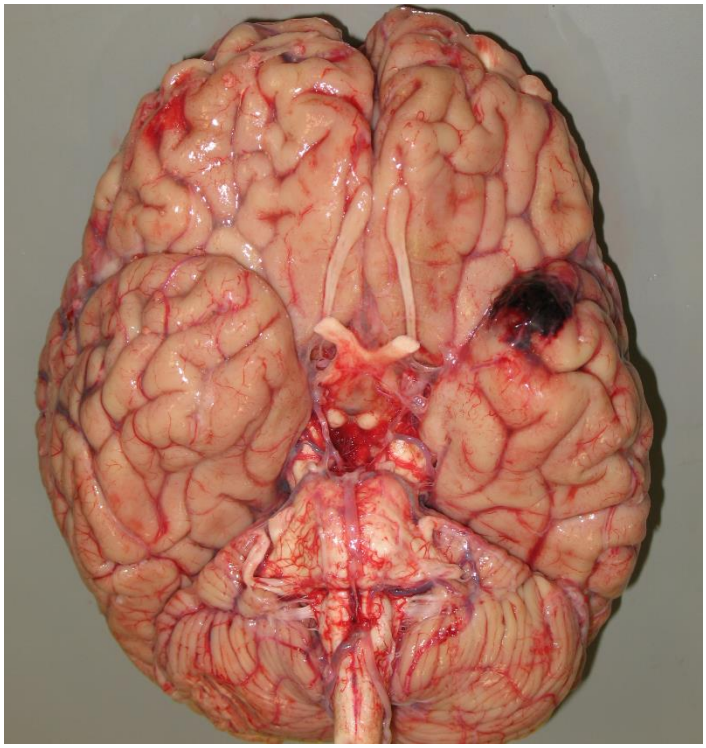

Fig. 8D.1 **Contusion**

Isolated lesion with a hemorrhagic character at the left temporal lobe.

Fig. 8D.2 **Contusion**

Subarachnoid hemorrhage overlying areas with cerebral contusions.

Fig. 8D.3 **Contusion**

Close-up view of cerebral contusion with overlying subarachnoid hemorrhage in a formalin-fixed brain.

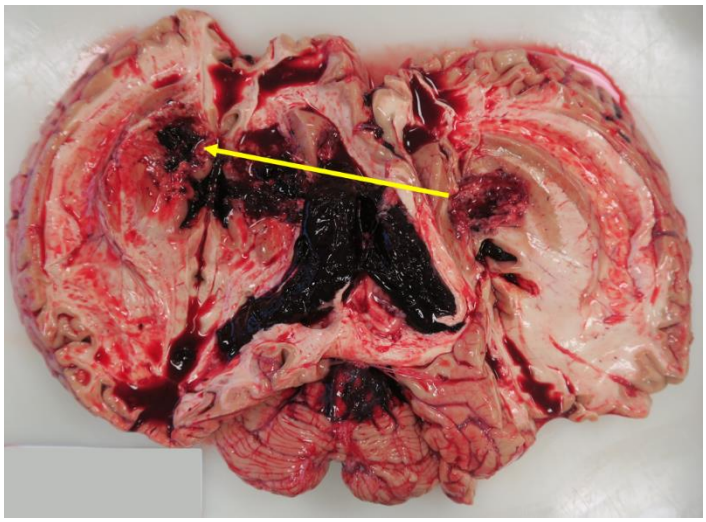

Fig. 8D.4 **Contusion**

Cerebral contusion with intracerebral hemorrhage in a perforating firearm injury to the head. Arrow is showing direction of the wound channel.

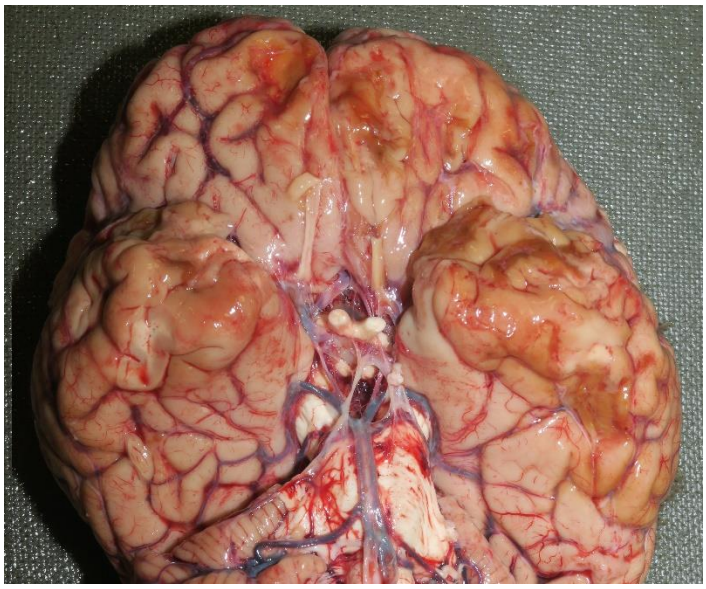

Fig. 8D.5 **Old contusion**

Old contusion of the frontal and temporal lobes with a depressed, brown-yellow appearance.

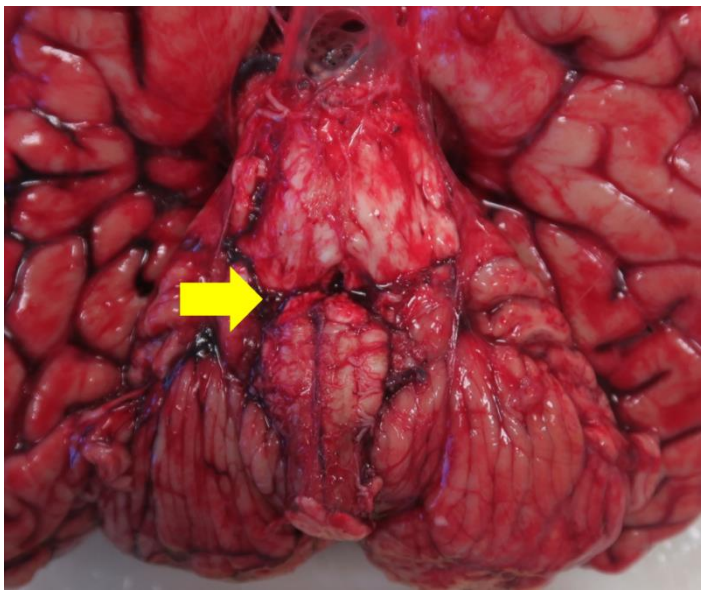

Fig. 8D.6 **Laceration**

Lacerations at the junction
of the pons and medulla.

Fig. 8D.7 **Edema**

Post traumatic cerebral edema
characterized by flattened
and widened gyri with narrowed sulci.

9 Skeletal System

9A | Skull fractures and defects

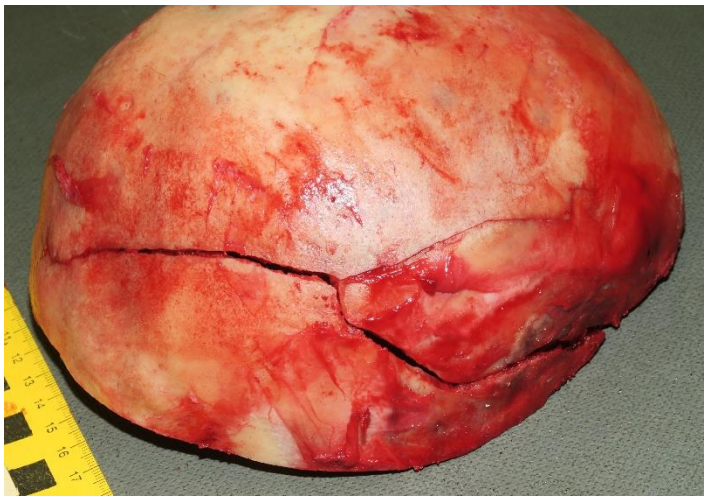

Fig. 9A.1 **Linear skull fracture**

Linear fracture of the right parietal and temporal bone.

Fig. 9A.2 **Diastatic skull fracture**

Fracture is present along the sagittal suture line.

Fig. 9A.3 **Depressed skull fracture**

Fracture of the right parietal and temporal bone with inward displacement of the fragments of the bone.

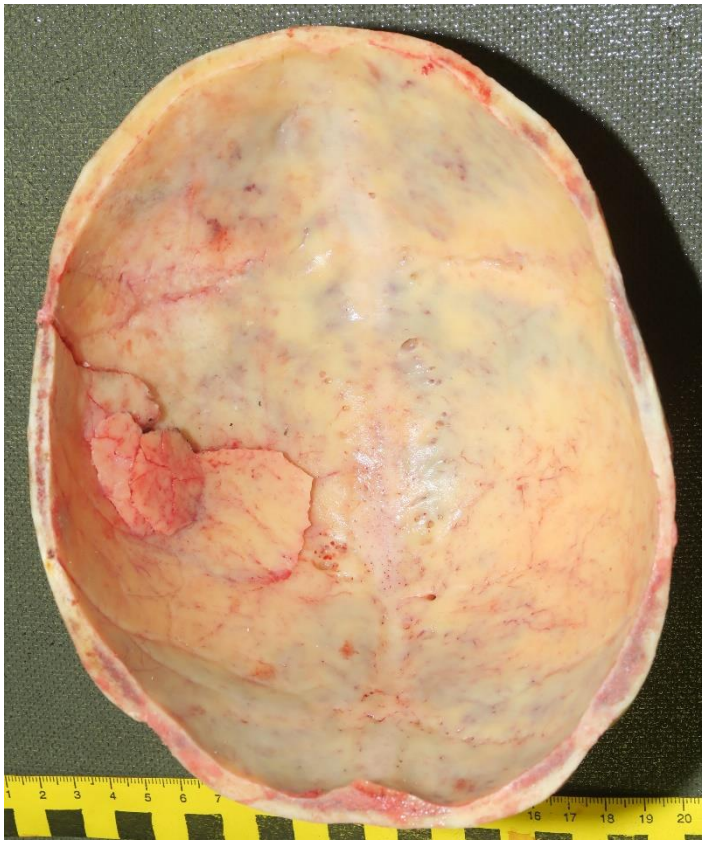

Fig. 9A.4 **Depressed skull fracture**

Inward displacement of the fragments of the bone visible on the inner surface of the skull.

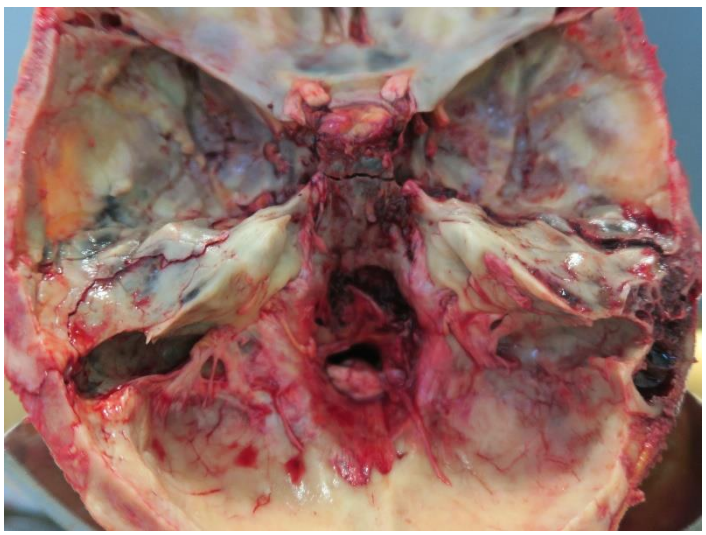

Fig. 9A.5 **Skull base fracture**

Middle cranial fossa fracture going from one side to the other (''hinge fracture'').

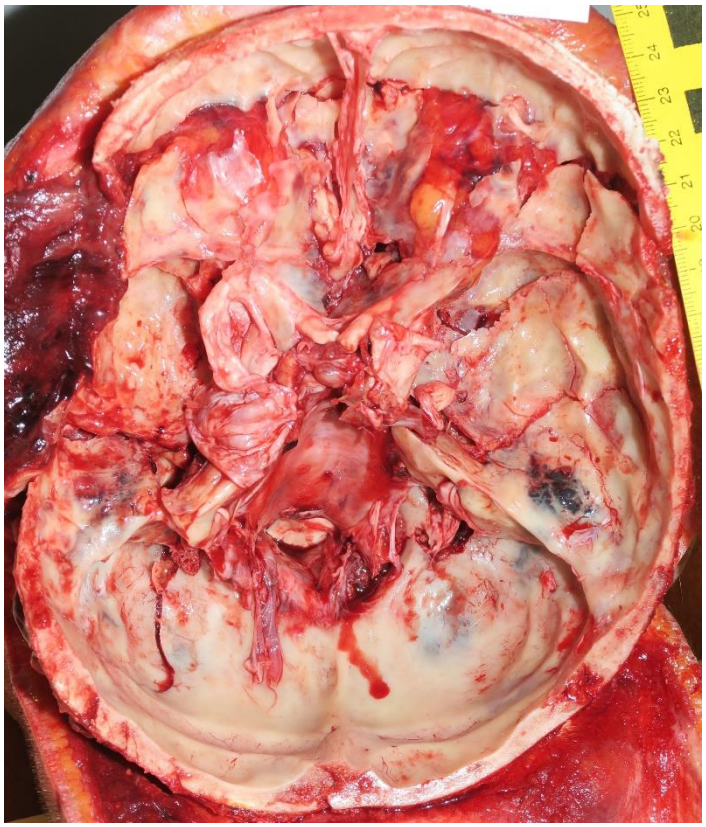

Fig. 9A.6 **Skull base fractures**

Multiple basilar skull fractures.

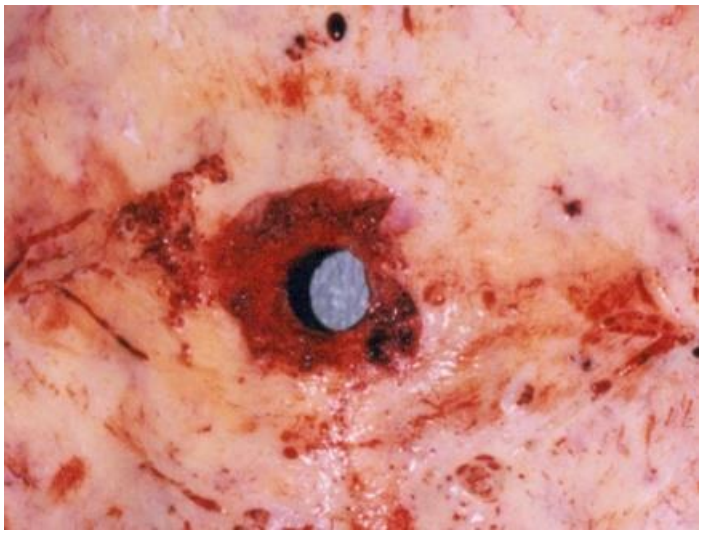

Fig. 9A.7 **Gunshot wound**

An inner view of a gunshot entrance wound to the skull showing cone-shaped bone erosion known as internal skull beveling.

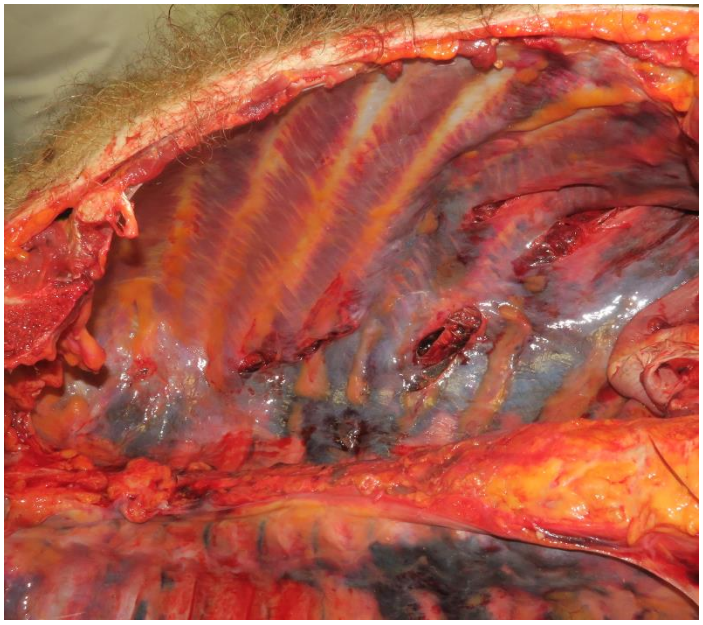

Fig. 9B.1 **Rib fractures**

Multiple rib fractures with pleural tears and intercostal hemorrhages.

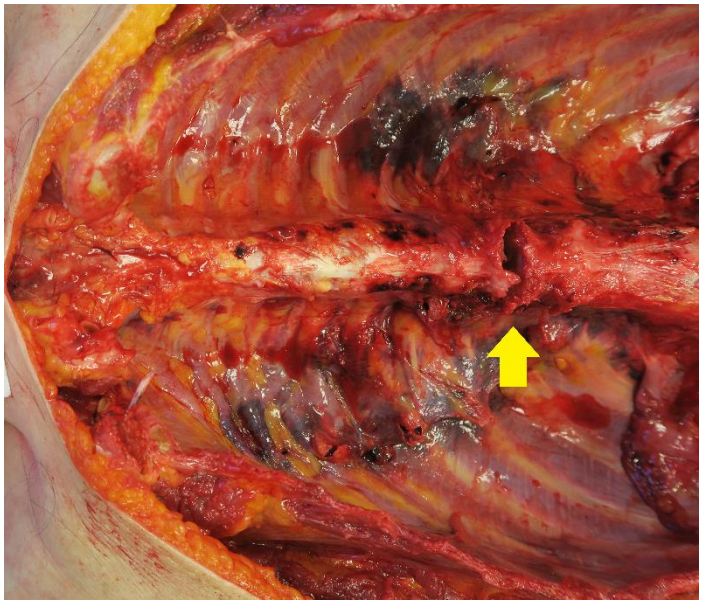

Fig. 9B.2 **Intervertebral disc disruption**

Disruption of intervertebral disc between the 9th and 10th thoracic vertebrae (arrow) and adjacent rib fractures on both sides.

10 Hypothermia

10A | External findings

Fig. 10A.1 **Frost erythema**

Pink discoloration of the skin over the extensor surfaces of both knees.

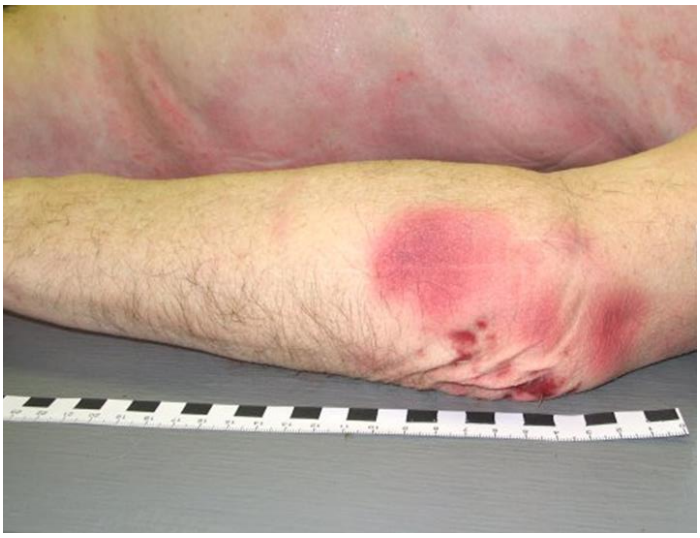

Fig. 10A.2 **Frost erythema**

Pink discoloration of the skin over the extensor surface of the left elbows.

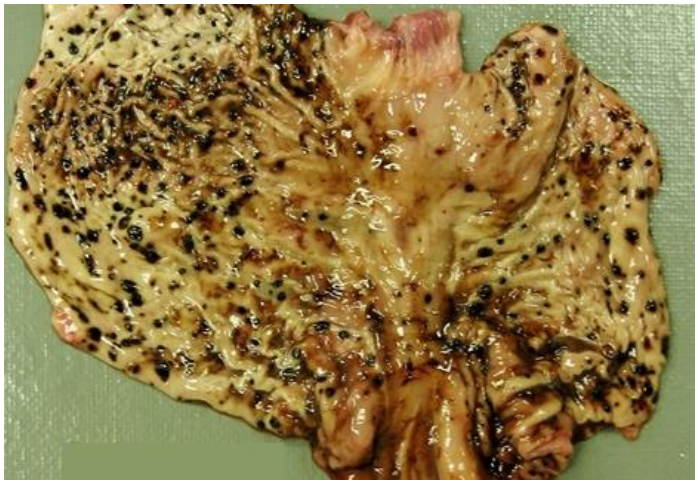

Fig. 10B.1 **Wischnewski spots**

Extensive dark oval-shaped lesions in the gastric mucosa that vary in sizes.

Fig. 10B.2 **Wischnewski spots**

Sporadic dark dot-shaped lesions in the gastric mucosa of 1 mm in diameter.

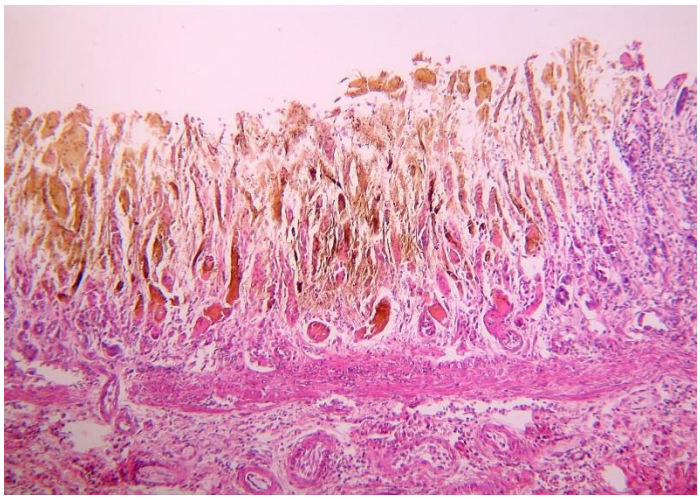

Fig. 10B.3 **Wischnewski spots**

Microscopic image of hemorrhagic erosion in the gastric mucosa (H&E).

11 Fire-related Death

11A | External findings

Fig. 11A.1 **Burned body**

Extensive external charring with focal splitting of the skin.

Fig. 11A.2 **Burned body**

So called ''boxer's'' or ''pugilistic'' attitude of the dead body with flexed elbow and clenched fist.

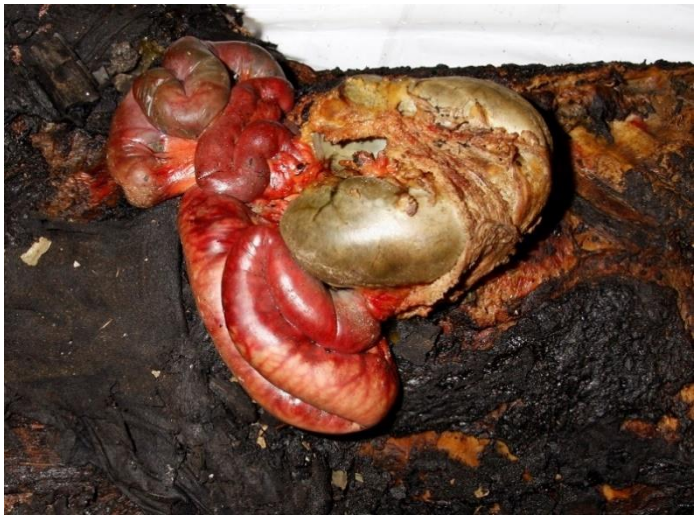

Fig. 11A.3 **Burned body**

Splitting of the abdominal wall with protrusion of the abdominal organs.

Fig. 11B.1 **Soot inhalation**

Soot within the trachea and main bronchi.

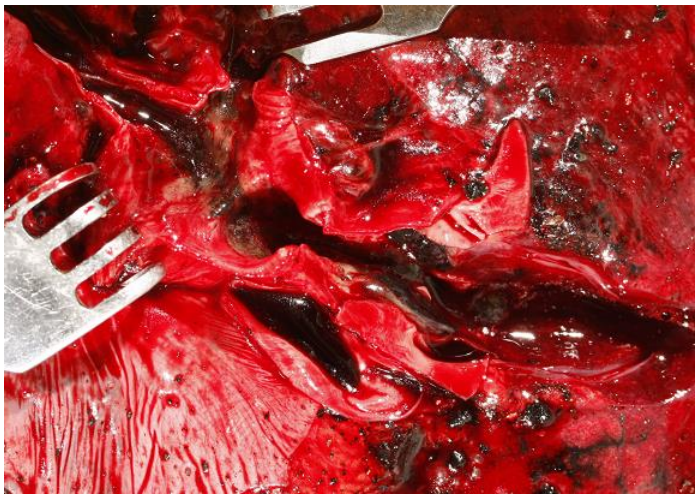

Fig. 11B.2 **Soot inhalation**

Soot within the bronchi at the lung hilum.

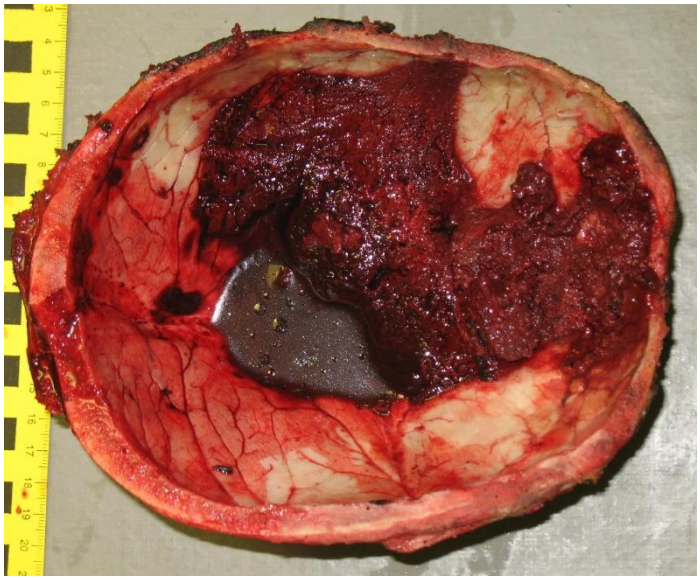

Fig. 11B.3 **Heat hematoma**

Scalp with a heat-induced epidural hematoma characterized by the presence of mud-like brick-red blood.

12 Drowning

12A | External findings

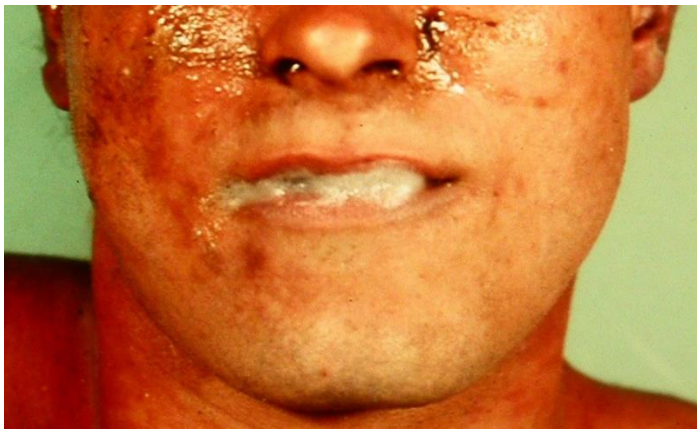

Fig. 12A.1 **The plume of foam**

Foam at the mouth produced by the mixture of drowning liquid, pulmonary surfactant, bronchial secretion, and air. It is also referred to as ''foam cone''.

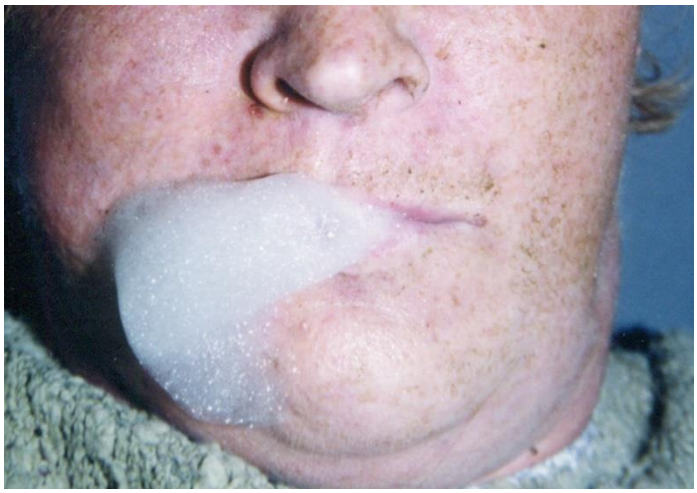

Fig. 12A.2 **The plume of foam**

Another example of the foam at the mouth.

Fig. 12A.3 **Washer woman's skin**

Wrinkled skin of the hand.

Fig. 12A.4 **Washer woman's skin**

Wrinkled skin of the foot.

Fig. 12A.5 **General appearance**

The image shows clothed corpse recovered from the river. The clothes are wet and dirty.

Fig. 12A.6 **General appearance**

The corpse from the previous image after undressing with mud adhered to the skin surface.

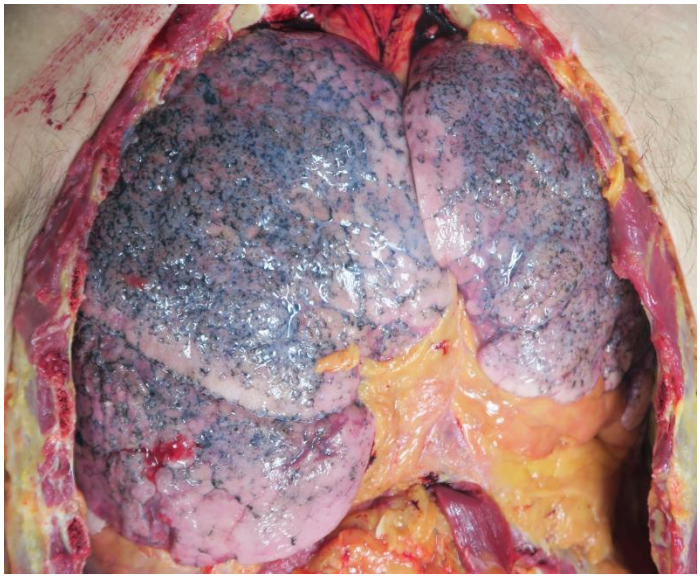

Fig. 12B.1 ***Emphysema aquosum***

Lungs are overdistended and occupy most of the pleural cavity; they may meet or overlap in the body midline, which is referred to as ''kissing lungs''.

Fig. 12B.2 ***Emphysema aquosum***

Overdistended lungs after evisceration do not collapse; they meet in the midline and obscure the pericardium.

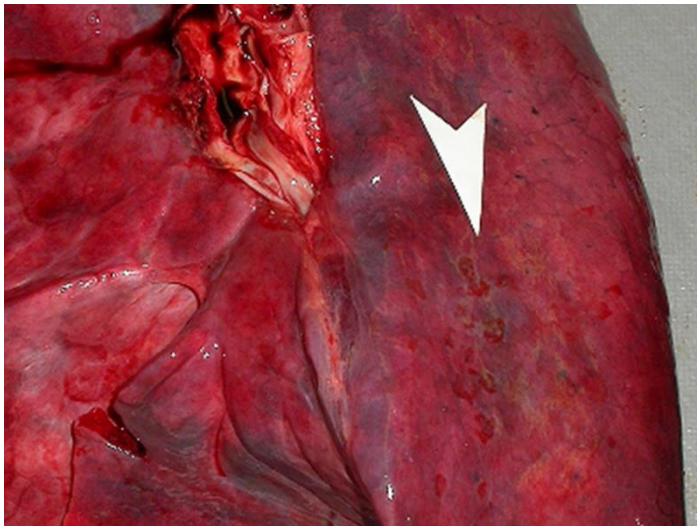

Fig. 12B.3 **Paltauf's spots**

Arrow pointing to the subpleural hemorrhages.

Fig. 12C.1 **Diatoms**

Microscopic image of various diatom species detected in lung tissue (unstained).

13 Strangulation

13A | External findings

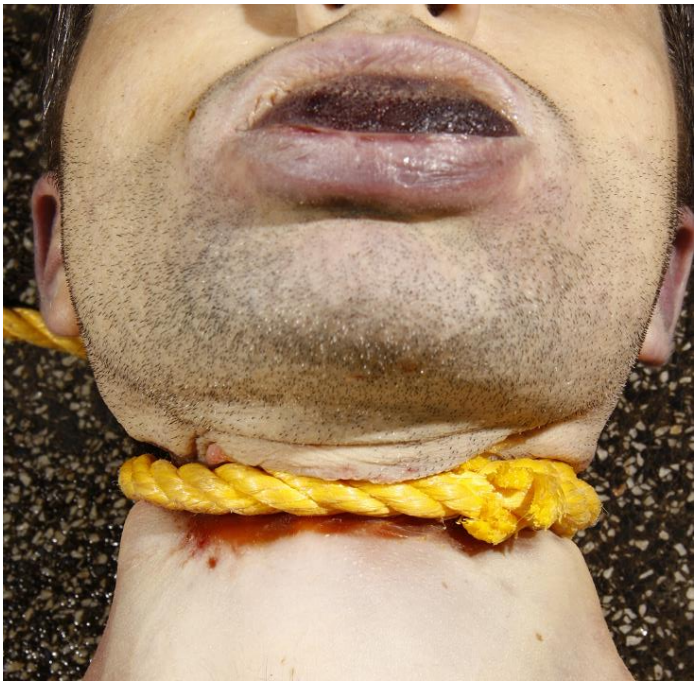

Fig. 13A.1 **Ligature mark**

A nylon rope around the neck in a case of suicidal hanging. The tongue protrudes from the mouth; it has a dark appearance as a result of drying.

Fig. 13A.2 **Ligature mark**

Dual ligature mark on the neck bearing the imprint of the ligature (rope).

Fig. 13A.3 **Ligature mark**

Non-patterned interrupted (non-continuous) ligature mark on the left side of the neck with marked upward angle; it has a parchment-like appearance.

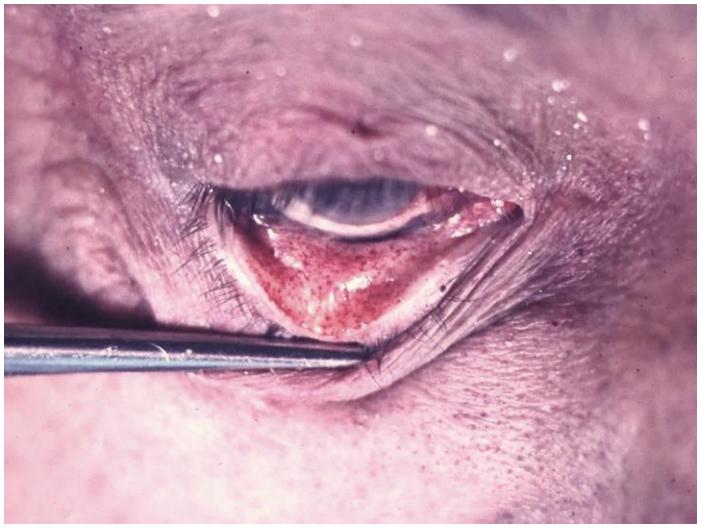

Fig. 13A.4 **Petechial hemorrhages**

Petechiae in the conjunctiva.

Fig. 13A.5 **Postmortem lividity**

Postmortem lividity on the lower extremities in the case of hanging with full suspension.

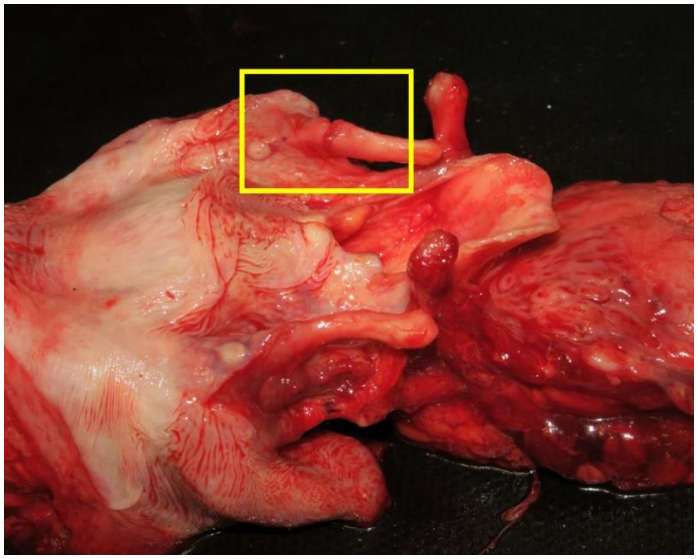

Fig. 13B.1 **Thyroid cartilage fracture**

Eviscerated neck complex with a fracture of the left superior cornu (yellow frame) of the thyroid cartilage.

Fig. 13B.2 **Hyoid bone fracture**

Eviscerated neck complex with a fracture of the left greater cornu of the hyoid bone (to the right of epiglottis on the image).

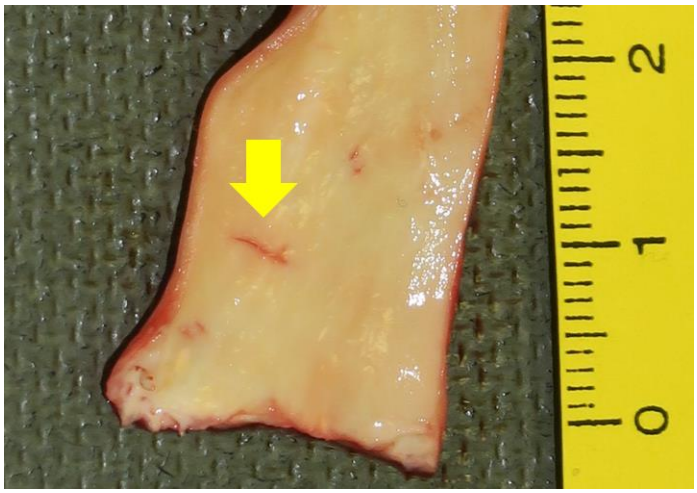

Fig. 13B.3 **Amussat's sign**

Arrow pointing to the intimal tear of the common carotid artery.

Fig. 13B.4 **Petechial hemorrhages**

Petechial hemorrhages in the cranial soft tissues dissected from the skull.

Fig. 13B.5 **Petechial hemorrhages**

Petechial hemorrhages under the visceral pericardium of the left ventricle below the left auricle.

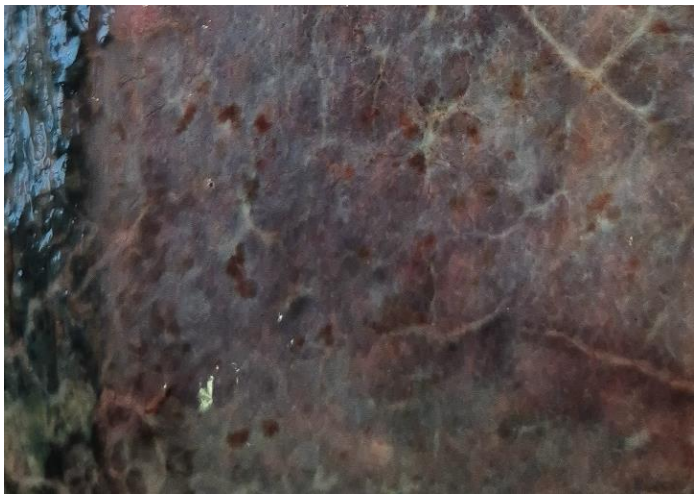

Fig. 13B.6 **Petechial hemorrhages**

Petechial hemorrhages under the visceral pleura of the interlobal surface of the lung.

TESTS

You can test your knowledge on the autopsy findings by taking picture-based tests.

The tests are created in MS Forms and comprise of picture-based questions.

There are four options to each question; always only one answer is correct.

The results and correct/incorrect answers will appear immediately after submitting the response.

Links can be accessed only by using the university account (@student.upjs.sk).

TEST No. 1 | https://forms.office.com/e/5fysDTyD55

TEST No. 2 | https://forms.office.com/e/aPjsSTu169

TEST No. 3 | https://forms.office.com/e/LUNkXEWTdj

References

ARMSTRONG, E. J., and K. L. ERSKINE. Investigation of Drowning Deaths: A Practical Review. Academic Forensic Pathology. 2018, **8**(1), 8 – 43. ISSN 19253621.

BAUM, G. R. et al. Gunshot Wounds: Ballistics, Pathology, and Treatment Recommendations, with a Focus on Retained Bullets. Orthopedic Research and Reviews. 2022, **14**, 293 – 317. ISSN 1179-1462.

BERAN, R. Legal and Forensic Medicine. Berlin: Springer Berlin, Heidelberg, 2013. ISBN 978-3-642-32337-9.

BURTON, J., S. SAUNDERS, and S. HAMILTON. Atlas of Adult Autopsy Pathology. Boca Raton: CRC Press, 2015. ISBN 978-1-4441-3753-8.

DIMAIO, V. J., and D. DIMAIO. Forensic Pathology. 2nd edition. Boca Raton: CRC Press, 2001. ISBN 978-0849300721.

DETTMEYER, R. B. Forensic Histopathology: Fundamentals and Perspectives. 2nd edition. Berlin: Springer, 2018.
ISBN 978-3-319-77996-6.

DETTMEYER, R. B., M. A. VERHOFF, and H. F. SCHÜTZ. Forensic Medicine: Fundamentals and Perspectives. Berlin: Springer Verlag, 2013. ISBN 978-3-642-38817-0.

HIRT, M. et al. Soudní lékařství: I. díl. Praha: Grada Publishing, a. s., 2015. ISBN 978-80-247-5680-6.

HIRT, M. et al. Soudní lékařství: II. díl. Praha: Grada Publishing, a. s., 2015. ISBN 978-80-271-0268-6.

JANÍK, M. et al. Forenzná patológia srdca a ciev. Multimediálna podpora výučby klinických a zdravotníckych disciplín: Portál Jesseniovej lekárskej fakulty Univerzity Komenského. Online. Available from: https://portal.jfmed.uniba.sk//clanky.php?aid=436. ISSN 1337-7396. [viewed 2023-10-10].

KRAJČOVIČ, J. Vybrané medicínsko-právne kapitoly v súdnom lekárstve. Multimediálna podpora výučby klinických
a zdravotníckych disciplín: Portál Jesseniovej lekárskej fakulty Univerzity Komenského. Online. Available from: https://portal.jfmed.uniba.sk//clanky.php?aid=205. ISSN 1337-7396. [viewed 2023-10-10].

MADEA, B. Handbook of Forensic Medicine. Oxford: Wiley Blackwell, 2014. ISBN 978-0-470-97999-0.

PALMIERE, C., G. TERESIŃSKI, and P. HEJNA. Postmortem diagnosis of hypothermia. International Journal of Legal Medicine. 2014, **128**(4), 607 – 614. ISSN 0937-9827.

PAYNE-JAMES, J. J. History of Forensic Medicine. In: J. J. PAYNE-JAMES, and R. BYARD, ed. Encyclopedia of Forensic and Legal Medicine. 2nd edition. Elsevier, 2016, p. 539 – 567. ISBN 978-0128000342.

PILIN, A. et al. Soudní lékařství. Praha: Univerzita Karlova, Nakladatelství Karolinum, 2022. ISBN 978-80-246-5013-5.

POPPER, H. Pathology of Lung Disease. 2nd edition. Berlin: Springer, 2021. ISBN 978-3030557423.

RAO, N. G. Textbook of Forensic Medicine and Toxicology. 2nd edition. Jaypee Brothers Medical Publishers (P) Ltd, 2010. ISBN 978-81-8448-706-0.

REDDY, K. S. N., and O. P. MURTY. The Essentials of Forensic Medicine and Toxicology. 33rd edition. New Delhi: Jaypee Brothers Medical Publishers Ltd., 2014. ISBN 978-8188230303.

SAUKKO, P., and B. KNIGHT. Knight's Forensic Pathology. 5th edition. CRC Press, 2016. ISBN 978-1-4441-6508-1.

ŠIDLO, J. Súdne lekárstvo: pitva. Bratislava: Univerzita Komenského v Bratislave, 2020. ISBN 978-80-223-4903-1.

ŠIDLO, J. Súdne lekárstvo: súdnolekárska tanatológia, súdnolekárska traumatológia. Bratislava: Univerzita Komenského v Bratislave, 2020. ISBN 978-80-223-4900-0.

ŠTEFAN, J., J. HLADÍK a kol. Soudní lékařství a jeho moderní trendy. Praha: Grada Publishing, a. s., 2012. ISBN 978-80-247-3594-8.

TESAŘ, J. Soudní lékařství. 2. vydanie. Praha: Avicenum, zdravotnické nakladatelství, 1976. ISBN 08-007-77.

VIJ, K. Textbook of Forensic Medicine and Toxicology: Principles and Practice. 5th edition. New Delhi: Elsevier, 2011. ISBN: 978-81-312-2684-1.

VOREL, F. et al. Soudní lékařství. Praha: Grada Publishing, 1999. ISBN 80-7169-728-1.

ATLAS OF FORENSIC MEDICINE: Autopsy findings in violent and non-violent deaths
University Textbook

Author: Dorota Sopková, MD, PhD., MBA

Publisher: Pavol Jozef Šafárik University in Košice
ŠafárikPress Publishing

Year: 2025
Pages: 118
Author's sheets: 9,87
Edition: first

DOI: https://doi.org/10.33542/AFM-0442-2
ISBN 978-80-574-0442-2 (e-publication)